MASS SPECTROMETRIC AND COMPUTATIONAL STUDIES OF *N*-HETEROCYCLES

by

NING WANG

A dissertation submitted to the

School of Graduate Studies

Rutgers, The State University of New Jersey

In partial fulfillment of requirements

For the degree of

Doctor of Philosophy

Graduate Program in Chemistry and Chemical Biology

Written under the direction of

Professor Jeehiun K. Lee

And approved by

_____

_____

_____

_____

New Brunswick, New Jersey

OCTOBER 2019

ABSTRACT OF THE DISSERTATION

Mass Spectrometric and Computational Studies of Heterocycles

by NING WANG

Dissertation Director:

Professor Jeehiun K. Lee

This dissertation focuses on the experimental and theoretical studies of thermodynamic properties and reactivity of two types of heterocyclic compounds: N-heterocyclic carbenes (NHCs) and imidazoles.

In recent years, triazolylidene carbenes have drawn broad attention in stereoselective organo-catalysis. These carbenes have dominated over thiazolylidene and imidazolylidene carbenes with drastic improvement in the achievable stereoselectivity in a variety of NHC-catalyzed reactions. Although intensively applied and studied in a great variety of catalytic transformations, the intrinsic properties of these carbenes remain mostly unknown. Our group therefore measured and calculated the gas phase acidities of a series triazolium pre-catalysts (the conjugate acids of triazolylidene carbenes), both achiral and chiral, with mass spectrometric experiments and quantum mechanical methods to probe their fundamental properties. It was found that the gas phase acidities of the triazolium pre-catalysts can be tuned by the subtle electronic properties of their substituents on the triazolium ring. The correlation between the thermodynamic properties and the catalytic reactivities has also

been discovered and further investigated. We have found the correlations between the gas phase acidities of these triazolium pre-catalysts and the stereoselectivity of two triazolylidene carbene-catalyzed *Umpolung* reactions. These correlations, the first of their kind, can be potentially used to provide guidance for future stereoselective catalyst design. These results are discussed in Chapter 2.

Carbon dioxide capture and sequestration (CCS) has become a research "hotspot" due to the increasing concern regarding their roles in the global greenhouse effect and subsequent climate change and environment destruction. We investigated the role that imidazolate anion plays in the absorption of carbon dioxide. A series of imidazoles with structural variations were characterized with both mass spectrometric experiments and computer modeling, in the gas phase and in an ionic liquid medium. By establishing correlations between the imidazolate properties and CO_2 absorption capacity, we hope to provide guidance for a future generation of greenhouse gas capture systems with improved efficiency and robustness. During this process, we have also analyzed the substitution effects on the imidazolate properties and CO_2 capture, and confirmed that mass spectrometry-based experiments can be designed to investigate tautomerism of imidazoles. These results are discussed in Chapter 3.

The difference in reactivity of organic species in solution phase compared to gas phase has interested many organic chemists. Gas phase studies using mass spectrometry allow us to penetrate the intrinsic property of various organic species and elucidate reaction mechanisms without solvent effects. Only charged species could be detected by mass spectroscopy, and organocatalysts with charged handles are therefore important for such purposes. In Chapter 4, we discussed how we could utilize the charge-handled NHCs in

Umpolung reactions such as Stetter reaction and benzoin condensation in the gas phase. Selected imidazolylidene, thiazolylidene and triazolylidene carbenes, either synthesized *ab initio* or commercially available, were examined both experimentally and theoretically.

Finally, in Chapter 5, we reported the preliminary data collected that explore the relationship between the gas-phase properties of ionic liquids (cations/anions) with proton conductivity/open-circuit potential (OCP) of ionic liquid-based electrolytes used in anhydrous fuel cells.

DEDICATION

To my grandparents, my parents and my love Yun.

ACKNOWLEDGEMENTS

First and foremost, I would like to thank my advisor, Prof. Jeehiun K. Lee, for giving me an opportunity to join her group, do research, and challenge myself to become a better scientist and professional under her supervision and guidance.

I would like to thank my committee members, Dr. Ralf Warmuth, Dr. Laurence Romsted, and Dr. Chen, for their help to improve my research, for their valuable time and discussions, and attention they devoted to my work.

I would like to thank Dr. Tomislav Rovis from Columbia University for the great collaboration.

I would like to thank Dr. Alexei Ermakov for all the valuable instructions he gave us on mass spectrometric instrument troubleshooting.

I would like to thank Dr. Geeta Govindarajoo for her help and guidance during my rewarding experience of academic teaching.

I would like to thank all the group members and alumni for their contribution to the research of Lee group, and for their support for my research and life: Dr. Yijie Niu, Jiahui Xu, Allison Krajewski, Lanxin Zhang, Damon Hinz, and Alec Levine.

I would like to thank all my family members and my friends for their encouragement.

TABLE OF CONTENTS

LIST OF FIGURES

LIST OF TABLES

Chapter 1. Introduction

1.1 Overview

Gas phase studies achieved by mass spectrometry have long been employed by scientist for identification and quantification of molecules, and to investigate ion-molecule interactions *in vacuo*.[1-5] Density functional theory (DFT) is a computational quantum mechanical modelling method widely used to investigate the electronic structure of many-body systems, in particular atoms, molecules, and the condensed phases. By using both mass spectrometry and DFT computational methods, we were able to characterize the thermodynamic properties and reactivity of two types of heterocyclic compounds: N-heterocyclic carbenes (NHCs) and imidazoles.

1.1.1 *N*-Heterocyclic Carbenes (NHCs)

A carbene is a molecule containing a neutral carbon atom with a valence of two and two unshared valence electrons. The general formula is R-(C:)-R' or R=C: where the R represent substituents or hydrogen atoms. The majority of carbenes are too reactive to be isolated and examined independently. *N*-heterocyclic carbenes (NHCs), as a type of stabilized carbene species, emerged during the second half of the 20th century. A brief comparison between the traditional carbenes and NHCs is shown in Figure 1.1.[6-9]

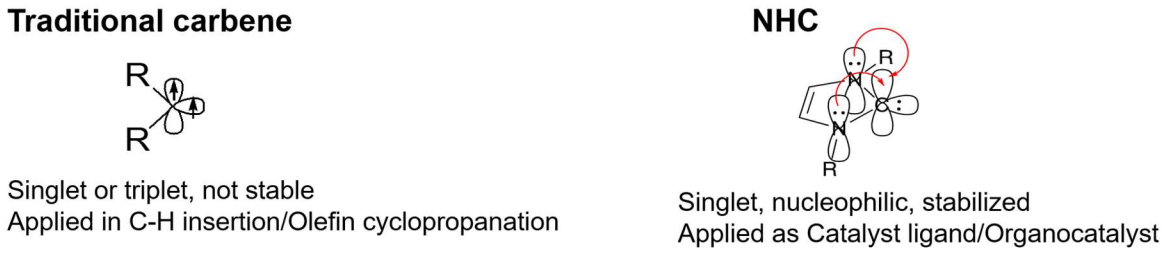

Figure 1. 1 Comparison between traditional carbenes and NHCs

In the early 1960's Wanzlick first investigated the reactivity and stability of N-heterocyclic carbenes. Shortly thereafter, Wanzlick reported the first application of NHCs as ligands for metal complexes, after which the field of NHCs as ligands in transition metal chemistry remained dormant for 23 years. In 1991, the successful isolation and characterization of *N*-heterocyclic carbenes were revealed in a report by Arduengo and co-workers. In this work, they reported the extraordinary stability, isolation and storability of crystalline NHC IAd. The synthesized *N*-heterocyclic carbenes are not only electronically stabilized by the nitrogen atom(s) adjacent to the center carbon, where the π-electrons of the nitrogen atom(s) donate to the empty *p* orbital of the center carbon, but also by the sterically hindered adamantyl group.

NHCs, based on the basic heterocyclic structure, can be derived from imidazole, imidazoline, thiazole or triazole (Figure 1.2).

Figure 1. 2 Different types of *N*-Heterocyclic carbenes

NHCs are considered as singlet ground state and are electron rich due to resonance, which makes them good sigma donors. Since the discovery and isolation of NHC, the rich chemistry of the nucleophilic lone pair on its center carbon and its relatively high stability has led to tons of applications in coordination chemistry and organocatalysis, both theoretically and experimentally.[10-26]

NHCs were widely used as ligands in the second-generation Grubbs catalyst (transition metal catalysts), which, compared to the first-generation Grubbs catalyst in which

tricyclohexylphosphine (PCy_3) was used, shows improved air and water resistance and higher catalytic reactivity on olefin metathesis.[27] The increased effectiveness of the catalysts with NHC ligands over phosphine ligands attracted many scientists to conduct examinations towards the principle underneath. Recently we published a review article where we discussed how the basicity of NHC would influence its catalytic ability. The fact that NHCs are generally more basic than the phosphine ligands might contribute to the increased efficiency of the second-generation Grubbs catalysts.

NHCs, in addition to serve as effective ligands for olefin metathesis, can themselves serve as efficient organocatalysts to induce *Umpolung* in a variety of organic transformations.[28] *Umpolung* (polarity inversion) is the chemical modification of a functional group with the aim of polarity reversal, which allows further reactions of this functional group that would otherwise not be available.[29-31] Catalysts such as *N*-Heterocyclic Carbenes (NHCs) have been using to achieve *Umpolung* of electrophilic aldehydes. These aldehydes are converted to nucleophiles to react with aromatic aldehydes (benzoin condensation) or with appropriate Michael acceptors (Stetter reaction). In 1958, Breslow postulated that the thiazolium moiety in thiamine can be deprotonated under mildly basic conditions to generate NHCs, which can be added to an activated carbonyl group, resulting in *Umpolung* of the latter. The resulting intermediate, known as ‘‘Breslow intermediate’’ since then, after a series of reaction steps, leads to decarboxylation of pyruvic acid, acetoin condensation, etc. The mechanisms of the two most intensively studied *Umpolung* reactions, benzoin condensation and the Stetter reaction, are shown in Figure 1.3.

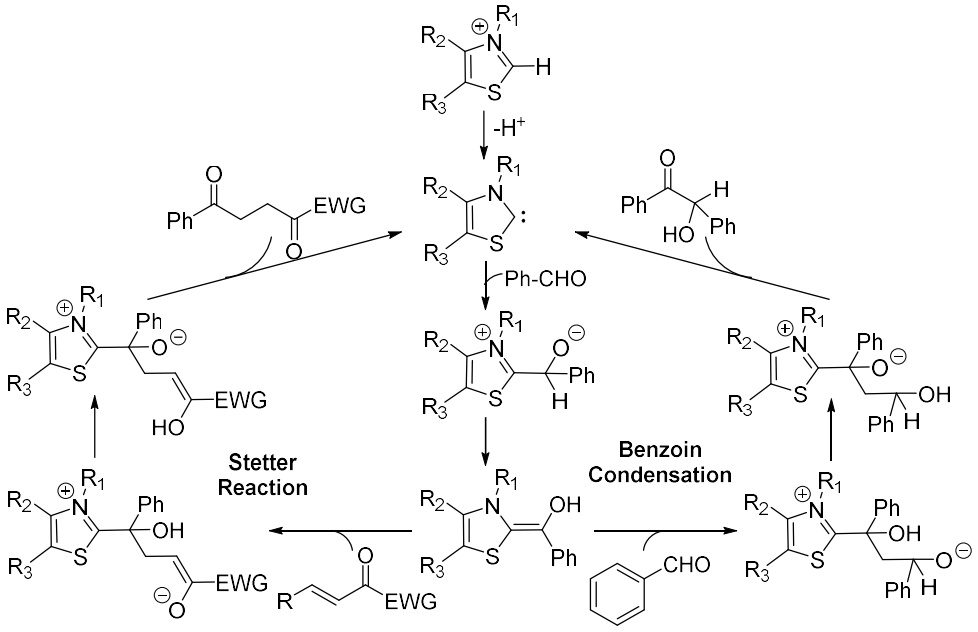

Figure 1. 3 Mechanisms of benzoin condensation and the Stetter reaction

Most organic transformations with NHCs as the catalysts were conducted in the condensed phase, where factors such as solvent effect and diffusion control make a difference towards the final results. Investigation on NHC-catalyzed reaction in a solvent-free environment to explore the intrinsic reactivity has been very rare. We utilize mass spectrometry technique and computational method to quantitatively measure the intrinsic, thermodynamic and kinetic properties of organic species, including a series of heterocyclic compounds such as NHCs and imidazoles. With both solution-phase and gas-phase data, we could help to lay the foundation towards a better understanding of various reaction mechanisms.

1.1.2 Carbon Dioxide Capture by Imidazolates

The prosperity of human society nowadays is supported by energy mostly coming from fossil fuels, which have released large amount of CO_2 into the atmosphere, and resulted in climate changes that in turn endanger human beings.[32] It is vital to find solutions to settle this imminent threat. Carbon capture and sequestration (CCS) is a process that includes the

initial capture of CO_2 emitted mainly from fossil fuels combustion, the CO_2 transportation that follows, and the final storage in geological formations.[33] CO_2 capture is the most costly step, while geological storage requires large capacity and bears concerns about its effects on the environment. Since the first International Conference on Carbon Dioxide Removal (ICCDR-1) held in in March 1992, Amsterdam, more and more researchers have been devoting themselves into this field, investigating new methods and materials for more efficient CCS process.[34]

Ionic liquids (ILs) have received much attention in the field of CCS due to their unique properties including low vapor pressure, high thermal stability, and a wide variety of cation/anion combinations that enables designability.[35] Compared to physical absorption which usually requires high pressure, chemisorption achieved by task-specific ILs (TSILs) can be applied in milder conditions with enhanced performance.[36] A major category of TSILs bear amine moieties within the cation/anion structures. One major issue associated with such TSILs is the dramatic viscosity increase after CO_2 absorption, which makes the absorption rate decrease along with time, as well as making the CO_2 desorption difficult to proceed. Molecular dynamics simulation indicates that the dramatic increase in viscosity is due to the formation of strong and dense hydrogen-bonded networks between the cation and anion species upon CO_2 absorption.[37]

As is shown in Figure 1.4, The partial charges on the individual atoms of the -NH2, $-NH3^+$, and $-NHCO2^-$ groups were calculated: there is a partial negative charge of -1.06 e on the amine nitrogen of A versus -0.52 e on the ammonium nitrogen of B, with other charges being comparable for terminal H and O atoms in the A, B, and C species. This points toward a hydrogen-bonding interaction between B⋯ C that is much stronger than that between

A ⋯ C. Upon CO_2 capture, strong hydrogen-bonded networks of $(B\cdots C)_n$ chains or clusters formed which results in the viscosity increase.

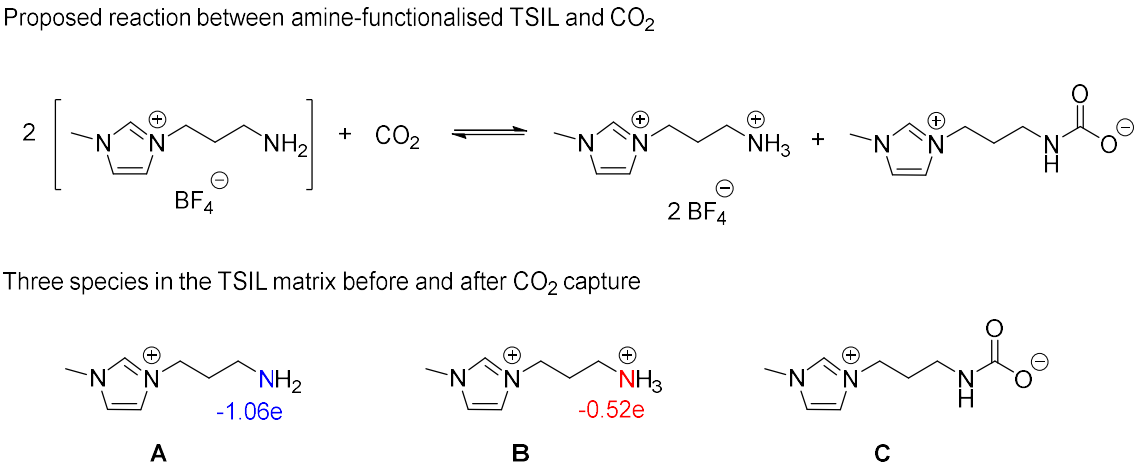

Figure 1. 4 Mechanism of viscosity increase of amino-functionalized ILs upon CO_2 capture

This drastic increase in viscosity makes the amino-functionalized TSILs less practical for carbon dioxide capture. Scientists have then adjusted the direction towards searching for "amino-free functionalized ILs", to improve carbon dioxide chemical absorption. Prominent within this type of IL are azolate ILs, which are also called aprotic heterocyclic anion (AHA) ILs.[38] Dai and Wang introduced this concept with a series of ILs that paired superbases such as 1,3,4,6,7,8-hexahydro-1-methyl-2H-pyrimido[1,2-a]pyrimidine (MTBD) and trihexyl(tetradecyl) phosphon-ium hydroxide ([P66614][OH]) with weak nitrogen acids such as imidazole, pyrazole, triazoles, tetrazoles and indoles.[39] In these AHA ILs, the anionic moiety (such as an imidazolate) nucleophilically attacks the carbon dioxide. Studies to date indicate that the basicity of the anion is important for carbon dioxide capture,

capacity, and solubility, while the effect of the countercation identity is weaker. Therefore, tuning the basicity is a key component for achieving effective CO_2 capture.[38]

Herein, we use computational and experimental methods to examine the acidity of fifty-six imidazoles, toward better understanding their properties. The experimental measurements provide valuable data to benchmark computations and lend insight into the inherent reactivity of these species. Gas-phase measurements are complemented by gas-phase and solution-phase calculations. We aim to achieve predictive power for such properties, which would allow for more facile tunability of potential ILs for carbon dioxide capture.

1.1.3 Charge-Handled *N*-Heterocyclic Carbene Catalyst

As mentioned above in **1.1.1**, Breslow and coworkers proposed a catalytic mechanism with the thiazolylidene as the catalytic species. The reaction mechanism he proposed involves a deprotonation of the thiazolium precatalyst to generate a thiazolyidene, which attacks an aryl aldehyde and yields a so-called Breslow intermediate after proton transfer. Although the Breslow mechanism is well accepted, other mechanisms, for example the one proposed by Lemal and Castells involving a thiazolyidine dimer, have also been postulated.[40-44] There has been debate among different mechanisms. On the other hand, limited work with detailed mechanistic studies for Stetter reaction impeded the development of intensive application of NHC-catalyzed asymmetric Stetter reactions.[45,46]

Gas phase studies in absence of solvent are able to reveal intrinsic organic reactivity and elucidate complicated reaction mechanisms. Neutral species are, however, undetectable by mass spectroscopy, and the reaction intermediates are usually unstable and have the propensity of fragmentation. Introducing a charged handle to NHC will address the first

issue, while using a "soft" electrospray ionization tandem mass spectrometry (ESI-MS/MS), which has achieved recognition as a tool to probe the reaction mechanisms over the years, will help the latter.[47] Therefore, we analyzed two categories of charged-handled carbenes both experimentally and calculationally. The first category includes two newly designed and synthesized triazolylidene NHCs with carboxylate charge tags; the second category includes two commercially available catalysts (one thiazolylidene and one imidazolylidene) with alkoxide and carboxylate charge tags, respectively (Figure 1.5).

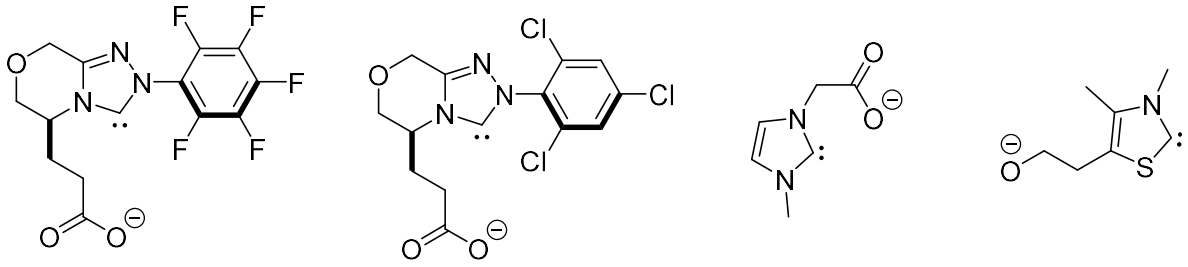

Figure 1. 5 The four charge-handled NHCs discussed in Chapter 4

The charged groups of these NHCs would not only make it possible to track the regents and intermediates of benzoin condensation and Stetter reaction in vacuum by mass spectrometry, but also serve as "proton shuttles" to effect the 1,2-proton transfer to form the Breslow intermediate. In addition, these charged NHC catalysts possess different ring structure (triazolylidene, thiazolylidene and imidazolylidene, respectively) so that we could compare their intrinsic catalytic reactivity.[48,49]

1.1.4 Heterocycle-based Ionic Liquids (ILs) Applied as Electrolytes in Anhydrous Fuel Cells

Anhydrous proton conductors (e.g. fuel cells) have many advantages as electrochemical units due to the absence of flammable and/or toxic solvents, which avoid the risk of dangerous chemical reactions such as the thermal runaway reaction that potentially poses

great damage to human beings and environment.[50] Thermal runaway is a complicated process. It is believed to be triggered by reaction of liquid electrolyte with electrode surfaces and releases a lot of heat and flammable H2/O2 gases, which further react and release heat, and finally result in fire or explosion.

Recently much attention has been paid to high temperature polymer electrolyte fuel cells (PEFCs) due to their advantages over conventional PEFCs which exhibit poor proton conductivity above 100°C due to their temperature and humidity dependence.[51] Therefore, ionic conducting membranes based on low-volatility solvents, i.e., heterocycle-based polymer or ILs-based polymer, have been widely studied. Heterocycles such as imidazole, pyrazole, triazole, and benzimidazole have been considered as proton solvents to replace water, so that high temperature polymer electrolyte fuel cells would be possible.[52,53]

Our gas-phase study is conducted in anhydrous conditions where the properties of the heterocycle-based electrolytes could be characterized *in vacuo*. By establishing the relationship between heterocycle properties and proton conductivity in fuel cells we could provide guidance for rational electrolytes design for novel anhydrous high temperature fuel cells.

1.2 Instrumentation

1.2.1 Electrospray Ion Source (ESI)

The electrospray ion source (ESI) is a technique used in mass spectrometry to produce ions using an electrospray in which a high voltage is applied to a liquid to create an aerosol. ESI, as a "soft" ion source, is not only applied in analysis of small molecules, but also especially useful in producing ions from macromolecules because it overcomes the propensity of these molecules to fragment when ionized, whereas the "hard" ion source (e.g. electron ionization (EI)) produces fragment ions that have mass-to-charge ratios less than that of the parent molecular ions. ESI could generate both cations and anions. ESI happens under atmospheric pressure.[54,55]

As is shown in Figure 1.6, the liquid passes through a capillary tube, the end of which bears a high electric field. Under the electric field, charges accumulate at the liquid surface at the end of the capillary, and break the liquid into charged droplets. The evaporation of solvent shrinks the droplets and the increasing repelling force break the droplets into small ones. After cascades of this process, the solvent is dried out and ions are desorbed from the solvent.[56]

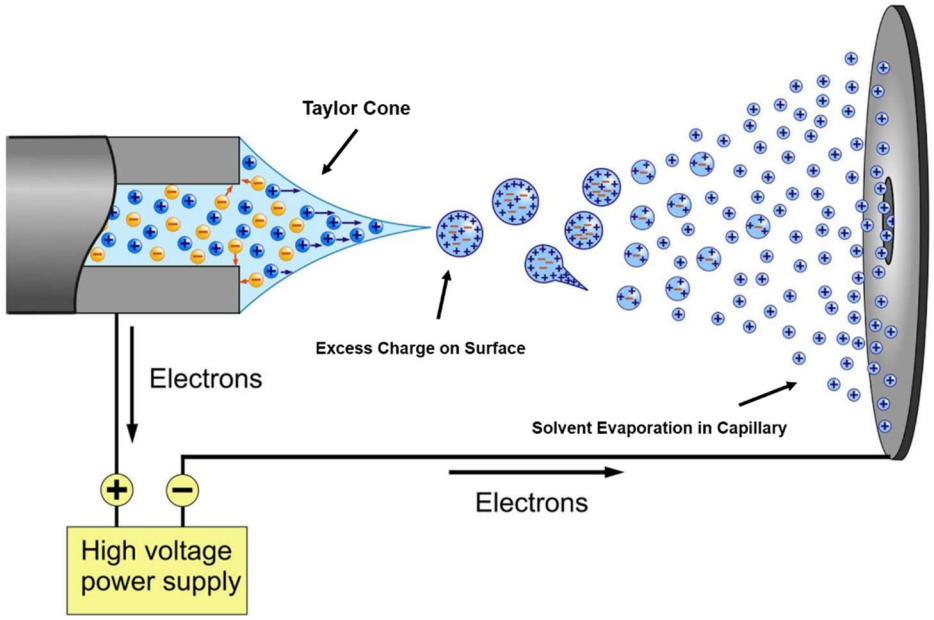

Figure 1. 6 Diagrammatic representation of ionization in an electrospray ion source (ESI)

1.2.2 Quadrupole Ion Trap Mass Spectrometer

A linear quadrupole mass spectrometer comprises four parallel rods of circular or hyperbolic cross-section. These are connected to radio-frequency($V_0 cos\omega t$) and direct-current (U) power supplies, as shown in Figure 1.7.[57]

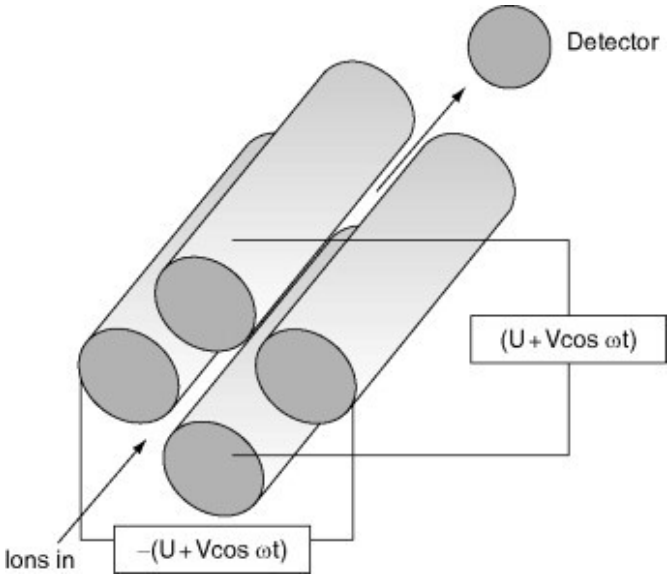

Figure 1. 7 Schematic diagram of a quadrupole mass spectrometer.

The quadrupole analyzes different mass-to-charge ratios using the stability of their trajectories. The rods opposite to each other always carry the same polarity, while the rods next to each other carry opposite polarity. A polarity reversal of the potential applied on the rods can change the ion travel direction before it hits the rods and discharges, thus stabilizing the ion. By operating the quadrupole in a stable region, the ions will be constrained to follow a path between the rods until they reach the detector. The mass spectrum is scanned by varying V_0 and U so that the ratio U/V_0 remains constant. The quadrupole mass analyzer acts as a mass filter, allowing one mass channel at a time to reach the detector as the mass range is scanned.

Ion trap mass analyzers use a combination of electric or magnetic fields to capture or "trap" ions inside the mass analyzer. There are multiple configurations of ion traps. For example, 3D ion traps, also called the Paul ion trap in honor of Wolfgang Paul, who invented the device and shared the Nobel Prize in Physics in 1989 for this work. The 3D ion trap basically works on the same principle as a quadrupole mass analyzer, using static DC current and RF oscillating electric fields, but the hardware is configured differently, where the parallel rods are replaced with two hyperbolic metal electrodes (end caps) facing each other, and a ring electrode placed halfway between the end cap electrodes; ions are trapped in a circular flight path based on the applied electric field (Figure 1.8).[58] Another configuration is the 2D trap, also named linear ion trap. A linear ion trap uses a set of quadrupole rods coupled with electrodes on each end to facilitate the ion trapping. Tandem mass analysis can be conducted on both 2D and 3D quadrupole ion traps. The magnetic field-based trap (ion cyclotron resonance, ICR) will be introduced in **1.2.3**.

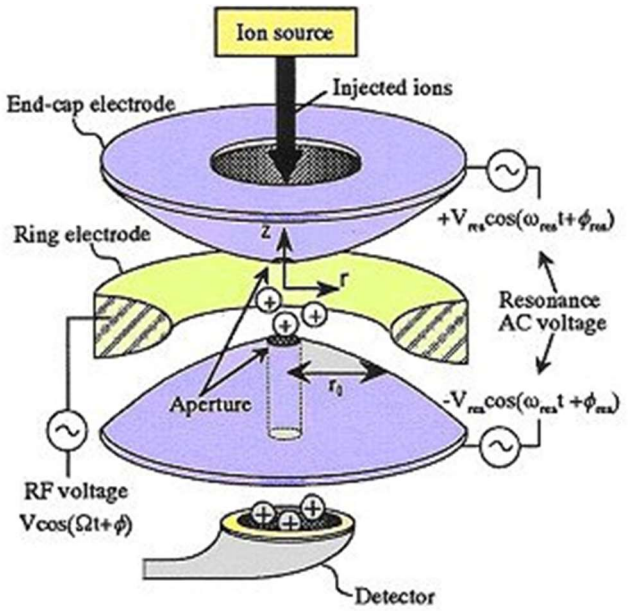

Figure 1. 8 Schematic diagram of a 3D ion trap.

Specifically, our group uses both a Finnigan LCQ DUO (ESI-3D quadrupole ion trap) mass spectrometer and a Finnigan LTQ (ESI-linear quadrupole ion trap) mass spectrometer for the Cooks kinetic experiments to measure gas phase acidity and proton affinity.

Our group also uses a house-modified Finnigan LCQ DUO (ESI-3D quadrupole ion trap) mass spectrometer for bracketing and gas-phase reaction mechanistic study. A schematic presentation is shown in Figure 1.9. The analyte sample solution could be introduced through ESI via a syringe pump, while a cross inlet was constructed on the buffering gas line in order to introduce the neutral references, thus making the 3D ion trap as both a "reaction container" where the reaction between charged analyte molecules and neutral reference molecules can be monitored, and a mass spectrometer.

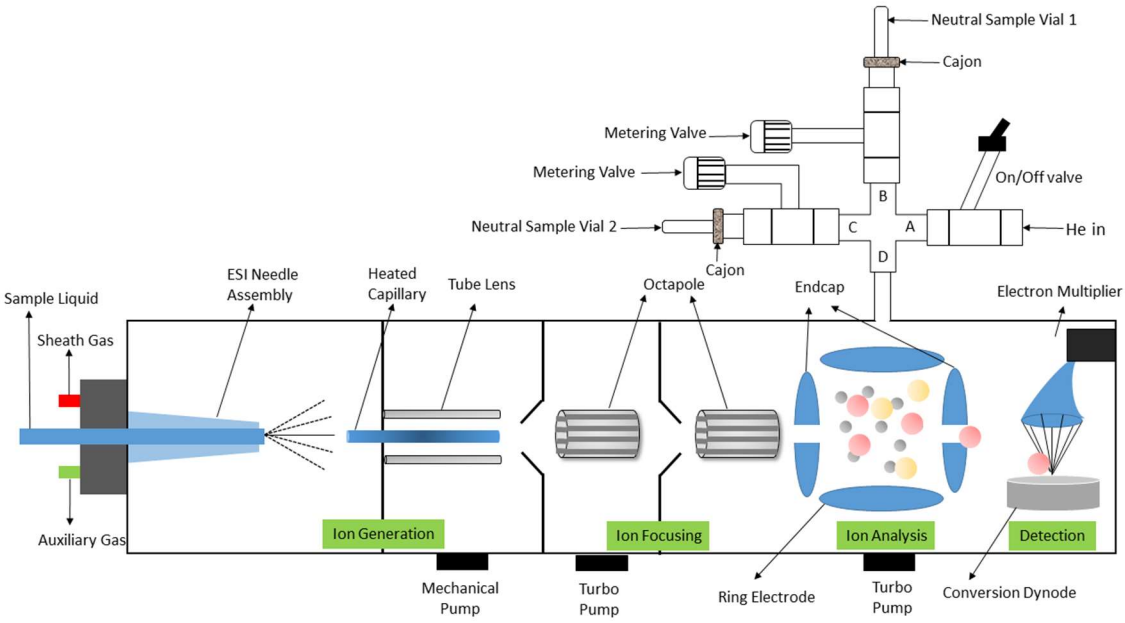

Figure 1. 9 The house-modified Finnigan LCQ DUO Mass Spectrometer in the Lee group

1.2.3 Fourier Transform Ion Cyclotron Resonance Mass Spectrometer (FT-ICR)

As we mentioned above in **1.2.2**, ion cyclotron resonance (ICR) traps use a strong magnetic field to induce a radial orbit of ions, where the frequency of orbit in the magnetic field is a function m/z for the ion. A Fourier transform algorithm is required for the signal processing. The advantage of an ICR trap is the ability to trap all ions at once and detect them on the basis of their detected frequencies.[59]

The circular motion of an ion in a magnetic field is subject to Lorentz force. The Lorentz force *F* that an ion feels in a magnetic field B can be depicted by Eq. 1.1.

$$F = qvB \qquad \textbf{Eq. 1.1}$$

where v is the velocity of the ion and q is the ion net charge.

The circular trajectory of the ion can be stabilized when the Lorentz force *F* balances the centrifugal force Fc (Eq. 1.2).

$$F = F_C = \frac{mv^2}{r} \qquad \textbf{Eq. 1.2}$$

where m is the mass of the ion and r is the circular radius of its trajectory.

Therefore, from Eq. 1.1 and Eq. 1.2, we could derive Eq. 1.3, represented in angular frequency:

$$\omega = 2\pi f = \frac{v}{r} = \frac{q}{m}B = \frac{1}{m/z}B \qquad \textbf{Eq. 1.3}$$

As shown in Eq. 1.3, the angular frequency ω ($\omega = 2\pi f$) of the ion motion is proportionally related to the mass-to-charge ratio (m/z) of the ion.

While the ion frequency is independent to its velocity, the trajectory radius is proportional to the velocity. After an ion is trapped in the ICR cell, it is excited by a radio electromagnetic wave that shares the same frequency as the circular motion, thus irradiating the ions and transferring energy to the ions via resonance absorption, which results in an increased motion trajectory radius. As the trajectory radius increases, the resonance ions end up hitting the detector and the subsequent alternating current, the image current, can be interpreted into frequency signals and further translated into mass-to-charge ratio of the ion (Figure 1.10).[60]

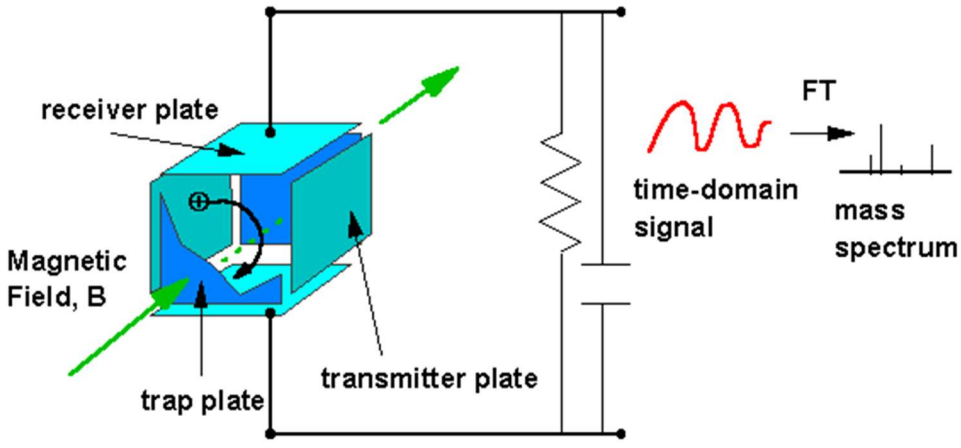

Figure 1. 10 Schematic diagram of an ion cyclotron resonance instrument

Our Finnigan 2001 FT-ICR mass spectrometer is equipped with two cubic ICR cells with 3.3 Tesla superconducting magnet field (Figure 1.11). We can introduce chemical compounds into the instrument via batch inlets, leak valves, pulsed valves and a heatable solids probe inlet. Chemical samples can be ionized by electron ionization (EI), chemical ionization (CI) and electrospray ion (ESI) sources. The dual cell system allows ions to be selectively transferred between two cells. This enables users to prepare ions in one cell and study the property of the ions in the other cell, which introduces flexibility of experimental designs.

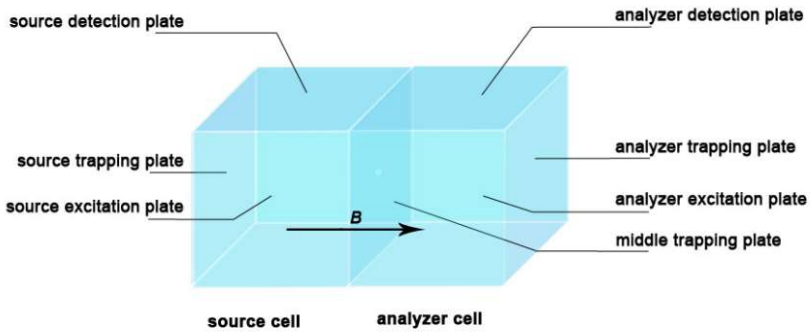

Figure 1. 11 Schematic diagram of the Finnigan 2001 FT-ICR duel cell setup

1.3 Methodology

1.3.1 Bracketing Method

The bracketing method is used to measure the gas phase proton affinity (PA) and acidity of organic bases and acids, respectively. Organic bases or acids with known proton affinity or acidity are used as references to "bracket" the corresponding thermodynamic property (PA or acidity) of the sample compounds into a narrow range (2-3 kcal/mol).

The reaction efficiency (Eq. 1.4) of the proton transfer reaction between a reference compound and a sample compound is measured and calculated. Assuming this process to

be barrier-free, this efficiency indicates the occurrence (indicated by the "+" symbol) or absence (indicated by the "-" symbol) of the proton transfer, with a cutoff of 10%.

$$\boldsymbol{efficiency}\ (\%) = \frac{\boldsymbol{k_{exp}}}{\boldsymbol{k_{coll}}} \times \mathbf{100}\% \qquad \textbf{Eq. 1.4}$$

For example, if a reference base B_1 is unable to deprotonate the conjugated acid of the sample compound, but another reference base B_2 can, then we could conclude that the PA of the sample is higher than PA of B_1 and lower than that of B_2.

Specifically, $k_{coll,}$ defined as the theoretical ion-molecule collision rate constant, can be calculated using the Average Dipole Orientation (ADO) program,[61.62] while k_{exp} (experimental rate constant of the reaction) can be measured by the reaction kinetics study using mass spectrometers (FT-ICR or quadrupole ion trap). Take the proton transfer reaction below as an example, the proton transfer happens between the protonated sample BH^+ and the neutral reference compound Ref. The concentration of the neutral reference is considered constant, and this reaction could be considered as *pseudo*-first order:

$$BH^+ + \text{Ref} \rightarrow B + \text{Ref-}H^+$$

$$\text{Rate} = k_{exp}\,[BH^+][\text{Ref}]$$

$$k' = k_{exp}\,[\text{Ref}]\ (\textit{pseudo}\text{-first order reaction})$$

$$Rate = k'\,[BH^+] = -\frac{d[BH^+]}{dt}$$

$$\int_{[BH^+]_0}^{[BH^+]_t} \frac{d[BH^+]}{[BH^+]} = -\int_0^t k'dt$$

$$ln\frac{[BH^+]_t}{[BH^+]_0} = -k't$$

$$ln[BH^+]_t = -k't + ln[BH^+]_0$$

$$slope = -k' = -k_{exp}\,[Ref]$$

$$k_{exp} = \frac{Rate}{[BH^+][Ref]} = -\frac{slope}{[Ref]} = -\frac{slope}{P_{ref}*\theta} \qquad \textbf{Eq. 1.5}$$

As shown in Eq. 1.5, *slope* is the slope for the plot of ln[BH^+] versus reaction time; P_{ref} is the pressure of the neutral reference which could be derived from the kinetic reaction; θ is the conversion factor of 3.239×10^{16} molecule·cm^{-3}·torr^{-1}.

1.3.1.1 Bracketing Method using FT-ICR

The FT-ICR mass spectrometer has a dual cell setup (described previously).[36-40] The magnetic field is 3.3 T; the baseline pressure is 1 x 10^{-9} Torr. The analyte sample is introduced into the cell via a heatable solids probe, while the reference acids are introduced via a system of heatable batch inlets or leak valves. Water is pulsed into the cell through the pulse valves, and is ionized by an electron beam (typically 8 eV (for HO^-), 20 eV (for H_3O^+), 6 μA (for H_3O^+), 9 μA (for HO^-), 0.5 s) to generate hydronium/hydroxide ions. The reactions between the analyte sample compounds and reference compounds are measured in both directions. In one direction, the sample cations/anions are generated by reaction of the sample with the hydronium/hydroxide ions, respectively. The charged sample species are then selected and transferred from one cubic cell to another via a 2-mm hole in the middle trapping plate. Transferred ions are then cooled with pulsed argon gas that allows the pressure to rise to 10^{-5} Torr. Reaction with the neutral reference compounds is then tracked. In the opposite direction, the charged reference compounds are generated by reaction with hydronium/hydroxide. These ions are then transferred to the second cell to react with neutral sample molecules. The experiments are conducted at ambient temperature. The typical protocol for obtaining gas phase rate constants has been described previously in literatures[36,37,40-42] and also in **1.3.1**. The experiments are run under *pseudo-*

first-order conditions with the neutral reactant in excess, relative to the analyte ions. Reading the pressure of the neutral reference compounds from the ion gauges is not always accurate; therefore, we "back out" the neutral substrate pressure from fast control reactions (described previously).[36,42-46]

1.3.1.2 Bracketing Method using LCQ Mass Spectrometer

The LCQ (Liquid Chromatography Quadrupole Ion Trap) mass spectrometer in our lab has been modified with a cross inlet bearing two needle valves in the buffer gas line, in order to introduce the neutral reference vapor into the ion trap. The analyte sample is dissolved in organic solvents such as methanol and acetonitrile to make a homogeneous solution with concentrations of 10^{-4} to 10^{-5} M. The solution is then injected into the system by a syringe pump and ionized by ESI. The charged analyte will then react with the neutral reference molecules in the ion trap, and the resultant ions after proton transfer could be collected and measured by the detector.

1.3.2 Cooks Kinetic Method

First developed by Cooks in 1977, the Cooks kinetic method is another technique to measure proton affinity and acidity of organic compounds using mass spectrometers.[63] Thermodynamic properties, such as PA and acidity, can be obtained from the collision-induced dissociation (CID) pattern of a proton-bound dimer (Figure 1.12).

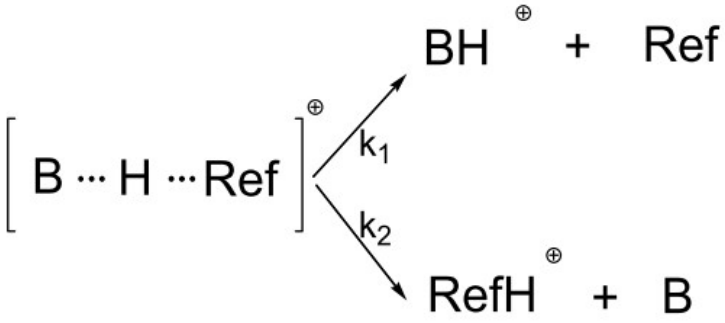

Figure 1. 12 CID-induced fragmentation pattern for a proton-bounded dimer of analyte and reference

For example, after isolating the proton-bound dimer between a sample base B and a reference base Ref (with known proton affinity), collision-induced dissociation (CID) energy is applied and the dimer can be dissociated in two different pathways: forming a protonated BH^+ and a neutral Ref, or yielding a protonated $RefH^+$ and a neutral B (Figure 1.11). The relative intensity of two product ion peaks can be used to calculate the proton affinity of B.[64-66]

1.3.3 Computational Method

Computational methods are used to study the thermodynamic properties and structural information of molecules described in this dissertation. All ground state calculations were performed using density functional theory (B3LYP/6-31+G(d), and B3LYP/6-311++G(d,p)) as implemented in Gaussian 09 and Gaussian 16.[67-72] All the geometries were fully optimized and frequencies were calculated; no scaling factor was applied. The optimized structures had no negative frequencies. The temperature for the calculations was set to be 298 K.

Both acidity and proton affinity (PA) can be calculated. The ΔH_{acid} is the enthalpy associated with the deprotonation of HA, and the ΔG_{acid} is the free energy associated with the deprotonation of HA; likewise, the ΔH_{PA} is the enthalpy associated with the deprotonation of BH^+, and the ΔG_{PA} is the free energy associated with the deprotonation of BH^+.

$$HA \rightarrow A^- + H^+ \qquad \Delta H_{rxn} = \Delta H_{acid};\ \Delta G_{rxn} = \Delta G_{acid}$$

$$BH^+ \rightarrow B + H^+ \qquad \Delta H_{rxn} = \Delta H_{PA};\ \Delta G_{rxn} = \Delta G_{PA}$$

For the transition state (TS) calculations, the SMD model was used and M06/6-31+G(d,p) solution-phase single-point energy calculations (on the B3LYP/6-31+G(d) geometry) were conducted. Reported energetics are the sum of the Gibbs free energy correction at B3LYP/6-31+G(d) applied to the solution-phase single-point energy at M06/6-31+G(d,p). For the solvation calculations, the SMD model was used with ionic liquid [DBUH][OTf] as the solvent. The solvent descriptors for [DBUH][OTf] were derived based on the "SMD-GIL" method developed by Cramer, Truhlar and coworkers.[73]

1.4 References

(1) Moon, J. H.; Yoon, S.; Bae, Y. J.; Kim, *M. S. Mass Spectrom. Rev.* **2015**, *34*, 94.
(2) Palii, S. P.; *John Wiley & Sons Ltd.,* **2014**, p 65.
(3) Nibbering, N. M. M. *Int. J. Mass Spectrom.* **2015**, *377*, 10.
(4) Chen, C.-C.; Lin, P.-C., *Anal. Methods*, **2015**, *7*, 6947.
(5) Richardson, D. E.; Plattner, D. A.; *Elsevier Ltd.*: **2007**; *Vol.* 1, p 801.
(6) IUPAC, *Compendium of Chemical Terminology,* 2nd ed. (the "Gold Book"), **1997**.
(7) Anslyn, E. V.; Dougherty, D. A. *Modern Physical Organic Chemistry* University Science Books, **2006**.
(8) Igau, A.; Grutzmacher, H.; Baceiredo, A.; Bertrand, G. *J. Am. Chem. Soc.* **1988**, *110*, 6463.
(9) Arduengo, A. J. I.; Harlow, R. L.; Kline, M. *J. Am. Chem. Soc.* **1991**, *113*, 361.
(10) Sharma, S.; Lee, J. K. *J. Org. Chem.* **2002**, *67*, 8360.
(11) Lee, J. K. *Int. J. Mass. Spectrom.* **2005**, 240.
(12) Kurinovich, M. A.; Lee, J. K. *J. Am. Soc. Mass. Spectrom.* **2002**, *13*, 985.
(13) NIST Chemistry WebBook, NIST Standard Reference Database Number 69; retrieved in 2011. Linstrom, P. J.; Mallard, W. G., Eds.; National Institute of Standards and Technology: Gaithersburg, MD 20899, http://webbook.nist.gov.
(14) Huisgen, R.; Szeimies, G.; Mobius, L. *Chem. Ber.* **1967**, *100*, 2494.
(15) Kolb, H. C.; Fin, M. G.; Sharpless, K. B. *Angew. Chem. Int. Ed.* **2001**, *40*, 2004.
(16) Kolb, H. C.; Sharpless, K. B. *Drug Discovery Today* **2003**, *8*, 1128.
(17) Bock, V. D.; Hiemstra, H.; van Maarseveen, J. H. *Eur. J. Org. Chem.* **2005**, *1*, 51.
(18) Whiting, M.; Muldoon, J.; Lin, Y.-C.; Silverman, S. M.; Lindstrom, W.; Olson, A. J.; Kolb, H. C.; Finn, M. G.; Sharpless, K. B.; Elder, J. H.; Fokin, V. V. *Angew. Chem. Int. Ed.* **2006**, *45*, 1435.
(19) Bock, V. D.; Speijer, D.; Hiemstra, H.; van Maarseveen, J. H. *Org. Biomol. Chem.* **2007**, *5*, 971.
(20) Ye, C.; Gard, G. L.; Winter, R. W.; Syvret, R. G.; Twamley, B.; Shreeve*, J. M. Org. Lett.* **2007**, *9*, 3841.
(21) Struble, J. R.; Kaeobamrung, J.; Bode, J. W. *Org. Lett.* **2008**, *10*, 957.
(22) Welton, T. *Chem. Rev.* **1999**, *99*, 2071.
(23) Formentin, P.; Garcia, H.; Leyva, A. *J. Mol. Catal. A: Chemical* **2004**, *214*, 137.
(24) Wasserscheid, P.; Keim, W. *Angew. Chem. Int. Ed. Engl.* **2000**, *39*, 3772.
(25) Dupont, J.; Spencer, *J. Angew. Chem. Int. Ed. Engl.* **2004**, *43*, 5296.
(26) Debray, J.; Leveque, J.-M.; Philouze, C.; Draye, M.; Demeunynck, M. *J. Org. Chem.* **2010**, *75*, 2092.
(27) Scholl, M.; Ding, S.; Lee, C. W.; Grubbs, R. H, *Org. Lett.* **1999**, *1*, 953.
(28) Enders, D.; Niemeier, O.; Balensiefer, T., *Angew. Chem. Int. Ed.* **2006**, *45*, 1463.
(29) Seebach, D., *Angew. Chem. Int. Ed. Engl.* **1979**, *18*, 239.
(30) Gröbel, B. T.; Seebach, D., *Synthesis* **1977**, *5*, 357.
(31) Seebach, D. *Angew. Chem. Int. Ed.* **1979**, *18*, 239.
(32) Chu, S., Carbon capture and sequestration. *Science* **2009,** *325* (5948), 1599.
(33) Smit, B.; Reimer, J. A.; Oldenburg, C. M.; Bourg, I. C., *Introduction to Carbon Capture and Sequestration*. World Scientific: 2014.

(34) Herzog, H. J., What future for carbon capture and sequestration? *Environmental Science & Techonolgy* **2001,** *35* (7), 148A-153A.
(35) Zeng, S.; Zhang, X.; Bai, L.; Zhang, X.; Wang, H.; Wang, J.; Bao, D.; Li, M.; Liu, X.; Zhang, S., Ionic-liquid-based CO2 capture systems: structure, interaction and process. *Chemical reviews* **2017,** *117* (14), 9625-9673.
(36) Yu, C.-H.; Huang, C.-H.; Tan, C.-S., A review of CO2 capture by absorption and adsorption. *Aerosol and Air Quality Research* **2012,** *12* (5), 745-769.
(37) Gutowski, K. E.; Maginn, E. J., Amine-functionalized task-specific ionic liquids: a mechanistic explanation for the dramatic increase in viscosity upon complexation with CO2 from molecular simulation. *Journal of the American Chemical Society* **2008,** *130* (44), 14690-14704.
(38) Cui, G.; Wang, J.; Zhang, S. Active Chemisoprtion Sites in Functionalized Ionic Liquids for Carbon Capture. *Chemical Society Reviews* **2016**, *45*, 4307-4339.
(39) Wang, C.; Luo, X.; Luo, H.; Jiang, D.-e.; Li, H.; Dai, S. Tuning the Basicity of Ionic Liquids for Equimolar CO_2 Capture. *Angew. Chem. Int. Ed.* **2011**, *50*, 4918-4922.
(40) Lemal, D. M.; Lovald, R. A.; Kawano, K. I. *J. Am. Chem. Soc.* **1964**, *86*, 2518.
(41) Ukai, T.; Tanaka, S.; Dokawa, S. *J. Pharm. Soc. Jpn.* **1943**, *63*, 296.
(42) Lapworth, A. *J. Chem. Soc.* **1903**, *83*, 995.
(43) Breslow, R. *J. Am. Chem. Soc.* **1958**, *80*, 3719.
(44) Mizuhara, S.; Handler, P. *J. Am. Chem. Soc.* **1954**, *76*, 571.
(45) Stetter, H.; Raemsch, R. Y.; Kuhlmann, H. *Synthesis* **1976**, *11*, 733.
(46) Stetter, H.; Kuhlmann, H. *Organic Reactions* **1991**, *40*, 407.
(47) Fenn, J. B.; Mann, M.; Meng, C. K.; Wong, S. F.; Whitehouse, C. M. *Science.* 1989, 246, 64-71.
(48) Tian, Y.; Lee, J. K. *J. Org. Chem.* **2015**, *80*, 6831.
(49) Zeng, H.; Wang, K.; Tian, Y.; Niu, Y.; Greene, L.; Hu, Z.; Lee, J. K. *Int. J. Mass. Spec.* **2015**, *378*, 169.
(50) Takahashi, T.; Tanase, S.; Yamamoto, O.; Yamauchi, S. J. *J. Solid State Chem.* **1976**, *17*, 353.
(51) Cho, E.; Park, J.-S.; Sekhon, S.; Park, G.-G.; Yang, T.-H.; Lee, W.-Y.; Kim, C.-S.; Park, S.-B. J. *J. Electrochem. Soc.* **2009**, *156*, B197.
(52) Noda, A.; Susan, M. A. B. H.; Kudo, K.; Mitsushima, S.; Hayamizu, K.; Watanabe, M. J. T. *J. Phys. Chem. B.* **2003**, *107*, 4024.
(53) Miran, M. S.; Yasuda, T.; Susan, M. A. B. H.; Dokko, K.; Watanabe, M. J. *RSC Advances,* **2013**, *3*, 4141.
(54) Yamashita, M.; Fenn, J. B. *Phys. Chem.* **1988**, *88*, 4451.
(55) Yamashita, M.; Fenn, J. B. *Phys. Chem.* **1988**, *88*, 4671.
(56) Kebarle, P.; Tang, L. *Anal. Chem.* **1993**, *65*, 972A.
(57) Douglas, D. J.; Frank, A. J.; Mao, D. *Mass Spec. Rev.* **2005**, *24*, 1.
(58) Paul, W. *Angew. Chem.* **1990**, *102*, 780.
(59) Comisarow, M. B.; Marshall, A. G. *Chem. Phys. Lett.* **1974**, *25*, 282.
(60) Amster, I. J. *J. Mass Spectrom.* **1996**, *31*, 1325.
(61) Chesnavich, W. J.; Su, T.; Bowers, M. T. *J. Chem. Phys*. **1980**, *72*, 2641.
(62) Su, T.; Chesnavich, W. J. *J. Chem. Phys.* **1982**, *76*, 5183.
(63) Cooks, R. G.; Kruger, T. L. *J. Am. Chem. Soc.* **1977**, *99*, 1279.

(64) MuLuckey, S. A.; Cameron, D.; Cooks, R. G. *J. Am. Chem. Soc.* **1981**, *103*, 1313.
(65) Brodbelt-Lustig, J. S.; Cooks, R. G. *Talanta* **1989**, *36*, 255.
(66) Green-Church, K. B.; Limbach, P. A. *J. Am. Chem. Soc. Mass Spectrom.* **2000**, *11*, 24.
(67) *GAUSSIAN09*, R. A.; Frisch, M. J.; Trucks, G. W.; Schlegel, H. B.; Scuseria, G. E.; Robb, M. A.; Cheeseman, J. R.; Scalmani, G.; Barone, V.; Mennucci, B.; Petersson, G. A.; Nakatsuji, H.; Caricato, M.; Li, X.; Hratchian, H. P.; Izmaylov, A. F.; Bloino, J.; Zheng, G.; Sonnenberg, J. L.; Hada, M.; Ehara, M.; Toyota, K.; Fukuda, R.; Hasegawa, J.; Ishida, M.; Nakajima, T.; Honda, Y.; Kitao, O.; Nakai, H.; Vreven, T.; Montgomery, J., J. A.; Peralta, J. E.; Ogliaro, F.; Bearpark, M.; Heyd, J. J.; Brothers, E.; Kudin, K. N.; Staroverov, V. N.; Kobayashi, R.; Normand, J.; Raghavachari, K.; Rendell, A.; Burant, J. C.; Iyengar, S. S.; Tomasi, J.; Cossi, M.; Rega, N.; Millam, J. M.; Klene, M.; Knox, J. E.; Cross, J. B.; Bakken, V.; Adamo, C.; Jaramillo, J.; Gomperts, R.; Stratmann, R. E.; Yazyev, O.; Austin, A. J.; Cammi, R.; Pomelli, C.; Ochterski, J. W.; Martin, R. L.; Morokuma, K.; Zakrzewski, V. G.; Voth, G. A.; Salvador, P.; Dannenberg, J. J.; Dapprich, S.; Daniels, A. D.; Farkas, Ö.; Foresman, J. B.; Ortiz, J. V.; Cioslowski, J.; Fox, D. J., Gaussian, Inc., Wallingford CT, 2009.
(68) Lee, C.; Yang, W.; Parr, R. G. *Phys. Rev. B* **1988**, *37*, 785.
(69) Kohn, W.; Becke, A. D.; Parr, R. G. *J. Phys. Chem.* **1996**, *100*, 12974.
(70) Becke, A. D. *J. Chem. Phys.* **1993**, *98*, 5648.
(71) Becke, A. D. *J. Chem. Phys.* **1993**, *98*, 1372.
(72) Stephens, P. J.; Devlin, F. J.; Chabalowski, C. F.; Frisch, M. J. *J. Phys. Chem.* **1994**, *98*, 11623.
(73) Bernales, V. S.; Marenich, A. V.; Contreras, R. H.; Cramer, C. J.; Truhlar, D. G. Quantum Mechanical Continuum Solvation Models for Ionic Liquids. *J. Phys. Chem. B* **2012**, *116*, 9122-9129.

Note: Major parts of this chapter have been submitted to Journal of the American Chemical Society: *Niu, Y.; *Wang, N.; Munoz, A.; Xu, J.; Zeng, H.; Rovis, T.; Lee, J. K. "Experimental and Computational Gas Phase Acidities of Conjugate Acids of Triazolylidene Carbenes: Rationalizing Subtle Electronic Effects", *J. Am. Chem. Soc.* **2017**, 139, 42, 14917-14930.

Chapter 2. Proton Affinity of Triazolylidene Carbenes: Rationalizing Subtle Electronic Effects

2.1 Introduction

Since the discovery of stable carbenes, first reported independently by Bertrand and Arduengo, these species have become key players in organic and organometallic chemistry.[1,2] *N*-Heterocyclic carbenes (NHCs), particularly imidazolylidenes, have come to the forefront as effective ligands for transition-metal catalysts, with perhaps the best-known example being the Grubbs second-generation ruthenium catalysts for olefin metathesis.[3] In addition to their role as key ligands for organometallic catalysts, NHCs themselves can also function as organocatalysts, and in recent years, triazolylidene carbenes have emerged as the most prominent structure.[4,5] Work in this field has encompassed both *Umpolung* and non-*Umpolung* reactions, with an eye to stereoselectivity.[4-6]

For reactions catalyzed by triazolylidene carbenes, the carbene is often generated *in situ* by deprotonation of the corresponding triazolium precatalyst. The resultant carbene behaves as a nucleophile; for most reactions catalyzed by NHCs, the first step in the catalytic cycle is NHC attack of an electrophile. An example of an NHC-catalyzed reaction from our lab, the intramolecular Stetter reaction, is shown in Figure 2.1. Because of the requisite deprotonation of the precatalyst and the nucleophilic nature of the carbene, the

acidity of the triazolium precatalyst (which is equivalent to the basicity of the free carbene) and the nucleophilicity of the triazolylidene carbene catalyst are of great interest.

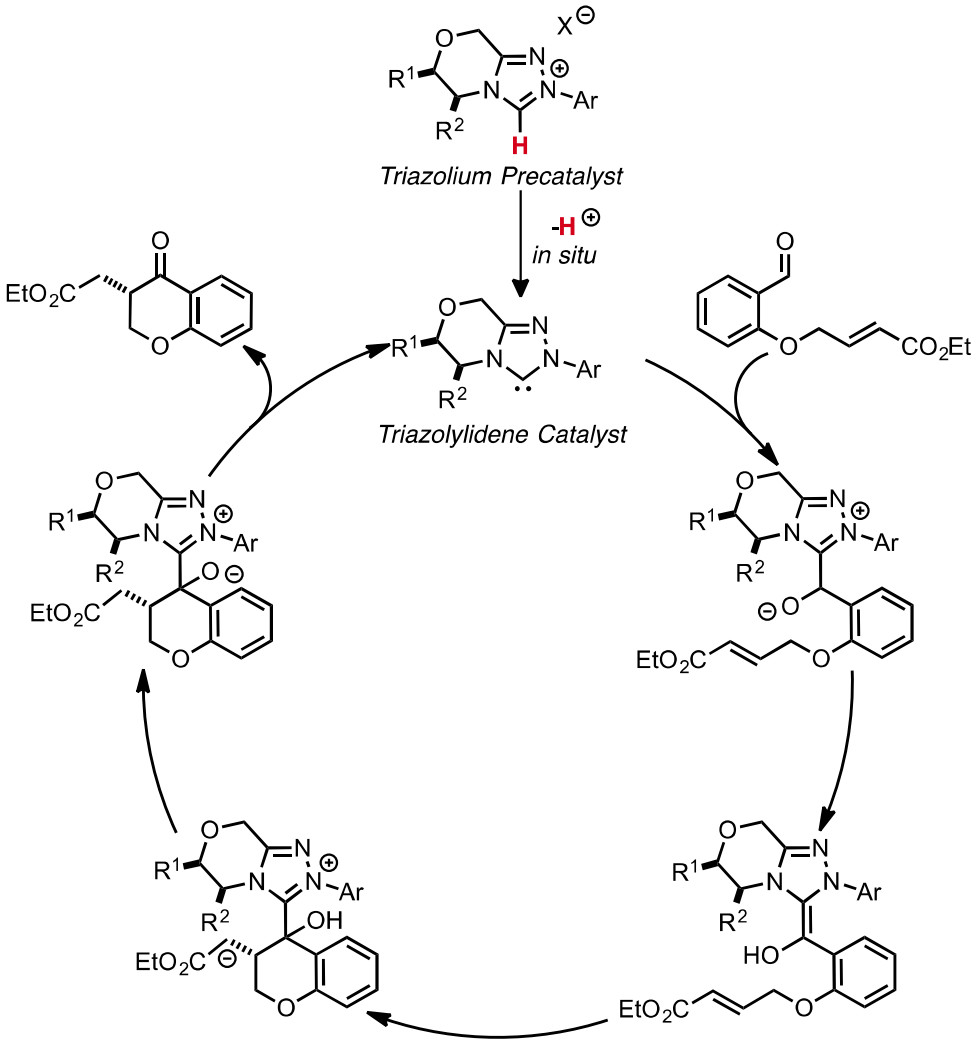

Figure 2. 1 Intramolecular Stetter reaction cycle as catalyzed by a triazolylidene NHC

Despite great progress in the development and optimization of triazolylidene carbenes as catalysts for enantioselective reactions, fundamental studies of these species are relatively limited. With respect to the evaluation of the acidity of these triazoliums, Smith, O'Donoghue and coworkers conducted a seminal study that yielded the acidity of twenty triazolium salts in aqueous solution.[7,8] Mayr and coworkers examined a series of NHCs to

evaluate nucleophilicity and Lewis basicity. [9] They found that triazolylidene **2c** is less nucleophilic than imidazolylidene **2a** and imidazolinylidene **2b**; all three had moderate nucleophilicity relative to a high Lewis basicity (Figure 2.2).

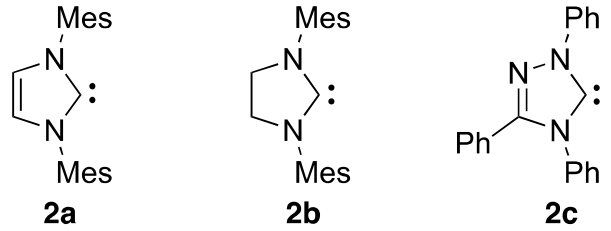

Figure 2. 2 NHCs studied by Mayr Group

In this chapter, we describe our studies of two series of triazolium cations that, upon deprotonation, deliver catalysts that are active in a variety of transformations. [4] We use experiment and theory to characterize the intrinsic basicity of triazolylidenes by measuring and computing the acidity of the corresponding triazolium cations in the gas phase, for a wide range of achiral and chiral species not heretofore examined *in vacuo*.

2.2 Experimental

The synthesis of the protonated carbenes studied herein have been previously described.[4] The reference bases were purchased from Sigma-Aldrich and used as received.

Bracketing experiments were conducted using a house-modified quadrupole ion trap mass spectrometer as previously described (1.3.3).[10] To generate the protonated carbene ions via electrospray ionization (ESI), the triazolium cations were dissolved in 1:10 water/methanol. About 2 μL formic acid was added into every 10ml water/methanol solution to facilitate ionization. Final concentrations of these solutions were ~10^{-4} M.

The flow rates of ESI injection were 15-25 μL/min. The capillary temperature was 190°C. Neutral reference bases were added with helium gas flow. The protonated carbene ions were allowed to react with neutral reference bases for 0.03-10000 ms. A total of 10 scans were averaged. The typical electrospray needle voltage was ~1.80 kV.

All calculations were performed using density functional theory (B3LYP/6-31+G(d)) as implemented in Gaussian 09.[11-16] All the geometries were fully optimized and frequencies were calculated; no scaling factor was applied. The optimized structures had no negative frequencies. The temperature for the calculations was set to be 298 K. For the enol TS calculations, the SMD model was used with ethanol as the solvent. M06/6-31+G(d,p) solution-phase single-point energy calculations (on the B3LYP/6-31+G(d) geometry) were conducted.[17-21] Reported energetics are the sum of the Gibbs free energy correction at B3LYP/6-31+G(d) applied to the solution-phase single-point energy at M06/6-31+G(d,p).

2.3 Results and Discussion

2.3.1 Achiral pyrrolidine-based triazoliums

i. Calculations: Achiral pyrrolidine-based triazolium cations

We first studied a series of achiral pyrrolidine-based triazolium cations as shown in Figure 2.3. These compounds were chosen to assess the electronic effect of the various substituted phenyl moieties; also, the aqueous pK_a has been measured for some of these, which would allow us to compare gas and solution phase values. The calculated acidities of the triazolium cations, which correspond to the proton affinity of their respective triazolylidene carbenes, are listed in Figure 2.3 and Figure 2.4. In our experience, density functional theory (DFT) methods generally yield accurate values for thermochemical properties of heterocyclic rings, so we utilized B3LYP/6-31+G(d) to calculate the acidities (ΔH_{acid}).[22-27]

The overall trend in terms of acidity for these substrates is as follows (from most acidic to least acidic; note that as with pK_a values, more acidic species have lower ΔH_{acid} values): **3c** > **3b** = **3e** > **3g** > **3f** > **3i** > **3h** > **3a** > **3l** > **3d** > **3j** > **3k.** Overall, this trend makes sense: **3c** is most acidic, with a 3,5-di-CF_3 substitution on the phenyl, followed by perfluorophenyl and 4-cyanophenyl. Ultimately the least acidic is **3k**, with a largely electron donating N-aryl group substituent.

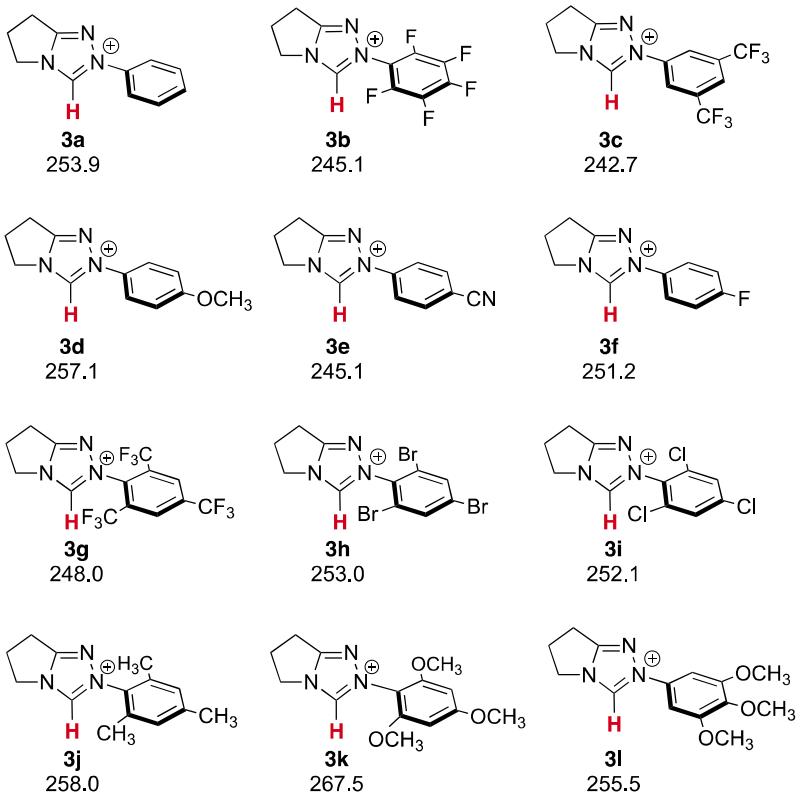

Figure 2. 3 Calculated acidities for a series of pyrrolidine-based achiral triazolium cations (kcal/mol). Calculations were conducted at B3LYP/6-31+G(d); reported values are ΔH at 298 K

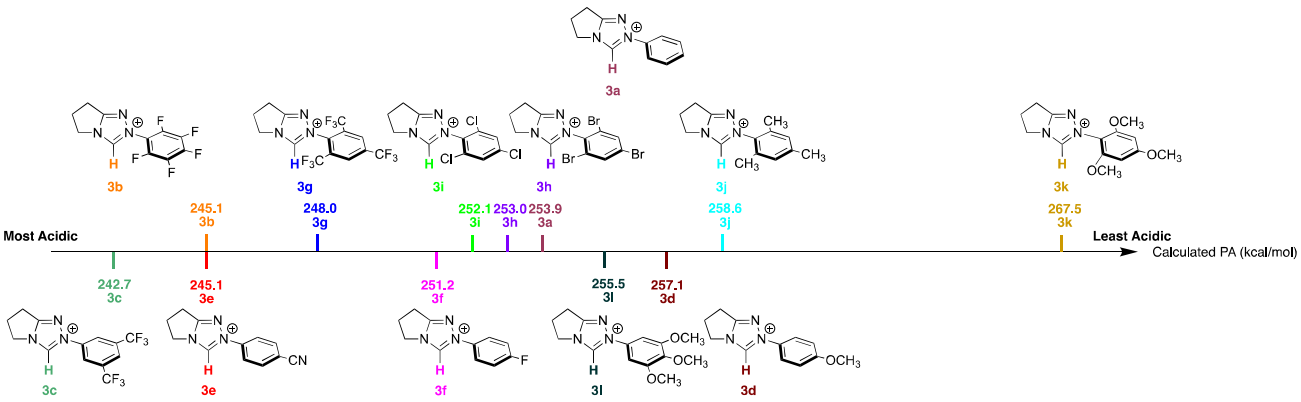

Figure 2. 4 Calculated acidities for a series of pyrrolidine-based achiral triazolium cations (kcal/mol), arranged in the order of acidity

There is one surprise in this trend, however, which is the higher acidity of **3c** (242.7 kcal/mol) versus **3g** (248.0 kcal/mol). **3c** has a phenyl ring with 3,5-di-CF_3 substitution while **3g** has a phenyl ring with an additional trifluoromethyl group, as well as diortho substitution (2,4,6-tri-CF_3). One might initially expect **3g** to be more acidic than **3c**, due to the additional electron withdrawing trifluoromethyl group. However, we suspected that the additional trifluoromethyl group (as well as the diortho substitution pattern) alters the phenyl ring geometry unfavorably, which calculations confirmed (Figure 2.5). For **3c**, the phenyl ring is relatively planar relative to the triazolium ring; the dihedral angle for the calculated structure (for the atoms labeled 1-2-3-4) is 34.7˚. For **3g**, however, the relatively bulky trifluoromethyl groups, placed at the ortho positions of the phenyl ring, cause the ring to become nearly perpendicular to the triazolium ring (dihedral 90.4˚). A perpendicular disposition of the aryl ring leads to reduced orbital overlap with the azolium and a minimization of its impact on the electronic character of the carbene center. Therefore, although the additional trifluoromethyl would be expected to increase the acidity, the lack of planarity of the phenyl ring relative to the triazolium core mitigates the effect of the third

CF_3. This is reminiscent of the surprisingly similar acidities of diphenylmethane and triphenylmethane; the third phenyl ring is less effective than might be expected due to the inability of all three phenyl rings to be in the same plane.

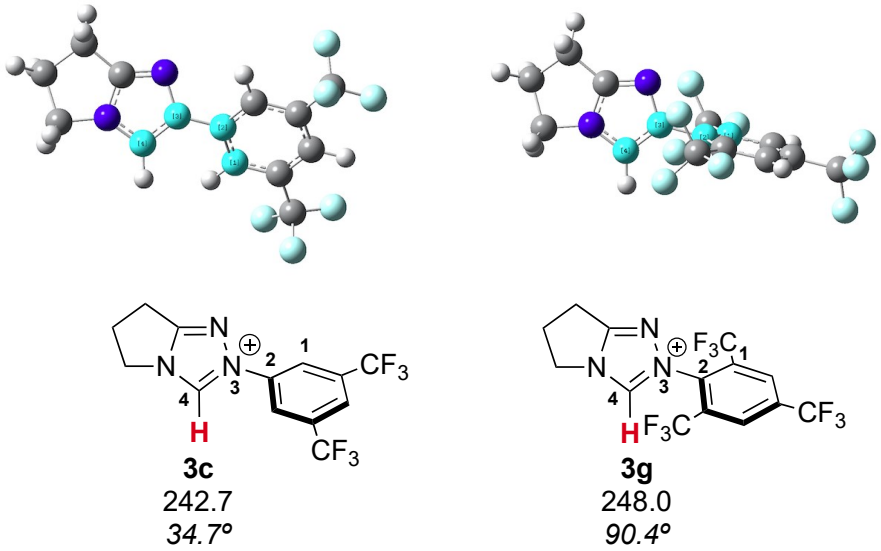

Figure 2. 5 Calculated (B3LYP/6-31+G(d)) geometries of the **3c** and **3g** achiral triazolium cations

To avoid this type of complication when looking at trends, a more reasonable comparison is to focus on structures that have the same substitution pattern. For example, among the 2,4,6-substituted phenyl compounds, the order from most to least acidic is: **3g** (2,4,6-tri-CF_3) > **3i** (2,4,6-tri-Cl) > **3h** (2,4,6-tri-Br) > **3j** (2,4,6-tri-CH_3(mesityl)) > **3k** (2,4,6-tri-OCH_3). In terms of electron withdrawing capability, this trend is reasonable: the most acidic is the compound with the 2,4,6-tri-CF_3-phenyl moiety and the least acidic has a 2,4,6-tri-OCH_3-phenyl group. For the 4-substituted phenyls, the acidity order is (from most to least acidic): **3e** (4-CN) > **3f** (4-F) > **3d** (4-OMe), which also makes sense.

ii. Experiments: Achiral pyrrolidine-based triazolium cations

To experimentally measure the gas phase acidity of the achiral triazolium cations, we utilized mass spectrometry and proton transfer reactions between the protonated carbene precursors and various bases in the gas phase whose proton affinities are known. Electrospray ionization of the protonated carbene successfully yields the triazolium cation as the major signal. Reference bases are then added and the presence or absence of proton transfer is assessed.

DBU (PA = 250.5 kcal/mol) is unable to deprotonate **3a**, but MTBD (PA = 254.0 kcal/mol) can. We therefore bracket the acidity of **3a** to be between DBU and MTBD (252 ± 4 kcal/mol). For **3b**, as well as **3e**, *N,N,N′,N′*-tetramethyl-1,3-propanediamine (PA = 247.4 kcal/mol) is unable to effect deprotonation, but DBN (PA = 248.2 kcal/mol) can, placing the acidity of **3b** and **3e** at 248 ± 3 kcal/mol. 1-(Cyclopent-1-en-1yl)pyrrolidine (PA = 243.6 kcal/mol) cannot deprotonate **3c**, but *N,N,N′,N′*-tetramethyl-1,3-propanediamine (PA = 247.4 kcal/mol) can; we therefore bracket the acidity of **3c** to be 246 ± 4 kcal/mol. For **3d**, no reaction is observed with MTBD (PA = 254.0 kcal/mol), but proton transfer occurs with HP_1(dma) (PA = 257.4 kcal/mol), placing the acidity of **3d** at 256 ± 4 kcal/mol. For **3f**, **3h** and **3i**, no proton transfer is observed with DBU (PA = 250.5 kcal/mol) but MTBD (PA = 254.0 kcal/mol) deprotonates all three, allowing us to bracket the acidity of **3f**, **3h** and **3i** to be the same, 252 ± 4 kcal/mol. **3j** is least acidic; HP_1(dma) (PA = 257.4) cannot deprotonate it, but $tbuP_1$(dma) (PA = 260.6) can, bracketing the acidity of **3j** to 259 ± 4 kcal/mol. MTBD (PA = 254.0 kcal/mol) does not deprotonate **3l**, but HP_1(dma) (PA = 257.4 kcal/mol) does, placing the acidity of **3l** at 256 ± 4 kcal/mol.

The overall trend for the experimental acidity values tracks reasonably well with calculation (from most acidic to least acidic): **3c** > **3b** = **3e** > **3a** = **3f** = **3h** = **3i** > **3d** = **3l** >

3j (Table 2.1). Reference bases are limited in this region, which is at the high basicity range for compounds in the gas phase. Therefore, although calculations indicate that **3a**, **3f**, **3h**, and **3i** have different acidities (ranging from about 251-254 kcal/mol), all four substrates have a measured acidity of 252 ± 4 kcal/mol. There are simply not enough reference bases to differentiate within this region. However, the calculations and experiments are in agreement, within the experimental uncertainty.

Table 2. 1 Summary of results for gas phase acidity bracketing of achiral pyrrolidine-based triazoliums

Reference base[a,b]	*PA (kcal/mol)*[c]	*Proton transfer to reference base*[d]									
		3c	**3b**	**3e**	**3f**	**3i**	**3h**	**3a**	**3l**	**3d**	**3j**
N,N,N',N'-tetramethylethylenediamine	242.1	–									
1-(cyclopent-1-en-1yl)pyrrolidine	243.6	–	–	–		–					
N,N,N',N'-tetramethyl-1,3-propanediamine	247.4	+	–	–		–	–	–			
DBN	248.2	+	+	+	–	–	–	–			
DBU	250.5	+	+	+	–	–	–	–	–	–	
MTBD	254.0				+	+	+	+	–	–	–
HP_1(dma)	257.4				+	+	+	+	+	+	–
$tBuP_1$(dma)	260.6								+	+	+
$tOctP_1$(dma)	262.0										+

[a] Reference[28] ; [b]DBN = 1,5-Diazabicyclo[4.3.0]non-5-ene; DBU = 1,8-diazabicyclo[5.4.0]undec-7-ene; MTBD = 7-Methyl-1,5,7-triazabicyclo[4.4.0]dec-5-ene; HP_1(dma) = Imino-tris(dimethylamino)phosphorane; *t*BuP_1(dma) = *tert*-Butylimino-tris(dimethylamino)phosphorane; *t*$OctP_1$(dma) = *tert*-Octylimino-tris(dimethylamino)phosphorane; BEMP = 2-*tert*-Butylimino-2-diethylamino-1,3-dimethylperhydro-1,3,2-diazaphosphorine. [c] Reference base PAs typically have an error of ±2 kcal/mol. [d] The "+" symbol indicates the occurrence and the "–" symbol indicates the absence of proton transfer.

The aqueous pK_a values for some of these achiral triazoliums have been determined.[7] In Table 2.2, we list our calculated and experimental gas phase acidity values as well as known pK_a values. The data in Table 2.2 is arranged in order of decreasing calculated gas phase acidity. The aqueous acidity trend more or less reflects the gas phase trend, meaning, as one moves down the table, the acidity generally decreases for both the gas phase and solution. There are two exceptions: the first is for **3b** (-F_5 substituted phenyl) versus **3e** (4-CN). The gas phase calculations predict the same gas phase acidity but in water **3e** is less acidic than **3b** by 0.4 pK_a units. The second exception is for **3d** (4-OMe) versus **3j** (1,3,5-trimethyl (Mes)). Calculations predict that **3d** is more acidic than **3j**, by 1.5 kcal/mol. In water, **3d** is less acidic than **3j** by 0.1 pK_a units.

Table 2. 2 Calculated (B3LYP/6-31+G(d); 298 K) and experimental data for achiral triazolium cations.[a]

Substrate	Calculated ΔH_{acid}	Experimental ΔH_{acid} [b]	pK_a [c]
3c	242.7	246	
3b	245.1	248	16.5
3e	245.1	248	16.9
3g	248.0		
3f	251.2	252	17.4
3i	252.1	252	
3h	253.0	252	
3a	253.9	252	17.5
3l	255.5	256	
3d	257.1	256	17.8
3j	258.6	259	17.7
3k	267.5		

[a] ΔH_{acid} values are in kcal/mol; [b] Error is ±3-4 kcal/mol; [c] Reference[7]

It is well known that acidity trends will sometimes differ in the gas versus solution phases; the classic case is that *tert*-butanol is more acidic than methanol in the gas phase, while the opposite is true in water.[29] In the gas phase, the polarizable methyl groups in *tert*-butoxide stabilize the anion; this is less keenly felt in solution, and also, water molecules may more poorly solvate the bulkier *tert*-butyl group. For our substrates, the gas phase results indicate that perfluoro and 4-CN phenyl moieties in **3b** and **3e**, respectively, have similar intrinsic anion stabilizing ability. In solution, however, the polarizability of the cyano group may have less of an influence, causing **3e** to be slightly less acidic than **3b**.

The other feature that is true for relative gas phase versus solution phase acidities is that the range is generally wider in the gas phase than solution. Thus, in Table 2.2, the range of gas phase acidities for those cations for which we have solution phase data is 13.5 kcal/mol (245.1 kcal/mol for **3b** to 258.6 kcal/mol for **3j**). The pK_a range is 16.5 to 17.7, which is 1.2 pK_a units, or roughly 1.6 kcal/mol at room temperature. This tighter range for the solution phase acidities makes it less surprising that **3d** and **3j**, which only differ by 1.5 kcal/mol in the gas phase, have a mere 0.1 pK_a unit difference in solution (0.14 kcal/mol).

The wider range of acidity for the catalysts in the gas phase also implies that differences in reactivity of catalysts will be more pronounced in nonpolar environments. Thus, for example, using a less polar solvent will allow for nuances among catalyst reactivity to stand out. Also, less solvent interference can increase catalyst efficacy; recent work by Kimura and coworkers using NHCs in solvent-free benzoin and Stetter reactions indicated efficient reactions with low catalyst loading.[30]

2.3.2 Chiral aminoindanol-based triazoliums

i. Calculations: Chiral triazolium cations

We also studied a series of chiral aminoindanol-based triazoliums that over the years have been used as precatalysts for a wide range of reactions.[4-6] The calculated acidities of the triazolium cations are shown in Figure 2.6 and Figure 2.7. The overall trend from most to least acidic, in the gas phase, is: **4f** > **4d** > **4j** = **4c** > **4g** > **4i** = **4h** ≥ **4l** > **4k** = **4a** > **4m** > **4b** > **4e**. As with the achiral triazoliums, the overall trend in acidity seems reasonable, with the most acidic species being the 3,5-bis(trifluoromethylphenyl) and the least being the mesityl-substituted catalyst. One perhaps surprising ordering is **4a** versus **4m**; the aminoindanol triazolium with an unsubstituted phenyl is more acidic than that with a 2,6-

dibromo substituted phenyl. As with the achiral series, however, we find that the dihedral angle for **4a** indicates a nearly flat phenyl ring (36.6˚) whereas for **4m**, the dibromophenyl substituent is perpendicular (95.0˚) to the triazolium ring. Presumably that perpendicularity will mean less of an electronic influence on the carbene center basicity (triazolium acidity) (Figure 2.8).

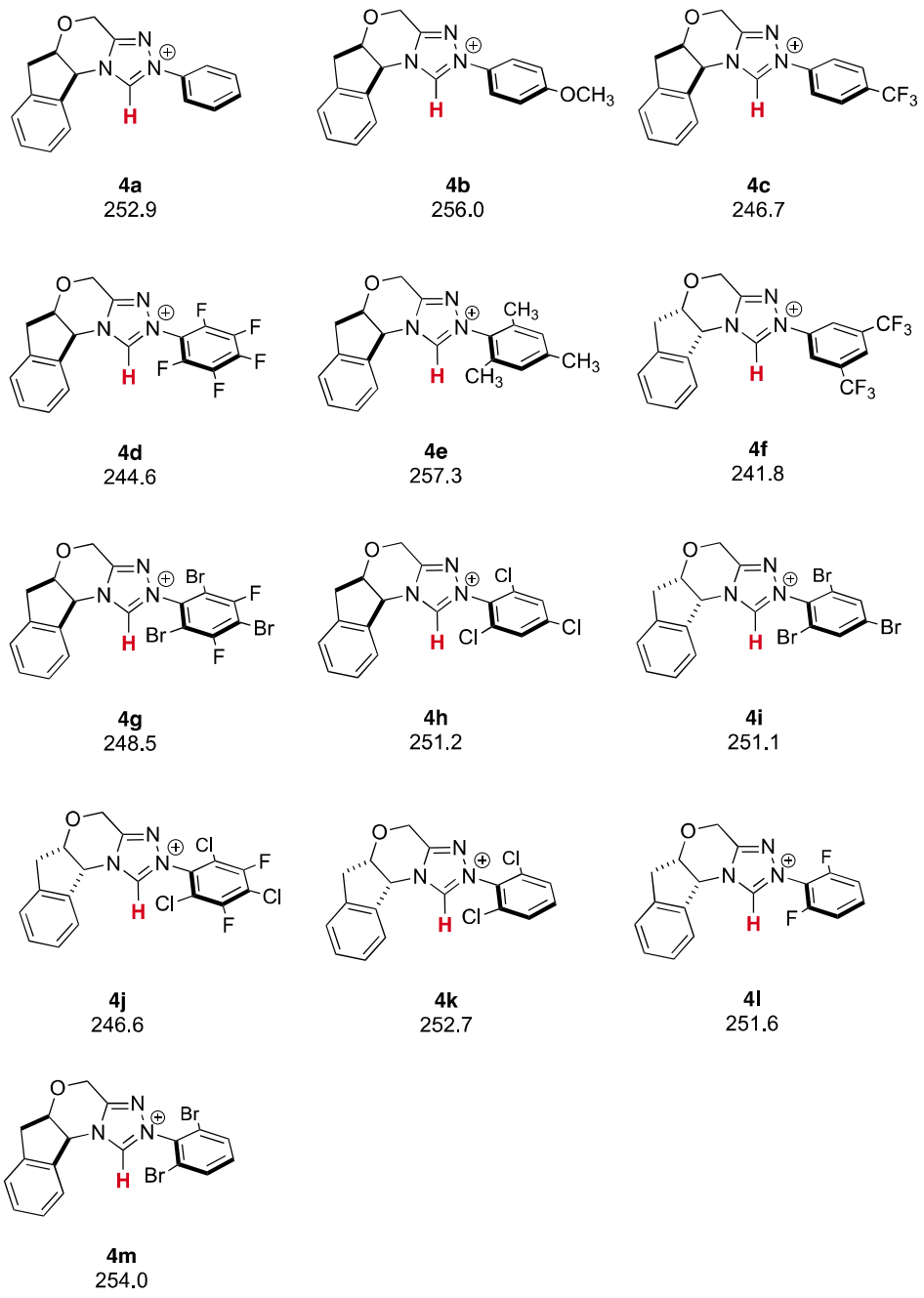

Figure 2. 6 Calculated acidities for a series of aminoindanol-based chiral triazolium cations, in kcal/mol. Calculations were conducted at B3LYP/6-31+G(d); reported values are ΔH at 298 K

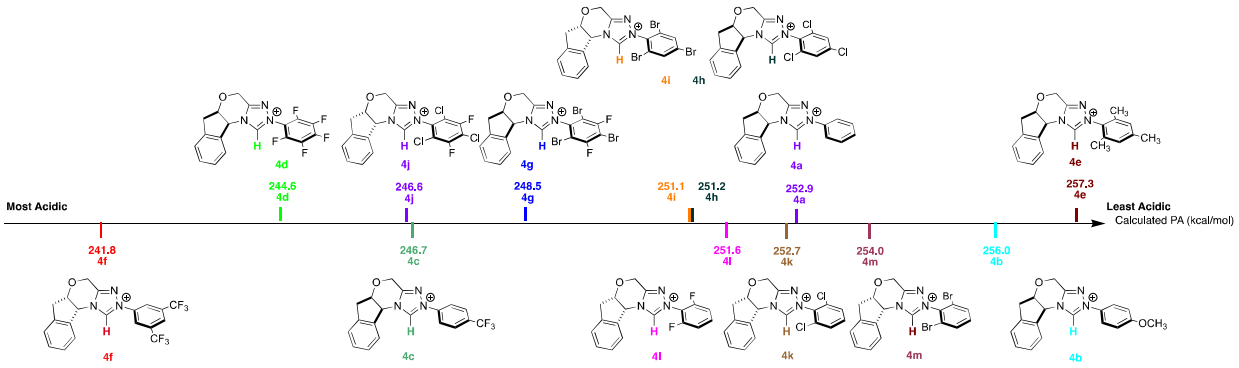

Figure 2. 7 Calculated acidities for a series of aminoindanol-based chiral triazolium cations (kcal/mol), arranged in the order of acidity

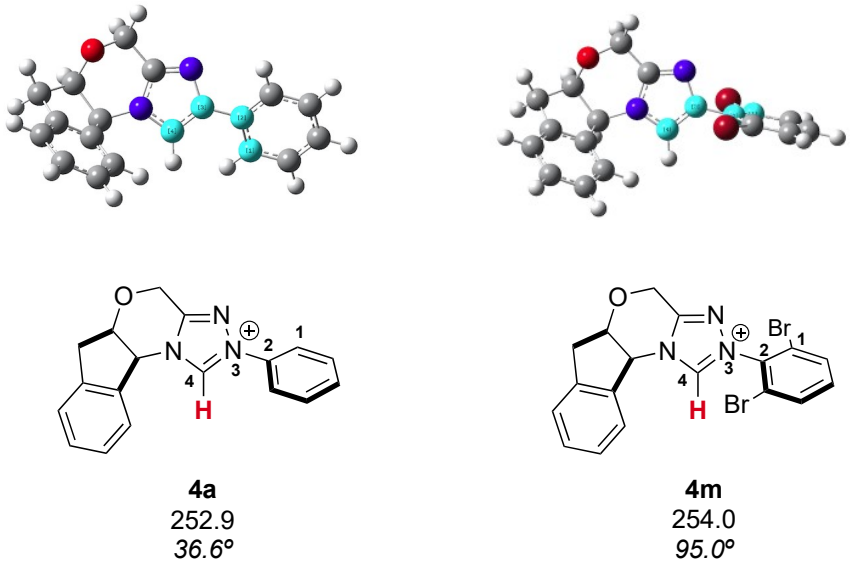

Figure 2. 8 Calculated (B3LYP/6-31+G(d)) geometries of the **4a** and **4m** chiral triazolium cations.

A comparison between achiral and chiral triazoliums and phenyl substitution also shows consistency in terms of the influence of the phenyl ring substitution on the triazolium carbene center acidity. Both series have a 3,5-bis(trifluoromethylphenyl) substituent that renders the triazolium to be the most acidic of their respective groups (**3c** and **3f**). This is followed by the perfluorophenyl substituted triazoliums and the 1,3,5-trihalophenyl

substituted species, for both the **3** and **4** series. The acidity trend then continues for both series with an unsubstituted phenyl followed by 4-OMe then mesityl.

ii. Experiments: Chiral triazolium cations

The experimental bracketing for the **4** series are shown in Tables 3.3. DBU (PA = 250.5 kcal/mol) cannot deprotonate **4a** but MTBD (PA = 254.0 kcal/mol) can, placing the acidity of **4a** at 252 ± 4 kcal/mol. Triazoliums **4k** and **4m** bracket to the same acidity. For **4b**, MTBD (PA = 254.0 kcal/mol) cannot deprotonate the triazolium but HP_1(dma) (PA = 257.4 kcal/mol) can, which allows us to bracket the acidity of **4b** to be 256 ± 4 kcal/mol. We find that *N,N,N′,N′*-tetramethyl-1,3-propanediamine (PA = 247.4 kcal/mol) is unable to effect deprotonation of **4c**, but DBN (PA = 248.2 kcal/mol) can, placing the acidity of at 248 ± 3 kcal/mol. Triazoliums **4d** and **4j** bracket to 248 kcal/mol as well. For **6e**, HP_1(dma) (PA = 257 kcal/mol) cannot effect deprotonation but $tBuP_1$(dma) (PA = 260.6 kcal/mol) does, placing the acidity of **4e** at 259 ± 4 kcal/mol. 1-(Cyclopent-1-en-1yl)pyrrolidine (PA = 243.6 kcal/mol) cannot deprotonate **4f** but N,N,N',N'-tetramethyl-1,3-propanediamine (PA = 247.4 kcal/mol) can, which gives an acidity of 246 ± 4 kcal/mol. Last, DBN (PA = 248.2 kcal/mol) cannot deprotonate **4g**, but DBU (PA = 250.5 kcal/mol) can. We thus bracket **4g** to be 249 ± 3 kcal/mol; substrates **4h**, **4i**, and **4l** have the same acidity.

Table 2. 3 Summary of results for acidity bracketing of chiral aminoindanol-based triazolium **4a-4m**

Reference base[a,b]	*PA (kcal/mol)*[c]	*Proton transfer to reference base*[d]												
		4f	**4d**	**4j**	**4c**	**4g**	**4i**	**4h**	**4l**	**4k**	**4a**	**4m**	**4b**	**4e**
TMEDA	242.1	–	–											
1-CP	243.6	–	–	–	–	–		–				–	–	
TMPDA	247.4	+	–	–	–	–	–	–	–			–	–	
DBN	248.2	+	+	+	+	–	–	–	–	–	–	–	–	
DBU	250.5	+	+	+	+	+	+	+	+	–	–	–	–	–
MTBD	254.0		+	+	+	+	+	+	+	+	+	+	–	–
HP_1(dma)	257.4			+		+	+		+	+	+	+	+	–
$tBuP_1$(dma)	260.6										+		+	+
$tOctP_1$(dma)	262.0										+			+
BEMP	263.8										+			+

[a]Reference[28]; [b] TMEDA = *N,N,N′,N′*-tetramethylethylenediamine; 1-CP = 1-(cyclopent-1-en-1yl)pyrrolidine ; TMPDA = *N,N,N′,N′*-tetramethyl-1,3-propanediamine; DBN = 1,5-Diazabicyclo[4.3.0]non-5-ene; DBU = 1,8-diazabicyclo[5.4.0]undec-7-ene; MTBD = 7-Methyl-1,5,7-triazabicyclo[4.4.0]dec-5-ene; HP_1(dma) = Imino-tris(dimethylamino)phosphorane; $tBuP_1$(dma) = *tert*-Butylimino-tris(dimethylamino)phosphorane; $tOctP_1$(dma) = *tert*-Octylimino-tris(dimethylamino)phosphorane; BEMP = 2-*tert*-Butylimino-2-diethylamino-1,3-dimethylperhydro-1,3,2-diazaphosphorine. [c]Reference base PAs typically have an error of ±2 kcal/mol. [d]The "+" symbol indicates the occurrence and the "–" symbol indicates the absence of proton transfer.

The computed and experimental gas phase acidity values for the chiral triazoliums are compiled in Table 2.4; the catalysts are listed in order of decreasing calculated gas phase acidity. The experiment gas phase acidities roughly track with the calculated values. Given the small number of available reference bases in this superbasic range, it is not surprising that some of the experimental values are not exactly the same as the calculated values, though all are within error. Taken together, the achiral and chiral experimental data benchmark B3LYP/6-31+G(d) as a reasonable method and level to calculate the triazolium acidities.

Table 2. 4 Calculated (B3LYP/6-31+G(d); 298 K) and experimental data for chiral triazolium cations.[a]

Substrate	Calculated ΔH_{acid}	Experimental ΔH_{acid} [b]
4f	241.8	246
4d	244.6	248
4j	246.6	248
4c	246.7	248
4g	248.5	249
4i	251.1	249
4h	251.2	249
4l	251.6	249
4k	252.7	252
4a	252.9	252
4m	254.0	252
4b	256.0	256
4e	257.3	259

[a] ΔH_{acid} values are in kcal/mol; [b] Error is ±3-4 kcal/mol.

2.3.3 Acidity and diastereoselectivity

To further explore the relationship between the acidity of triazolylidenes **3** and reactivity, we explored the NHC-catalyzed homoenolate addition of cinnamaldehyde to nitroalkenes, shown in Figure 2.9.[31-33]

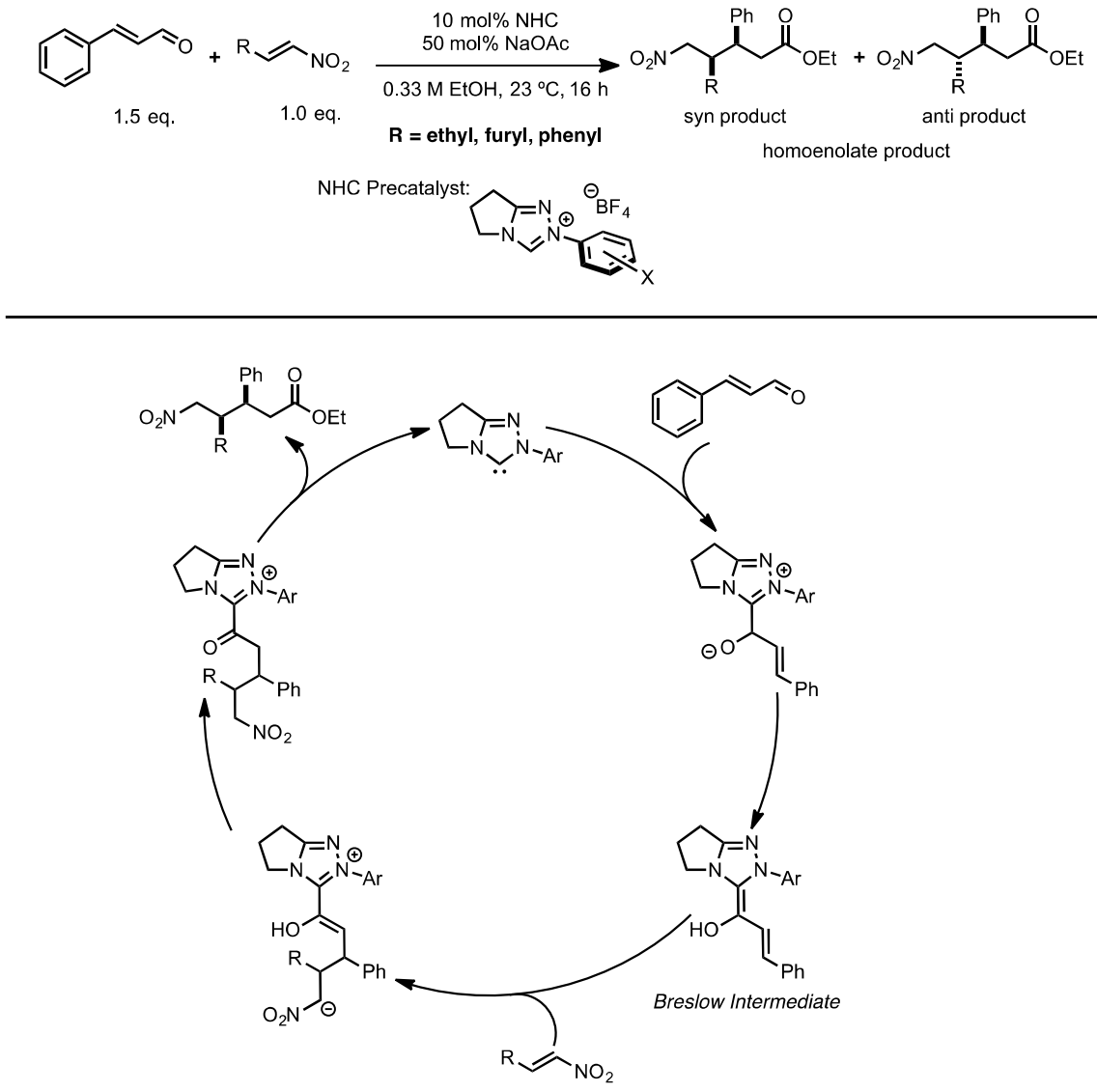

Figure 2. 9 NHC-catalyzed homoenolate addition of enals to nitroalkenes, with proposed catalytic mechanism

This reaction has two potential products, *anti* and *syn* (one enantiomer of each is shown in Figure 2.9, but this racemic reaction yields both enantiomers for *anti* and for *syn*). An examination of the *anti* versus *syn* preference reveals a correlation to gas phase acidity. Figure 2.10 shows a plot of the natural log of the ratio of the *anti* to *syn* products versus the calculated acidity, for the reaction with (E)-1-nitrobut-1-ene. A correlation is observable, wherein a more acidic triazolium precatalyst corresponds to more *syn* product, and conversely, decreasing acidity correlates to increasing *anti* selectivity.[34]

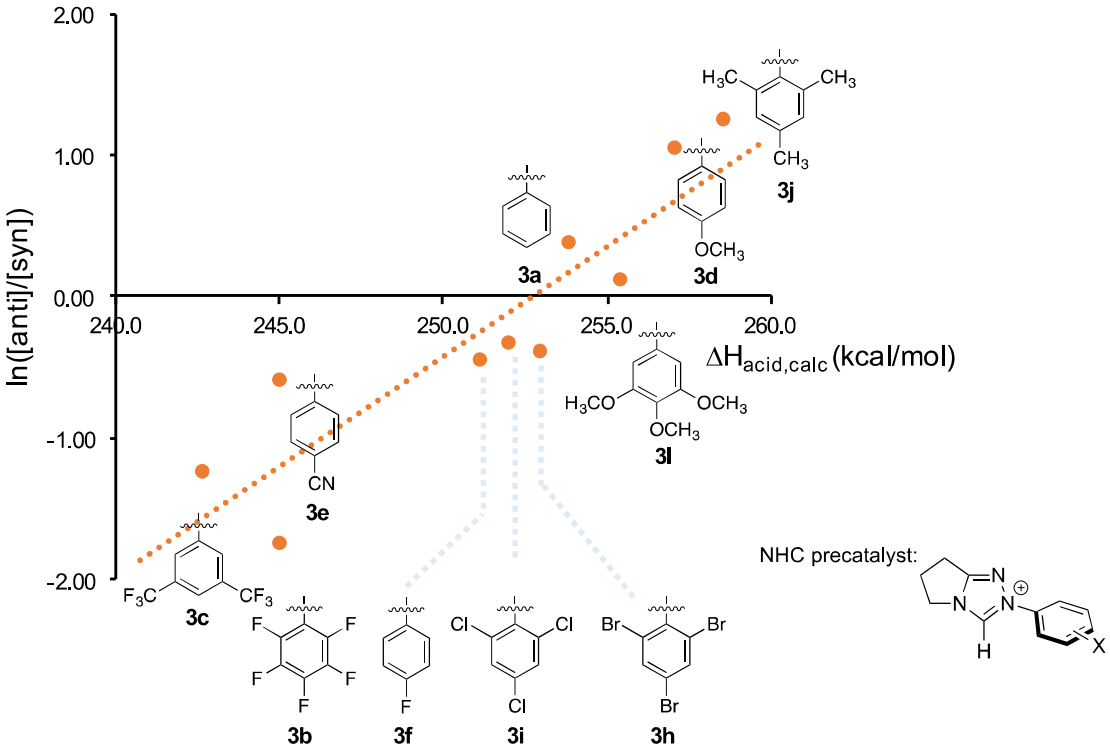

Figure 2. 10 Natural log plot of the *anti/syn* ratio for the reaction in Figure 2.9 (R=Et) versus calculated gas phase acidity of the precatalyst

While there is a clear overall trend, one pair of data points stands out: **3b** and **3e**. Both of these precatalysts have the same acidity (245.1 kcal/mol); however, they have different anti/syn selectivity, with 4-CN precatalyst **3e** showing more anti selectivity than the

perfluorinated precatalyst **3b**. We suspect this difference is related to the substitution pattern for the two precatalysts. The N-aryl group on **3b** has diortho substitution, while **3e** does not.[35] Therefore, we also composed separate analyses, one with precatalysts that have diortho substituents and one with precatalysts that do not (Figures 2.11 and 2.12); these plots show the same trend (more acidic, more *syn* selectivity), but with slightly better correlations. In a study with this same class of catalysts, for the benzoin and Stetter reactions, O'Donoghue, Smith and coworkers proposed that perpendicularity of the N-aryl group, which should be greater with diortho substitution, influences reactivity.[36] Our calculations do indicate that the catalysts with diortho substitution examined herein adopt geometries with a more perpendicular *N*-aryl group, which we assume influences the selectivity slightly differently than those catalysts without diortho substituents, which are less nonplanar.

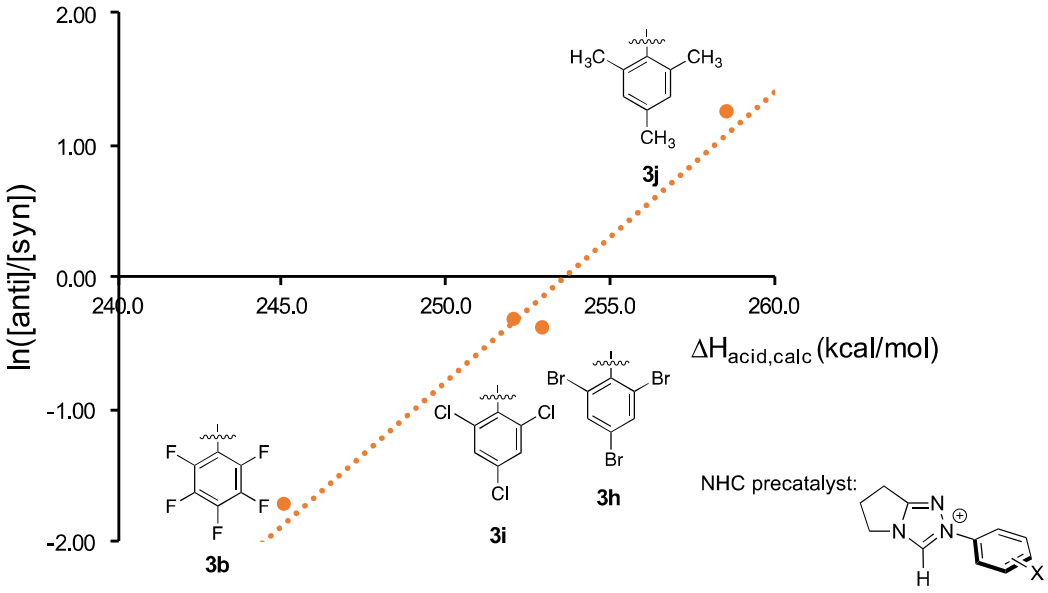

Figure 2. 11 Natural log plot of the *anti/syn* ratio for the reaction in Figure 2.9 (R=Et) versus calculated gas phase acidity of the precatalyst, for catalysts with diortho aryl substitution

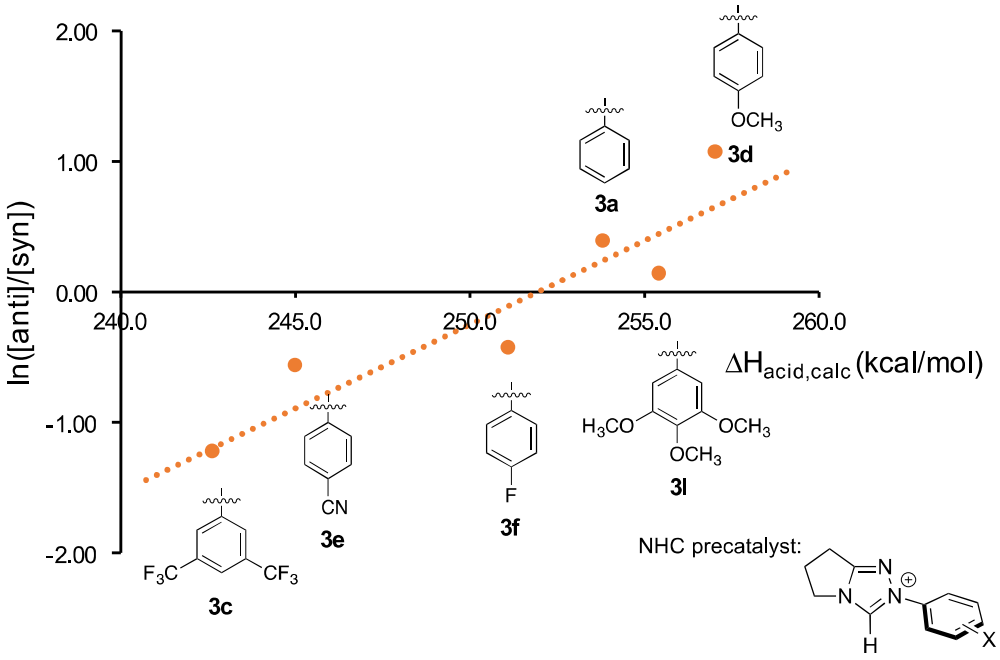

Figure 2. 12 Natural log plot of the anti/syn ratio for the reaction in Figure 2.9 (R=Et) versus calculated gas phase acidity of the precatalyst, for precatalysts lacking diortho aryl substitution.

What is the provenance of this selectivity?

This type of reaction was first reported by Nair, using imidazolium precatalyst **5** (Figure 2.13), which yielded the *anti* product as the major diastereomer.[31] Enantioselective variations, using chiral triazolium precatalysts, were reported by the Rovis and Liu groups, respectively, in 2013 and 2012.[32,33] Liu's precatalyst, **6**, favors the *anti* isomer, while Rovis' precatalyst **7** favors the *syn* isomer. The difference in diastereoselectivity is proposed to arise from a difference in the Breslow intermediate geometry. Because the two chiral

precatalysts **6** and **7** only allow approach from one face, the observed stereochemistry can be explained by E versus Z Breslow enol geometry (Figure 2.14).

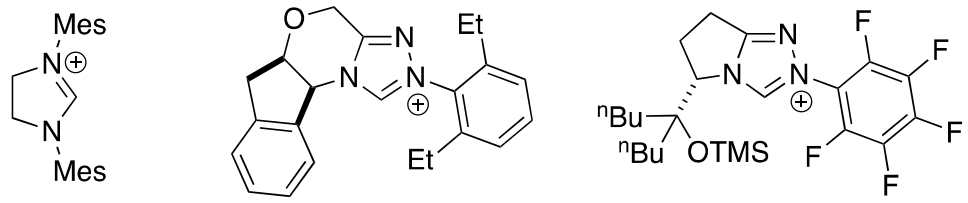

5 **6** **7**

Figure 2. 13 various NHC enantioselective precatalysts

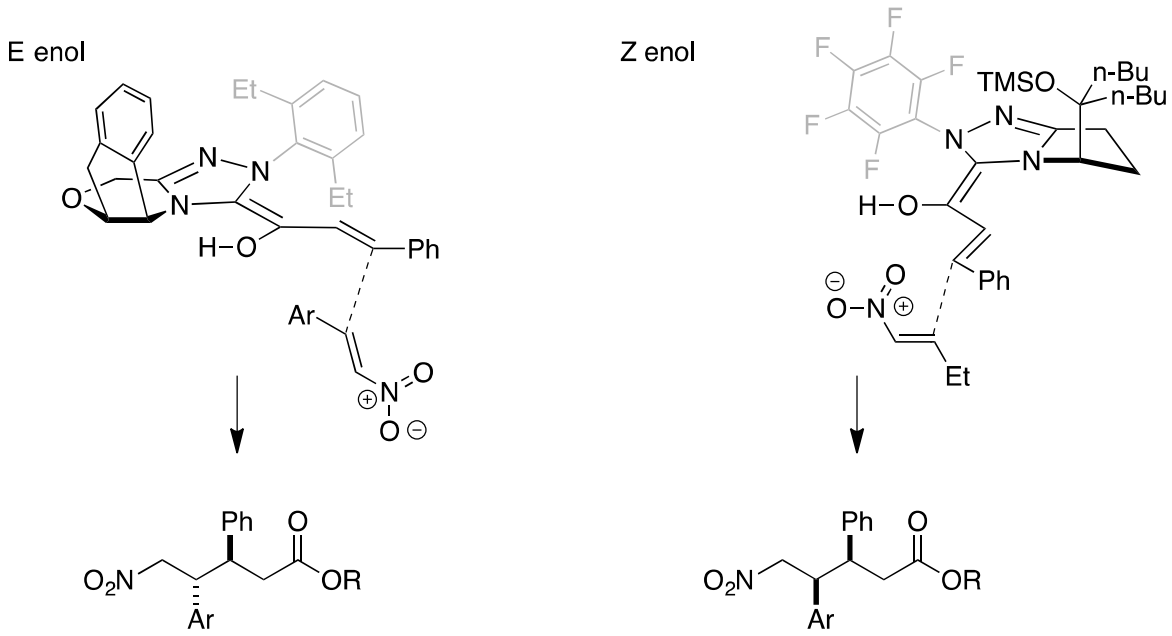

Figure 2. 14 Transition states leading to the observed major isomers in asymmetric homoenolate reactions

Applying what we learned from these chiral catalysts to our achiral system, we postulate that *anti* selectivity corresponds to a preference for the E enol, while *syn* selectivity arises from a preference for the Z enol. To further probe this hypothesis, we calculated the

transition states for the formation of the E and Z enols via deprotonation by acetate (Figure 2.15). Intermediate **8a** is deprotonated by acetate, via **TSa**, to form the E enol **9a**; intermediate **8b** reacts via **TSb** to form Z enol **9b.** For **3c** (Ar = 3,5-di-CF_3), experimentally, we see *syn* selectivity (Figure 2.10). Our calculations show that the transition state to form the Z enol (**TSb**) is *lower* than that to form the E enol (**TSa**) by 3.3 kcal/mol (Figure 2.16A). This is consistent with our hypothesis that *syn* selectivity arises from the Z enol. For **3d** (Ar = 4-OMe), we find that the transition state for Z enol formation is *higher* than that for E enol formation, by 1.5 kcal/mol (Figure 2.16). This reversal, as compared to **3c**, is consistent with the *anti* selectivity we experimentally observe for catalyst **3d**.

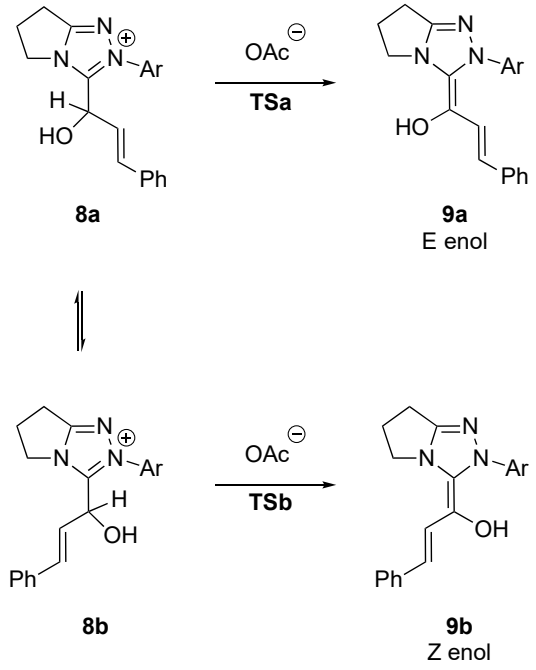

Figure 2. 15 Deprotonation to form either E or Z enol

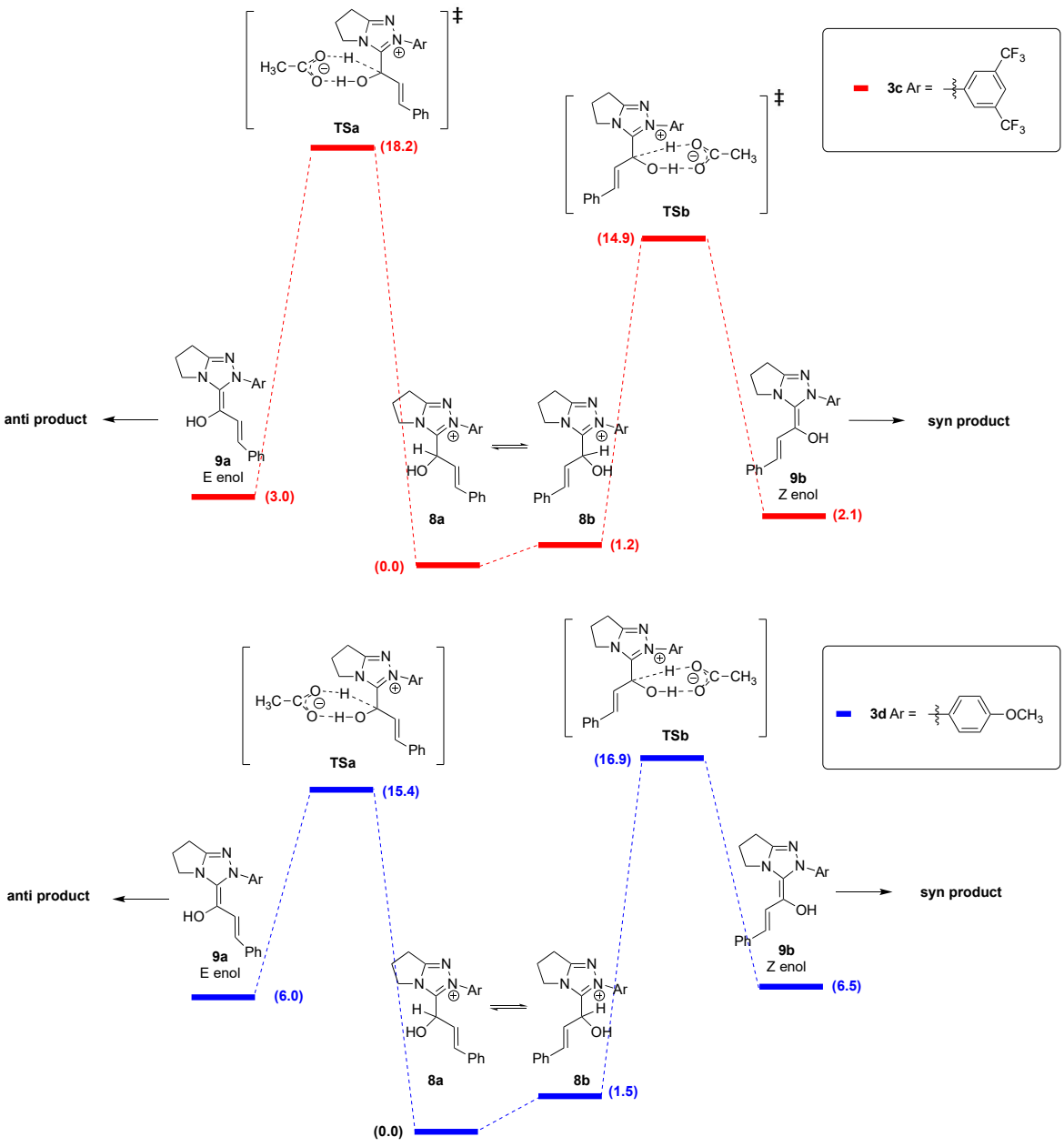

Figure 2. 16 Free energy profiles for E versus Z enol formation for **3c** (A) and **3d** (B)

We are not certain why electron withdrawing groups would favor Z-enol formation. An examination of the calculated geometries for the transition state leading to the Z-enol (**TSb**) indicates that **TSb** might be stabilized by an interaction between the enol oxygen and the *N*-aryl substituent (Figure 2.17). This interaction would be more favorable for an electron

deficient ring; we find that the distance between the enol oxygen and the N-aryl ring plane is indeed less for **3c** (2.23 Å) than for **3d** (2.39 Å), indicating a possibly stronger interaction.

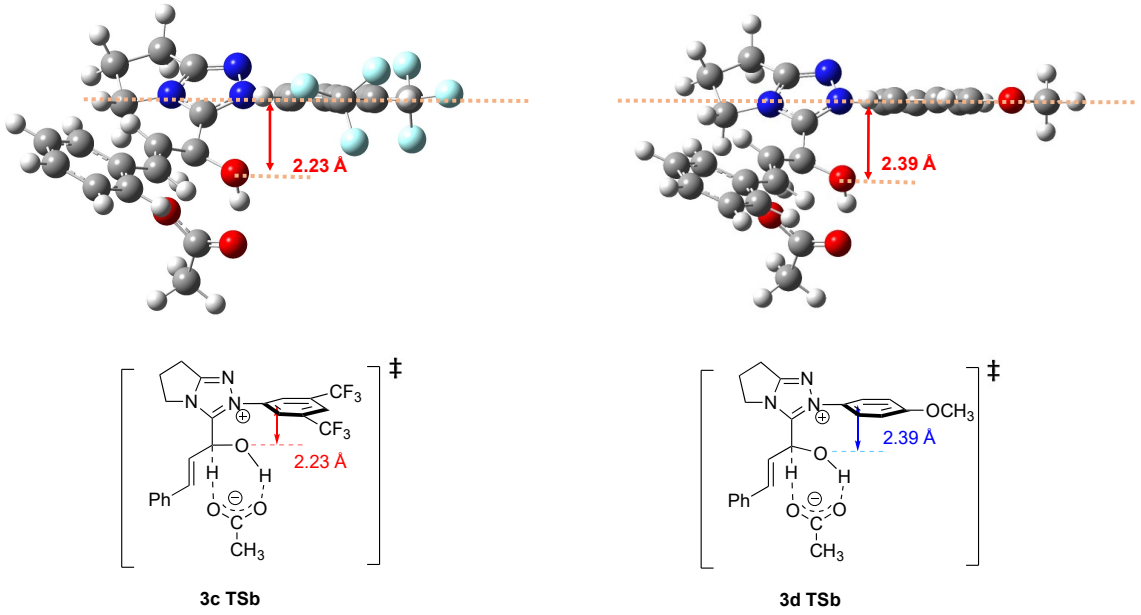

Figure 2. 17 Calculated TSb structures for **3c** and **3d**

The postulate that the E enol leads to *anti* selectivity and the Z enol to *syn* selectivity is also consistent with calculations conducted by Fu and coworkers on precatalyst **7**, which shows *syn* selectivity.[37] Their computations indicate that for **7**, the Z enol is afforded via a lower energy transition state relative to the E enol, consistent with the *syn* selectivity that **7** presents.

Thus, subtle electronic changes appear to exert their effect on these relative transition states, favoring formation of the Z enol for electron withdrawing groups, and the E enol for electron donating groups. These electronic changes are reflected nicely in the gas phase acidities.

2.3.4 Acidity and enantioselectivity

To explore whether a correlation between acidity and enantioselectivity exists for reactions catalyzed by chiral triazolylidenes **4,** we examined an NHC-catalyzed asymmetric intramolecular Stetter reaction (Figure 2.18).[38]

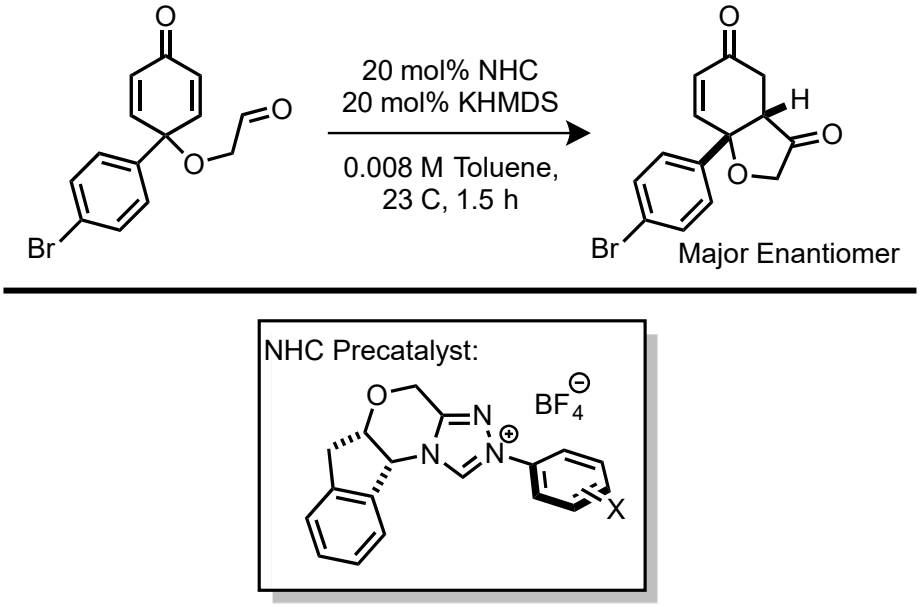

Figure 2. 18 NHC-catalyzed intramolecular Stetter reaction with dienones

An examination of the stereochemical outcome of this reaction reveals a linear correlation for the natural log of the ratio of major to minor enantiomer products versus the gas phase acidity of triazolium precatalysts **4** (Figure 2.19).[39] For this reaction, a more acidic triazolium corresponds to reduced enantioselectivities and a less acidic triazolium results in higher enantiomeric excesses.

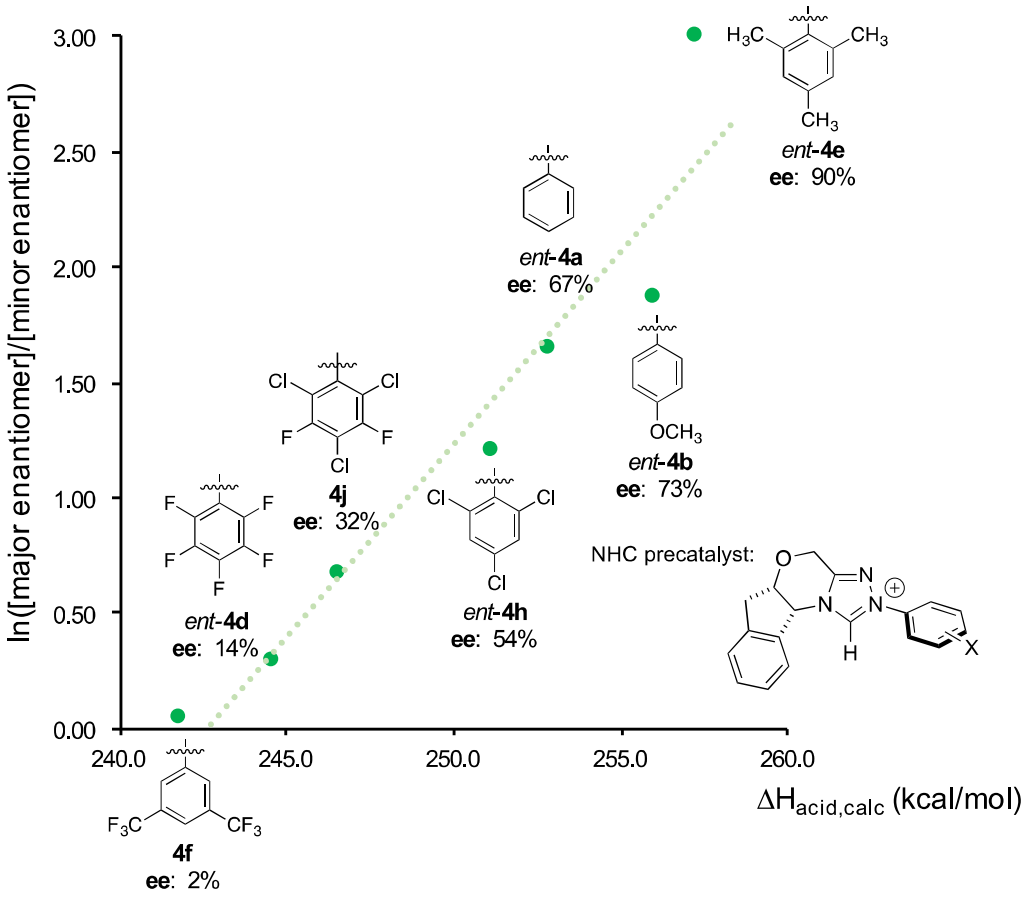

Figure 2. 19 Natural log plot of the major/minor enantiomer ratio for the reaction in Figure 2.18 versus the calculated gas phase acidity of the precatalyst

This correlation with acidity also allowed us to improve the ee of this reaction. The previous ee benchmark for this particular substrate and for the antipode of precatalyst **4b** was an acceptable 73%. Realizing that a precatalyst with a lower gas phase acidity should improve enantioselectivity, we tried precatalyst *ent*-**4e**, resulting in 90% ee, exceeding our previous benchmark for this substrate by 17% (~0.6 kcal/mol at ambient temperature). Thus, calculated and experimental acidities may aid in a more rational catalyst optimization for *Umpolung*-themed reactions.

We postulate that the correlation between acidity and enantioselectivity for this reaction may be related to a bimolecular event in the mechanism. In a previous study of this reaction, we found that when using a solvent mixture of toluene and isopropanol, increasing the concentration of the alcohol decreased the ee.[40]

We proposed that the alcohol was involved in the transition state structure via hydrogen bonding, either to the Breslow enol oxygen or the dienone carbonyl, or both. In the absence of alcohol, another species could provide the hydrogen bonding. Since more hydrogen bonding decreases the ee, then it should follow that a more acidic Breslow enol would favor hydrogen bonding, and decrease the ee. More electron withdrawing aryl substituents should increase the acidity of the precatalyst as well as the acidity of the Breslow intermediate. Thus, we see the correlation in Figure 2.19, between higher acidity and lower ee.

Our achiral and chiral selectivity studies, taken together, indicate that using gas phase acidity is a powerful and simple method to assess intrinsic properties of carbenes that can thus provide the backbone for predictive models for *Umpolung*-themed reactions. The nonpolar environment of the gas phase enhances the differences among acidities, making acidity trends clear. These acidity trends correlate with selectivity. Solution phase acidities should also correlate to selectivity, but are generally more difficult to obtain;[7,8,41-47] furthermore, it is potentially more difficult to ascertain acidity trends among pK_a values since the overall acidity range, as we show herein, is much tighter in solvent than in the gas phase. Gas phase acidity calculations are easily obtained, and the experimental measurements of acidity validate the calculations.

2.4 Conclusions

In this chapter, we calculate and measure the gas phase acidity of a series of achiral and chiral triazolium precatalysts whose acidities were heretofore unknown. The measurements benchmark the calculations, indicating that the DFT method (B3LYP/6-31+G(d)) is reasonably accurate. Calculations aid in the explanation of surprising trends in gas phase acidity, which are attributable to geometry and the planarity of the N-aryl substituent, relative to the triazolium ring. For the achiral catalysts, the few pK_a values that are known track reasonably well with the gas phase acidity values, though the acidity range is much tighter in solution than in the gas phase. This wider range of acidities in the gas phase allows for a clear correlation to be tracked between intrinsic acidity values and selectivity in both a homoenolate addition reaction, as catalyzed by achiral triazolylidene catalysts, and a Stetter reaction, as catalyzed by chiral triazolylidene catalysts. Acidity is shown to be a useful and powerful predictive tool for these types of reactions, and may well extend to other *Umpolung* reactions as well. We believe that different substituents affect the stereoelectronics of the system in such a way that is reflected in the acidity, allowing the gas phase acidity to track with selectivity.

2.5 References

(1) Igau, A.; Baceiredo, A.; Trinquier, G.; Bertrand, G. *Angew. Chem. Int. Ed.* **1989**, *101*, 617.
(2) Arduengo, A. J. I.; Harlow, R. L.; Kline, M. *J. Am. Chem. Soc.* **1991**, *113*, 361.
(3) Samojłowicz, C.; Bieniek, M.; Grela, K. *Chem. Rev.* **2009**, *109*, 3708.
(4) Flanigan, D. M.; Romanav-Michailidis, F.; White, N. A.; Rovis, T. *Chem. Rev.* **2015**, *115*, 9307.
(5) Enders, D.; Niemeier, O.; Henseler, A. *Chem. Rev.* **2007**, *107*, 5606.
(6) Bugaut, X.; Glorius, F. *Chem. Soc. Rev.* **2012**, *41*, 3511.
(7) Massey, R. S.; Collett, C. J.; Lindsay, A. G.; Smith, A. D.; O'Donoghue, A. C. *J. Am. Chem. Soc.* **2012**, *134*, 20421.
(8) O'Donoghue, A. C.; Massey, R. S. In *Contemporary Carbene Chemistry*; Moss, R. A., Doyle, M. P., Eds.; Wiley: Hoboken, New Jersey, 2013; Vol. 7, p 75.
(9) Maji, B.; Breugst, M.; Mayr, H. *Angew. Chem. Int. Ed.* **2011**, *50*, 6915.
(10) Liu, M.; Chen, M.; Zhang, S.; Yang, I.; Buckley, B.; Lee, J. K. *J. Phys. Org. Chem.* **2011**, *24*, 929.
(11) Lee, C.; Yang, W.; Parr, R. G. *Phys. Rev. B* **1988**, *37*, 785.
(12) Becke, A. D. *J. Chem. Phys.* **1993**, *98*, 5648.
(13) Becke, A. D. *J. Chem. Phys.* **1993**, *98*, 1372.
(14) Stephens, P. J.; Devlin, F. J.; Chabalowski, C. F.; Frisch, M. J. *J. Phys. Chem.* **1994**, *98*, 11623.
(15) Kohn, W.; Becke, A. D.; Parr, R. G. *J. Phys. Chem.* **1996**, *100*, 12974.
(16) GAUSSIAN09, R. A.; Frisch, M. J.; Trucks, G. W.; Schlegel, H. B.; Scuseria, G. E.; Robb, M. A.; Cheeseman, J. R.; Scalmani, G.; Barone, V.; Mennucci, B.; Petersson, G. A.; Nakatsuji, H.; Caricato, M.; Li, X.; Hratchian, H. P.; Izmaylov, A. F.; Bloino, J.; Zheng, G.; Sonnenberg, J. L.; Hada, M.; Ehara, M.; Toyota, K.; Fukuda, R.; Hasegawa, J.; Ishida, M.; Nakajima, T.; Honda, Y.; Kitao, O.; Nakai, H.; Vreven, T.; Montgomery, J., J. A.; Peralta, J. E.; Ogliaro, F.; Bearpark, M.; Heyd, J. J.; Brothers, E.; Kudin, K. N.; Staroverov, V. N.; Kobayashi, R.; Normand, J.; Raghavachari, K.; Rendell, A.; Burant, J. C.; Iyengar, S. S.; Tomasi, J.; Cossi, M.; Rega, N.; Millam, J. M.; Klene, M.; Knox, J. E.; Cross, J. B.; Bakken, V.; Adamo, C.; Jaramillo, J.; Gomperts, R.; Stratmann, R. E.; Yazyev, O.; Austin, A. J.; Cammi, R.; Pomelli, C.; Ochterski, J. W.; Martin, R. L.; Morokuma, K.; Zakrzewski, V. G.; Voth, G. A.; Salvador, P.; Dannenberg, J. J.; Dapprich, S.; Daniels, A. D.; Farkas, Ö.; Foresman, J. B.; Ortiz, J. V.; Cioslowski, J.; Fox, D. J., Gaussian, Inc., Wallingford CT, 2009.
(17) Marenich, A. V.; Cramer, C. J.; Truhlar, D. G. *J. Phys. Chem. B* **2009**, *113*, 6378.
(18) Miertuš, S.; Scrocco, E.; Tomasi, J. *Chem. Phys.* **1981**, *55*, 117.
(19) Pascual-Ahuir, J. L.; Silla, E.; Tuñón, I. *J. Comput. Chem.* **1994**, *15*, 1127.
(20) Zhao, Y.; Truhlar, D. G. *Theor. Chem. Acc.* **2008**, *120*, 215.
(21) Zhao, Y.; Truhlar, D. G. *Acc. Chem. Res.* **2008**, *41*, 157.
(22) Kurinovich, M. A.; Lee, J. K. *J. Am. Soc. Mass. Spectrom.* **2002**, *13*, 985.
(23) Xuejun, S.; Lee, J. K. *J. Org. Chem.* **2007**, *72*, 6548.
(24) Liu, M.; Li, T.; Amegayibor, F. S.; Cardoso, D. S.; Fu, Y.; Lee, J. K. *J. Org. Chem.* **2008**, *73*, 9283.

(25) Michelson, A. Z.; Chen, M.; Wang, K.; Lee, J. K. *J. Am. Chem. Soc.* **2012**, *134*, 9622.
(26) Liu, M.; Yang, I.; Buckley, B.; Lee, J. K. *Org. Lett.* **2010**, *12*, 4764.
(27) Liu, M.; Chen, M.; Zhang, S.; Yang, I.; Buckley, B.; Lee, J. K. *J. Phys. Org. Chem.* **2011**, *24*, 929.
(28) Kaljurand, I.; Koppel, I. A.; Kutt, A.; Room, E.-I.; Rodima, R.; Koppel, I.; Mishima, M.; Leito, I. *J. Phys. Chem. A* **2007**, *111*, 1245.
(29) Brauman, J. I.; Blair, L. K. *J. Am. Chem. Soc.* **1970**, *92*, 5986.
(30) Ema, T.; Nanjo, Y.; Shiratori, S.; Terao, Y.; Kimura, R. *Org. Lett.* **2016**, *18*, 5764.
(31) Nair, V.; Sinu, C. R.; Babu, B. P.; Varghese, V.; Jose, A.; Suresh, E. *Org. Lett.* **2009**, *11*, 5570.
(32) Maji, B.; Ji, L.; Wang, S.; Vedachalam, S.; Ganguly, R.; Liu, X.-W. *Angew. Chem. Int. Ed.* **2012**, *51*, 8276.
(33) White, N. A.; DiRocco, D. A.; Rovis, T. *J. Am. Chem. Soc.* **2013**, *135*, 8504.
(34) Plots of selectivity versus calculated acidity for the furyl and phenyl nitroalkenes, as well as a plot of selectivity versus experimental acidity for the ethyl nitroalkene are in the Supporting Information.
(35) H and F are not isosteric. F has an A-value of 0.25, and a van der Waals radius of 1.47 (compared to 1.22 for H).
(36) Collett, C. J.; Massey, R. S.; Maguire, O. R.; Batsanov, A. S.; O'Donoghue, A. C.; Smith, A. D. *Chem. Sci.* **2013**, *4*, 1514.
(37) Zhang, Q.; Yu, H.-Z.; Fu, Y. *Org. Chem. Front.* **2014**, *1*, 614.
(38) Liu, Q.; Rovis, T. *J. Am. Chem. Soc.* **2006**, *128*, 2552.
(39) For precatalysts **6a**, **6b**, **6d**, **6e** and **6h**, the enantiomers were utilized for the ee experiments; however, the gas phase acidity is still relevant since this value remains the same regardless of enantiomer.
(40) Liu, Q.; Rovis, T. *Org. Process Res. Dev.* **2007**, *11*, 598.
(41) Kim, Y.-J.; Streitwieser, A. *J. Am. Chem. Soc.* **2002**, *124*, 5757.
(42) Sievers, A.; Wolfenden, R. *J. Am. Chem. Soc.* **2002**, *124*, 13986.
(43) Washabaugh, M. W.; Jencks, W. P. *J. Am. Chem. Soc.* **1989**, *111*, 674.
(44) Alder, R. W.; Allen, P. R.; Williams, S. J. *J.C.S. Chem. Commun.* **1995**, 1267.
(45) Chu, Y.; Deng, H.; Cheng, J.-P. *J. Org. Chem.* **2007**, *72*, 7790.
(46) Amyes, T. L.; Diver, S. T.; Richard, J. P.; Rivas, F. M.; Toth, K. *J. Am. Chem. Soc.* **2004**, *126*, 4366.
(47) Higgins, E. M.; Sherwood, J. A.; Lindsay, A. G.; Armstrong, J.; Massey, R. S.; Alder, R. W.; O'Donoghue, A. C. *Chem. Comm.* **2011**, *47*, 1559.

Note: Major parts of this chapter have been submitted to the Journal of Organic Chemistry: Wang, N.; Lee, J. K. "Gas Phase and Ionic Liquid Experimental and Computational Studies of Imidazole Acidity and Carbon Dioxide Capture", *J. Org. Chem.* **2019**, in press.

Chapter 3 Imidazole Acidity and Carbon Dioxide Capture

3.1 Introduction

Fossil fuels have for many years been the primary source of energy worldwide. The burning of fossil fuels releases carbon dioxide, which has become an urgent environmental concern, primarily due to carbon dioxide's prominence as a greenhouse gas and related implications for climate change (Figure 3.1). The development of strategies to capture and store carbon dioxide is therefore a pressing research area.

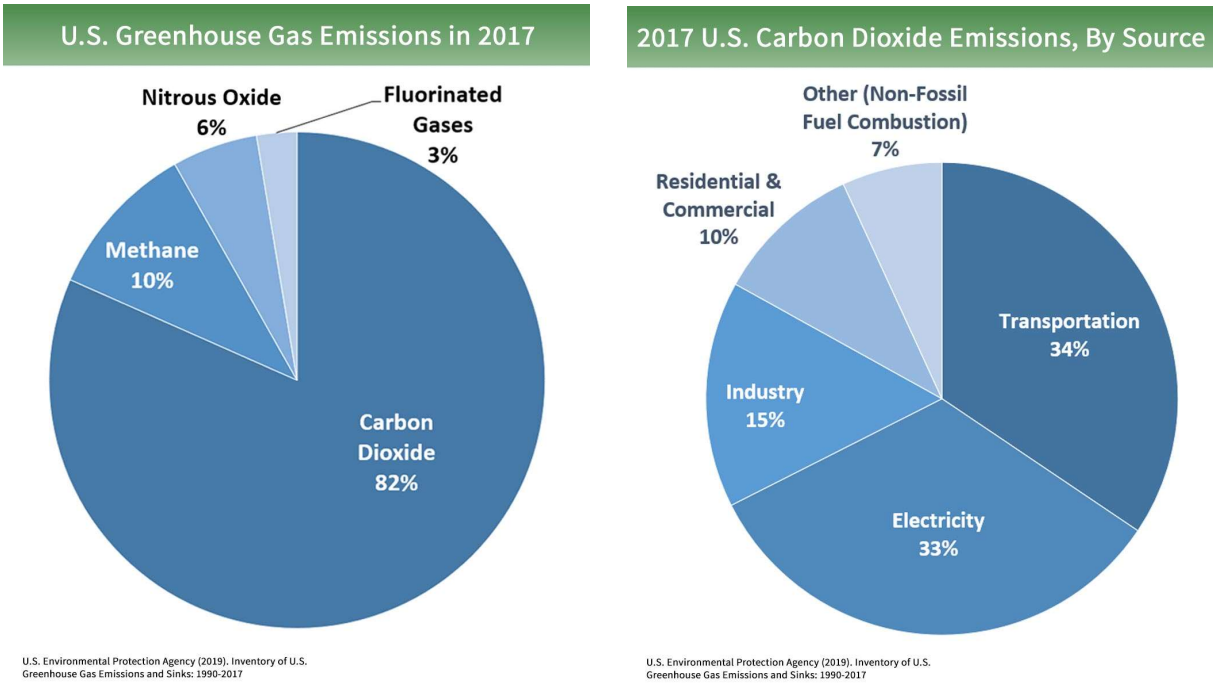

Figure 3. 1 Greenhouse gas emission within U.S. in 2017

In recent years, ionic liquids (ILs) have come to the forefront as an effective means of trapping carbon dioxide.[1-9] ILs have various advantages, including low vapor pressure,

high thermal stability, lack of flammability, property tunability, and a high solvent capacity.1 Early IL studies focused on the physical absorption of carbon dioxide; this method, however, was found to be limited by insufficient carbon dioxide absorption capacity, as the partial pressure and solubility of carbon dioxide is low post-combustion.[10]

To overcome this limitation, researchers turned to the development of "active site-containing" ILs. Such ILs contain a functionality that will chemically react with carbon dioxide, thus effecting chemical (as opposed to physical) CO2 absorption. Davis and co-workers developed the first of this kind, in which a primary amine was covalently tethered to the imidazolium cation of the ionic liquid.[2]

One drawback of such amino-functionalized ILs is a large increase in viscosity after carbon dioxide absorption, which has been attributed to a strong hydrogen-bonded network.[11-14] This increase in viscosity renders such ILs less practical. This issue led to the search for "amino-free functionalized ILs", to improve carbon dioxide chemical absorption. Prominent within this type of IL are azolate ILs, which are also called aprotic heterocyclic anion (AHA) ILs.[1,13,15-18] Dai and Wang introduced this concept with a series of ILs that paired superbases such as 1,3,4,6,7,8-hexahydro-1-methyl-2H-pyrimido[1,2-a]pyrimidine (MTBD) and trihexyl(tetradecyl)phosphonium hydroxide ([P66614][OH]) with weak nitrogen acids such as imidazole, pyrazole, triazoles, tetrazoles and indoles.[13,15] In these AHA ILs, the anionic moiety (such as an imidazolate) nucleophilically attacks the carbon dioxide. Studies to date indicate that the basicity of the anion is important for carbon dioxide capture, capacity, and solubility, while the effect of the countercation identity is weaker.[1,13,15,19] Therefore, tuning the basicity is a key component for achieving effective CO2 capture.[1,20-31]

Herein, we use computational and experimental methods to examine the acidity of fifty-six imidazoles, toward better understanding their properties. The experimental measurements provide valuable data to benchmark computations and lend insight into the inherent reactivity of these species. Gas-phase measurements are complemented by gas-phase and solution-phase calculations. We aim to achieve predictive power for such properties, which would allow for more facile tunability of potential ILs for carbon dioxide capture.

3.2 Experimental

All the experimentally measured imidazoles are commercially available and were used without further purification.

Measurement of the gas-phase acidities of imidazoles was carried out in a Fourier Transform ion cyclotron resonance mass spectrometer (FTMS). The FTMS has a dual cell setup (described previously).[36-40] The magnetic field is 3.3 T; the baseline pressure is 1 x 10^{-9} Torr. The imidazoles were introduced into the cell via a heatable solids probe, while the reference acids were introduced via a system of heatable batch inlets or leak valves. Water was pulsed into the cell, and ionized by an electron beam (typically 8 eV (for HO^-), 20 eV (for H_3O^+), 6 μA (for H_3O^+), 9 μA (for HO^-), 0.5 s) to generate hydronium ions. The reactions between the imidazoles and reference acids were measured in both directions. In one direction, the imidazolate anions were generated by reaction of the imidazoles with the hydroxide ions. The imidazolate anions were then selected and transferred from one cubic cell to another via a 2-mm hole in the middle trapping plate. Transferred ions were cooled with pulsed argon gas that allowed the pressure to rise to 10^{-5} Torr. Reaction with the reference acid was then tracked. In the opposite direction, the conjugate bases of the

reference acid were generated by reaction with hydroxide. These anions were then transferred to the second cell to react with neutral imidazoles. Experiments were conducted at ambient temperature. The typical protocol for obtaining gas phase rate constants has been described previously.[36,37,40-42] The experiments are run under pseudo-first-order conditions with the neutral reactant in excess, relative to the reactant anions. Reading the pressure of the neutral compounds from the ion gauges is not always accurate; therefore, we "back out" the neutral substrate pressure from fast control reactions (described previously).[36,42-46]

All calculations were performed using density functional theory (B3LYP/6-311++G(d,p)) as implemented in Gaussian 16.[47-51] All ground state geometries were fully optimized and frequencies were calculated; no scaling factor was applied. The optimized structures had no negative frequencies. For the solvation calculations, the SMD model was used with ionic liquid [DBUH][OTf] as the solvent. The solvent descriptors for [DBUH][OTf] were derived based on the "SMD-GIL" method developed by Cramer, Truhlar and coworkers (details in SI).[52] The temperature for the calculations was set to be 298 K.

3.3 Results and Discussion

3.3.1 Acidity

i. Gas Phase Acidity: Calculations.

Fifty-six imidazoles were examined computationally. Figure 1 depicts the imidazoles examined. Note that for the imidazoles, 4- and 5- substituted structures are tautomers. For benzimidazoles, the 5- and 6- substituted structures are tautomers. In Figure 3.2, the 4-substituted imidazoles and the 5-substituted benzimidazoles are shown.

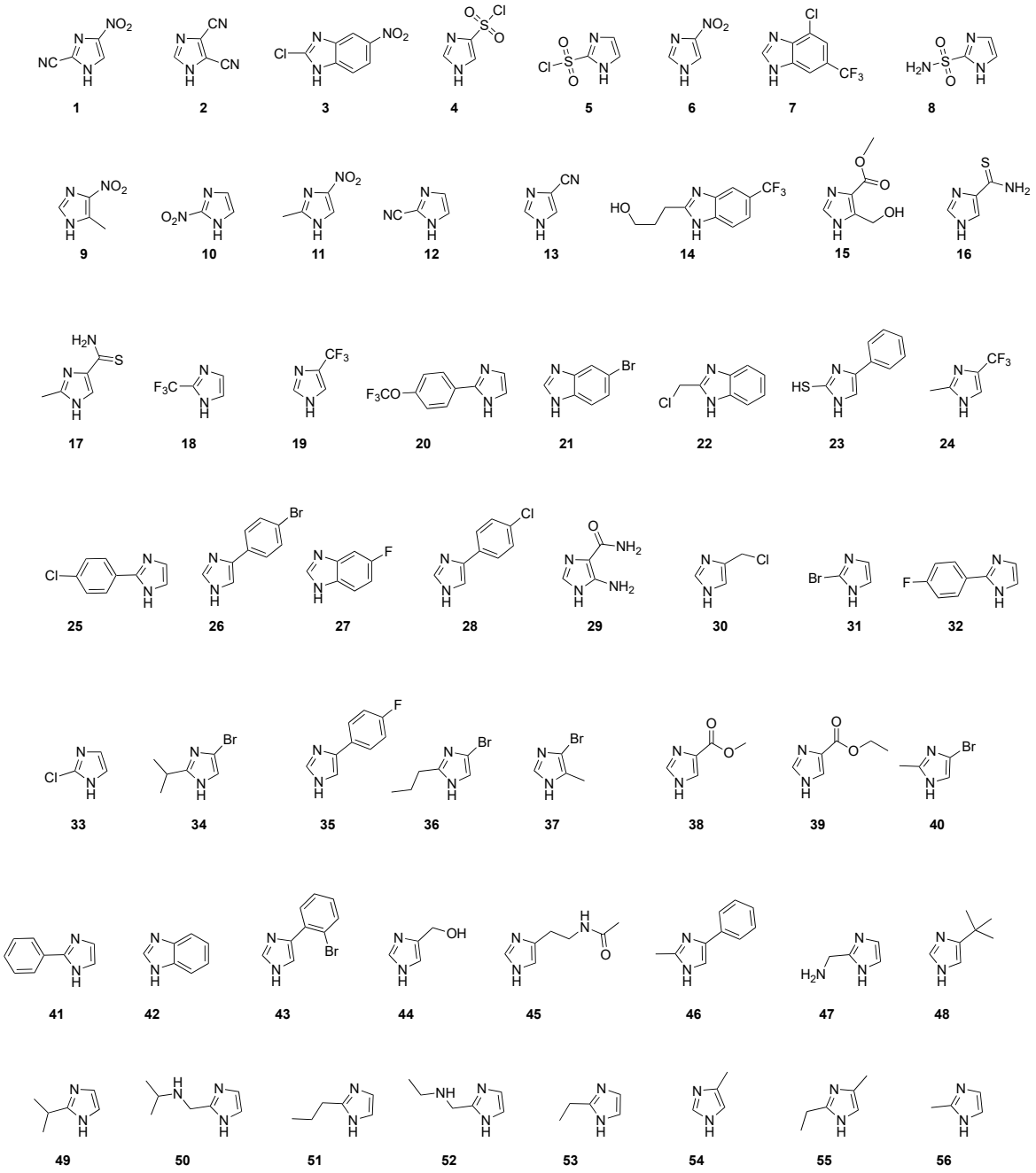

Figure 3. 2 The substrates studied herein. For imidazoles with possible tautomers, the 4-substituted structure is shown. For benzimidazoles, the 5-substituted structure is shown.

In Table 3.1, the calculated gas phase acidities of the fifty-six imidazoles, using B3LYP/6-311++G(d,p), are tabulated.[32] (The last column lists ΔG_{rxn} values, which will be discussed later). Both ΔH_{acid} and ΔG_{acid} values are shown; the substrates in Figure 1 are ordered in decreasing acidity. The ΔH_{acid} is the enthalpy associated with the deprotonation of the imidazole HA, and the ΔG_{acid} is the free energy associated with the deprotonation of the imidazole HA:

$$HA \rightarrow A^- + H^+ \qquad \Delta H_{rxn} = \Delta H_{acid};\ \Delta G_{rxn} = \Delta G_{acid}$$

For those imidazoles for which there is more than one tautomer, no "prime" mark next to the structure indicates that the most stable tautomer AH is the 4-substituted imidazole or 5-substituted benzimidazole (the structures shown in Figure 1). A "prime" (') next to the structure number indicates that the most stable tautomer AH is the 5-substituted imidazole or the 6-substituted benzimidazole.

Table 3. 1 Gas phase calculations (B3LYP/6-311++G(d,p)) on fifty-six substrates.

	Acidity, ΔH_{acid} (kcal/mol)	Acidity, ΔG_{acid} (kcal/mol)	ΔG_{rxn}, CO_2 addition, kcal/mol
1	306.7	299.4	3.5
2	311.4	304.0	3.3
3'	315.9	308.6	3.0
4	317.2	309.5	6.7
5	317.6	309.9	10.2
6'	324.5	316.9	3.1
7	324.7	317.3	3.6
8	325.0	317.5	8.1
9	325.4	318.2	4.5
10	326.2	318.5	2.4
11'	326.8	319.6	2.4
12	328.7	321.3	6.2
13	328.8	321.3	0.8
14	330.8	323.3	4.0

	Acidity, ΔH_{acid} (kcal/mol)	Acidity, ΔG_{acid} (kcal/mol)	ΔG_{rxn}, CO_2 addition, kcal/mol
15	331.5	324.9	1.6
16	332.3	324.4	1.1
17	333.1	326.2	2.2
18	333.2	325.7	7.2
19	333.6	325.9	-1.1
20	333.9	327.0	6.4
21'	334.0	326.5	0.2
22	334.6	327.2	5.1
23	334.7	327.7	-1.1
24	335.5	327.7	0.2
25	336.3	330.8	4.6
26	336.5	329.3	-1.7
27'	336.7	329.2	-1.1
28	337.1	329.8	-1.9
29	337.4	330.3	-4.3
30'	337.5	329.4	-1.1

	Acidity, ΔH_{acid} (kcal/mol)	Acidity, ΔG_{acid} (kcal/mol)	ΔG_{rxn}, CO_2 addition, kcal/mol
31	337.7	330.1	4.7
32	338.0	331.0	5.1
33	338.4	330.8	3.7
34	338.7	331.2	0.3
35	338.8	331.9	-2.8
36	339.2	331.7	-0.4
37	339.7	331.8	-1.4
38'	339.8	332.2	-1.2
39'	340.0	332.5	-1.2
40	340.2	332.4	-1.2
41	340.8	333.9	5.1
42	341.0	333.5	-2.4
43'	341.6	334.0	-2.3
44'	341.7	334.1	-0.4
45	341.8	334.4	-5.1
46	342.2	335.0	-1.8

	Acidity, ΔH_{acid} (kcal/mol)	Acidity, ΔG_{acid} (kcal/mol)	ΔG_{rxn}, CO_2 addition, kcal/mol
47	348.2	340.0	-5.6
48	348.9	341.2	-7.3
49	349.1	342.4	-4.8
50	349.6	341.7	-4.5
51	349.7	342.0	-4.9
52	349.9	342.0	-4.7
53	350.0	342.3	-6.5
54	350.9	343.3	-8.4
55	351.1	343.9	-5.7
56	351.1	343.3	-6.5

Overall, the acidity trends are as one might expect; substrates with electron withdrawing groups (for example, $-NO_2$, -CN, -X where X is a halide) are more acidic. The less acidic imidazoles are those that are substituted with more electron-donating alkyl groups. For example, the series **4**, **6'**, **13**, **19**, and **54** are all 4/5-substituted imidazoles, with, respectively, substituents $-SO_2Cl$, $-NO_2$, -CN, $-CF_3$, and $-CH_3$. Their acidity decreases with the trend: **4** > **6'** > **13** > **19** > **54**, where **4** is most acidic. This is consistent with the

substitution patterns. Likewise, for the 2-substituted imidazoles, the acidity trend is: **5** > **10** > **12** > **18** > **56**, where substitution is, respectively, $-SO_2Cl$, $-NO_2$, -CN, $-CF_3$, and $-CH_3$.

ii. Gas Phase Acidity: Experiments.

While calculations are valuable, the accuracy of any chosen method and level is always in question. To benchmark some of our calculated values, we measured imidazole gas phase acidity. We utilized acidity bracketing in a Fourier Transform mass spectrometer. We selected imidazoles that by computations represented a range in acidity. Proton transfer reactions between reference acids whose acidities are known and the conjugate base of the imidazoles, as well as the reverse reaction, were tracked. The presence or absence of proton transfer was assessed.

The results are shown in Tables 3.2 and 3.3. Column "a" represents the reaction between the conjugate base of the imidazole and the neutral reference acid. Column "b" represents the reaction between the deprotonated reference acid and the neutral imidazole. For imidazole **9**, the conjugate base of **9** cannot deprotonate 1,1,1-trifluoro-2,4-pentadione (ΔG_{acid} = 322.0 kcal/mol), but 1,1,1-trifluoro-2,4-pentadione enolate can deprotonate **9**. The conjugate base of **9** deprotonates trifluoroacetic acid (ΔG_{acid} = 317.4 kcal/mol), but the reverse reaction does not take place. We therefore bracket imidazole **9** to have a ΔG_{acid} of 320 ± 4 kcal/mol. Imidazole **11** reacts the same as **9**; thus **11** has a ΔG_{acid} also of 320 ± 4 kcal/mol. The conjugate base of **13** cannot extract a proton from difluoroacetic acid (ΔG_{acid} = 323.8 kcal/mol); however, difluoroacetate is basic enough to abstract a proton from **13**. The conjugate base of **13** is basic enough to proton transfer from 3,5-bis(trifluoromethyl)phenol (ΔG_{acid} = 322.9 kcal/mol), but the reverse reaction does not

occur, placing the ΔG_{acid} of **13** at 323 ± 3 kcal/mol. Pyruvate (ΔG_{acid} = 326.5 kcal/mol) can deprotonate **19**, while the reverse reaction does not occur. The conjugate base of **19** can deprotonate difluoroacetic acid (ΔG_{acid} = 323.8 kcal/mol) but difluoroacetate is not basic enough to deprotonate **19.** We place the ΔG_{acid} of **19** to be 326 ± 4 kcal/mol. For **34, 38**, and **40**, the deprotonated imidazoles do not react with methyl cyanoacetate (ΔG_{acid} = 334.5 kcal/mol) but deprotonated methyl cyanoacetate can deprotonate **34, 38** and **40**. The conjugate base of all three imidazoles can abstract a proton from trifluoro-*m*-cresol (ΔG_{acid} = 332.4 kcal/mol), but the cresolate does not deprotonate the imidazoles, placing the acidity for **34**, **38** and **40** at 333 ± 3 kcal/mol. The reaction of deprotonated **41** and acetylacetone (ΔG_{acid} = 336.7 kcal/mol) does not result in proton transfer; however, the reverse reaction between **41** and acetylacetone enolate does result in proton transfer. The conjugate base of **41** does deprotonate methyl cyanoacetate (ΔG_{acid} = 334.5 kcal/mol), but the reverse reaction does not occur, placing the ΔG_{acid} of **41** at 336 ± 3 kcal/mol. Imidazole **46** reacts the same as **41**, so its acidity is also 336 ± 3 kcal/mol. For imidazole **49**, reaction between the conjugate base and *p*-cresol (ΔG_{acid} = 343.4 kcal/mol) does not occur, but the reverse reaction does. Acetate (ΔG_{acid} = 341.1. kcal/mol) cannot deprotonate **49**, but the conjugate base of **49** can deprotonate acetic acid. We therefore bracket **49** to 342 ± 3 kcal/mol. The conjugate base of **56** cannot transfer a proton from 1-pentanethiol ((ΔG_{acid} = 346.2 kcal/mol), but 1-pentanethiolate can deprotonate **56**. The conjugate base of **56** can deprotonate *p*-cresol ((ΔG_{acid} =343.4 kcal/mol); the reverse reaction does not occur. The ΔG_{acid} of imidazole **56** is therefore 345 ± 4 kcal/mol.

Table 3. 2 Summary of results for gas phase acidity bracketing of imidazoles **9**, **11**, **13**, **19**, **34**, and **38**.

Reference acid	*Acidity*[a] *(ΔG_{acid}, kcal/mol)*	*Proton transfer*[b,c] *a) from reference acid; b) from imidazole*											
		9		**11**		**13**		**19**		**34**		**38**	
		a	**b**	**a**	**b**	**a**	**b**	**a**	**b**	**a**	**b**	**a**	**b**
formic acid	339.2 ± 1.5											–	+
acetylacetone	336.7 ± 2.0									–	+	–	+
methyl cyanoacetate	334.5 ± 2.0									–	+	–	+
trifluoro-*m*-cresol	332.4 ± 2.0							–	+	+	–	+	–
pyruvic acid	326.5 ± 2.8					–	+	–	+	+	–	+	–
difluoroacetic acid	323.8 ± 2.0	–	+	–	+	–	+	+	–				
3,5-bis(trifluoromethyl)phenol	322.9 ± 2.0	–	+	–	+	+	–	+	–				
1,1,1-trifluoro-2,4-pentadione	322.0 ± 2.0	–	+	–	+	+	–						
trifluoroacetic acid	317.4 ± 2.0	+	–	+	–								
3,5-bis(trifluoromethyl)pyrazole	317.3 ± 2.0	+	–	+	–								

[a]Reference [33];[b]The "+" symbol indicates the occurrence and the "–" symbol indicates the absence of proton transfer. [c] "a" represents the reaction between the deprotonated imidazole and the neutral reference acid; "b" represents the reaction between the deprotonated reference acid and the neutral imidazole.

Table 3. 3 Summary of results for gas phase acidity bracketing of imidazoles **40**, **41**, **46**, **49** and **56.**

Reference acid	*Acidity*[a] *(ΔG_{acid}, kcal/mol)*	*Proton transfer*[b,c] *a) from reference acid; b) from imidazole*									
		40		**41**		**46**		**49**		**56**	
		a	**b**	**a**	**b**	**a**	**b**	**a**	**b**	**a**	**b**
2-propanethiol	347.1 ± 2.0							–	+	–	+
1-pentanethiol	346.2 ± 2.5							–	+	–	+
p-cresol	343.4 ± 2.0							–	+	+	–
acetic acid	341.1 ± 2.0							+	–	+	–
butyric acid	339.5 ± 2.0			–	+	–	+	+	–	+	–
formic acid	339.2 ± 1.5	–	+	–	+	–	+	+	–		
acetylacetone	336.7 ± 2.0	–	+	–	+	–	+				
methyl cyanoacetate	334.5 ± 2.0	–	+	+	–	+	–				
trifluoro-*m*-cresol	332.4 ± 2.0	+	–	+	–	+	–				
pyruvic acid	326.5 ± 2.8	+	–								

[a]Reference [33];[b]The "+" symbol indicates the occurrence and the "–" symbol indicates the absence of proton transfer. [c] "a" represents the reaction between the deprotonated imidazole and the neutral reference acid; "b" represents the reaction between the deprotonated reference acid and the neutral imidazole.

iii. Computational versus experimental results

A summary of the computational and experimental results is shown in Table 3.4 and Figure 3.3. For the computational data, if an imidazole has more than one possible tautomer, the acidity of the most stable tautomer is listed first. As noted earlier, a "prime" mark next to the structure number indicates the 5-substituted imidazole structure.

Table 3. 4 Calculated (B3LYP/6-311++G(d,p); 298 K) and experimental gas phase acidity values for imidazoles.[a]

Substrate	Calculated ΔG_{acid} more stable/less stable tautomer	Experimental ΔG_{acid}
9	318.2	320 ± 4
11	319.6 (**11'**)/318.5 (**11**)	320 ± 4
13	321.3 (**13**)/321.1 (**13'**)	323 ± 2
19	325.9 (**19**)/324.7 (**19'**)	326 ± 4
34	331.2 (**34**)/330.1 (**34'**)	333 ± 3
38	332.2 (**38'**)/329.2 (**38**)	333 ± 3
40	332.4 (**40**)/330.7 (**40'**)	333 ± 3
41	333.9	336 ± 3
46	335.0 (**46**)/333.5 (**46'**)	336 ± 3

49	342.4	342 ± 3
56	343.3	345 ± 4

[a]Values are in kcal/mol

There is general agreement between the calculated acidity of the more stable tautomer, and the experimentally determined values, thus benchmarking the calculations (Figure 3.3). The basicity of the anionic component of the AHA ILs for carbon dioxide capture is important, and often assessed by calculation, but gas phase data to which those computed values can be directly compared is generally scarce.[1] Our experiments therefore help fill this knowledge gap.

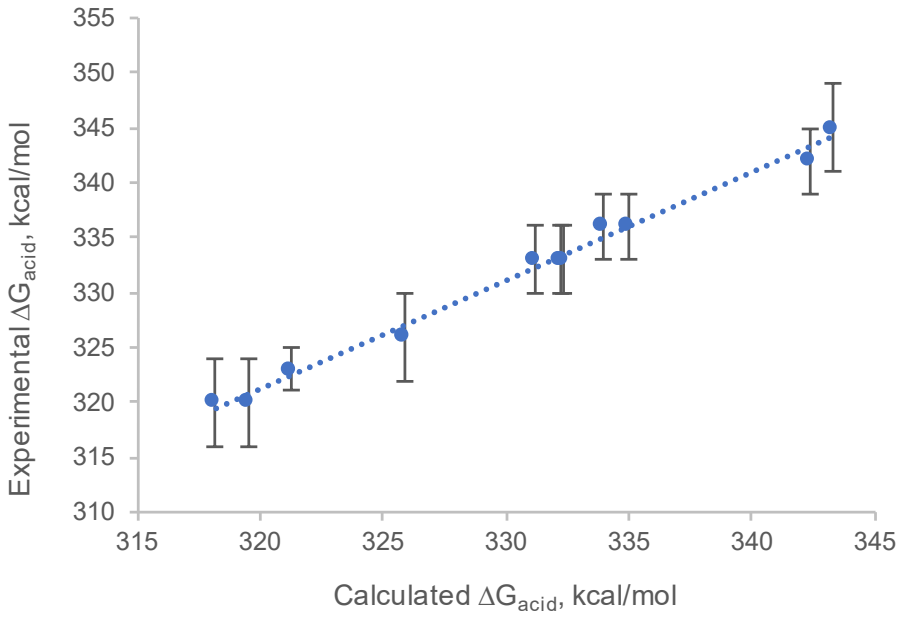

Figure 3. 3 Plot of experimental ΔG_{acid} versus calculated ΔG_{acid} (acidity of more stable tautomer used).

iv. Tautomers

One interesting possibility arising from these studies is the ability to ascertain whether the less stable tautomer is present under our conditions. If two tautomers are different enough in energy, their acidities will be different, and measurement of acidity could potentially be used to assess structure. For example, the 5-substituted tautomer **38'** has a calculated acidity of 332.2 kcal/mol. The less stable 4-substituted tautomer, **38**, has an acidity of 329.2 kcal/mol. The predicted behavior if one or both tautomers is present is shown in Figure 3.4. Direction "a" in Table 3.2 corresponds to the reaction of the conjugate base of **38** and a reference acid HA. The conjugate base of **38** is the same as the conjugate base of **38'**. Since the most basic site of this anion has a calculated $\Delta G_{acid,calc}$ of 332.2 kcal/mol, then, reaction would be expected to occur with any HA that has a ΔG_{acid} of about 332 kcal/mol or lower. In the opposite direction, "b", two scenarios are possible. If only the most stable tautomer **38'** is present, then the conjugate base of the reference acid HA (A^-) would need to be basic enough to deprotonate the N-H ($\Delta G_{acid,calc}$ = 332.2 kcal/mol). However, if both tautomers **38'** and **38** are present, a different proton transfer pattern will be seen. Since **38** has a $\Delta G_{acid,calc}$ of 329.2 kcal/mol, then proton transfer would be expected to occur as long as the conjugate base of the reference acid has a ΔG_{acid} of at least ~329 kcal/mol.

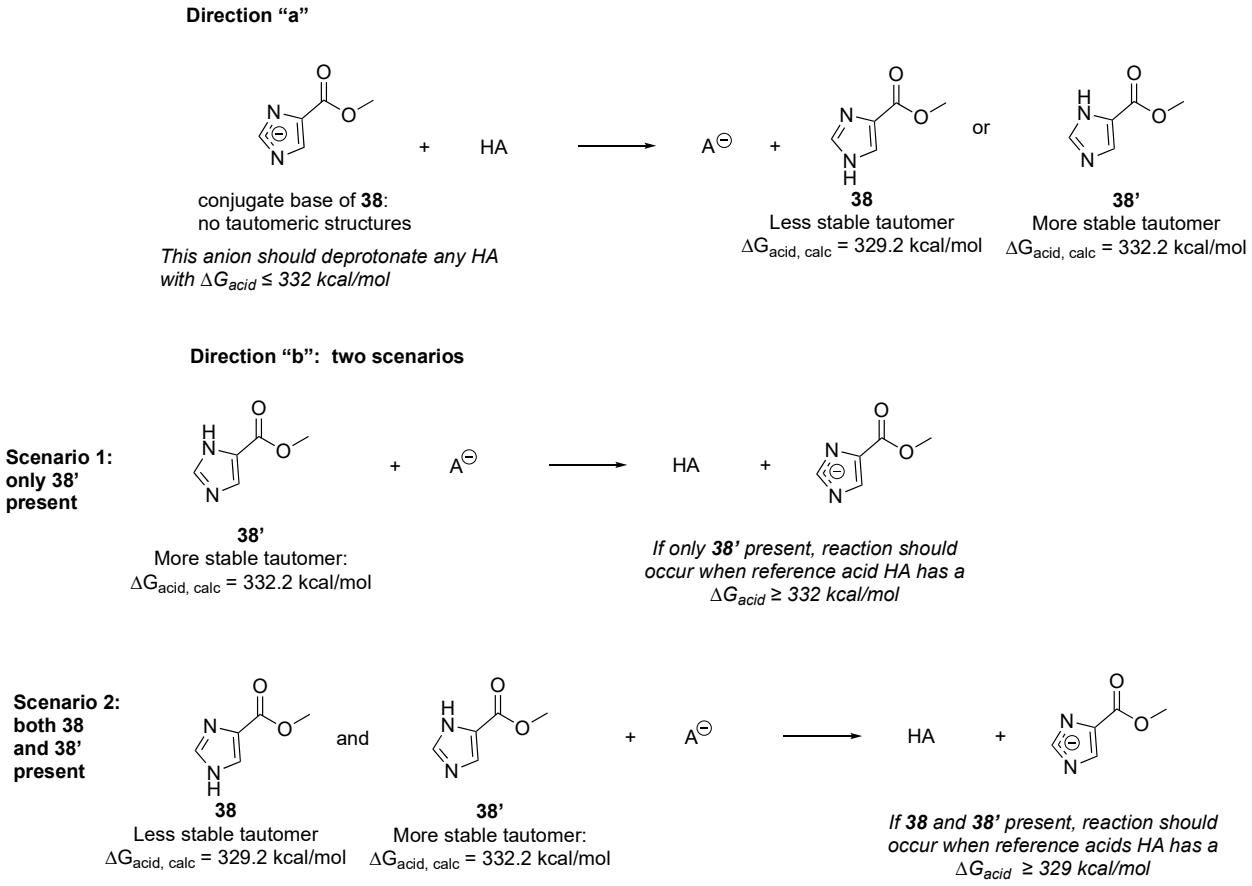

Figure 3. 4 Possible bracketing pathways for **38/38'**.

The resultant hypothetical bracketing table is shown in Table 3.5. The first and second columns (**a** and **b**) indicate the expected results If both the more stable **38'** and less stable **38** structures were present. If neutral **38** (calculated acidity 329.2 kcal/mol) were present, then trifluoro-*m*-cresolate ($\Delta G_{acid,\ expt}$ = 332.4 kcal/mol) and trifluoro-*p*-cresolate ($\Delta G_{acid,\ expt}$ = 330.1 kcal/mol) would be expected to deprotonate it ("+" in column b). The third and fourth columns (**a** and **b**) show our actual observations. The "–" in column b for trifluoro-*m*-cresolate ($\Delta G_{acid,\ expt}$ = 332.4 kcal/mol) and trifluoro-*p*-cresolate (($\Delta G_{acid,\ expt}$ = 330.1 kcal/mol) make it unlikely that the more acidic, less stable tautomer **38** ($\Delta G_{acid,\ calc}$ = 329.2

kcal/mol) is present. Our results indicate that only **38'** is present. Thus, under our gas phase conditions, the major structure is the 5-substituted tautomer **38'**, which is consistent with its greater computed stability.

Table 3. 5 Expected bracketing results if **38** and **38'** are both present (Figure 3).

Reference acid	*Acidity*[a] *(ΔG_{acid}, kcal/mol)*	*Proton transfer*[b,c] *a) from reference acid; b) from imidazole*			
		Expected results if 38' and 38 are present		**Actual results**	
		a	**b**	**a**	**b**
formic acid	339.2 ± 1.5	–	+	–	+
acetylacetone	336.7 ± 2.0	–	+	–	+
methyl cyanoacetate	334.5 ± 2.0	–	+	–	+
trifluoro-*m*-cresol	332.4 ± 2.0	+	+	+	–
trifluoro-*p*-cresol	330.1 ± 2.0	+	+	+	–
pyruvic acid	326.5 ± 2.8	+	–	+	–

[a]Reference [33];[b]The "+" symbol indicates the occurrence and the "–" symbol indicates the absence of proton transfer. [c] "a" represents the reaction between the deprotonated imidazole and the neutral reference acid; "b" represents the reaction between the deprotonated reference acid and the neutral imidazole.

3.3.2 Acidity and carbon dioxide absorption.

Prior studies have indicated that for ionic liquids with heterocyclic anions that capture carbon dioxide, the basicity of the anionic nucleophile (which is also the acidity of the nucleophile's conjugate acid) is important for tuning CO2 absorption capacity.1,13,15,19-30

To assess carbon dioxide capture, we computed the free energy of reaction shown in equation 1, for our fifty-six imidazoles. Prior studies have shown that the carbamate-type structure in equation 3.1 is the product of CO2 capture.13,19,34,35 We plotted the ΔGrxn for equation 1 versus computed imidazole acidity. The gas-phase data are in Table 3.1, and the resultant plot is shown in Figure 3.5.21

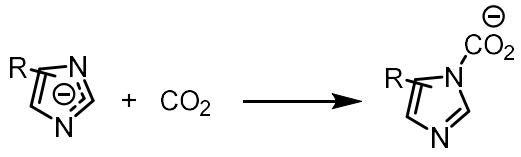

Eq. 3.1

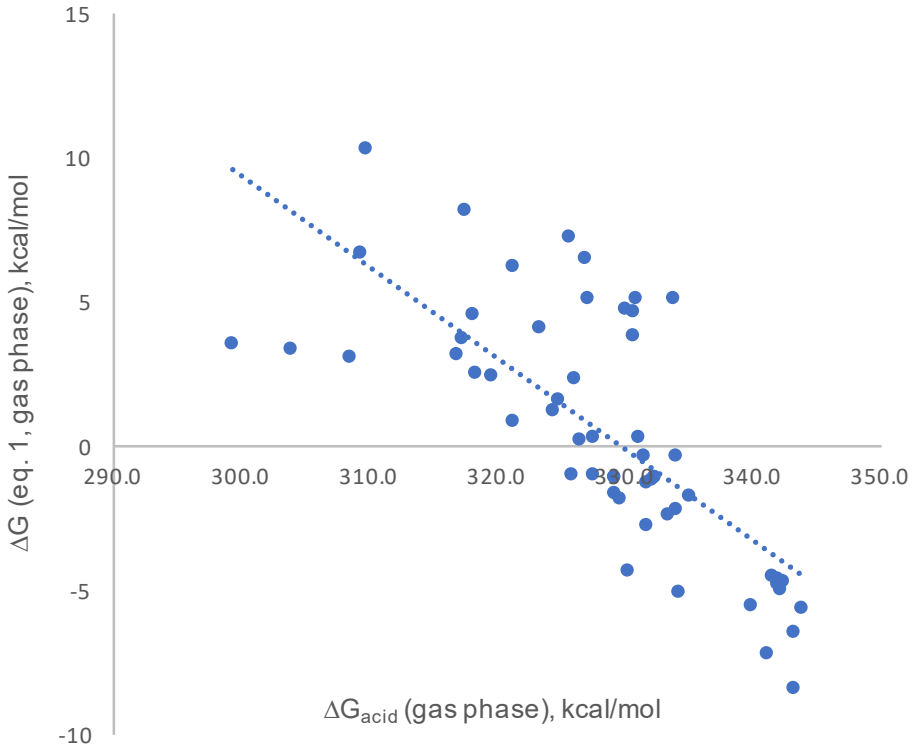

Figure 3. 5 Relationship between calculated gas phase ΔG_{rxn} for equation 1 and the calculated gas phase $\Delta G_{acid,\ calc}$ of imidazoles.

There is a rough linear correlation between the ΔG of formation of the imidazolate-carbon dioxide complex, and the acidity of the imidazole. The less acidic the imidazole (i.e. the more basic the imidazolate), the more exergonic the complexation reaction shown in equation 1. This result shows promise for the design/choice of imidazolates for CO_2 capture; our studies have benchmarked the calculations and show that the more basic anions yield more stable CO_2 adducts.

We also calculated the acidity of the 56 imidazoles in an ionic liquid medium. Prior work has indicated that calculations in solvent may be more relevant than gas phase computations for ionic liquid-based carbon dioxide capture systems.[22,27] Ji and Cheng and coworkers, in a recent study relating IL anion basicity to CO_2 absorption capacity, assessed anion basicity in the ionic liquid [$DBUH^+$][OTf^-]; we likewise used [$DBUH^+$][OTf^-] as a model.[22] The resultant plot is shown in Figure 3.6. The linear correlation is even clearer in this medium than in the gas phase, and again, the more basic imidazolates correspond to more favorable carbon dioxide complexation.

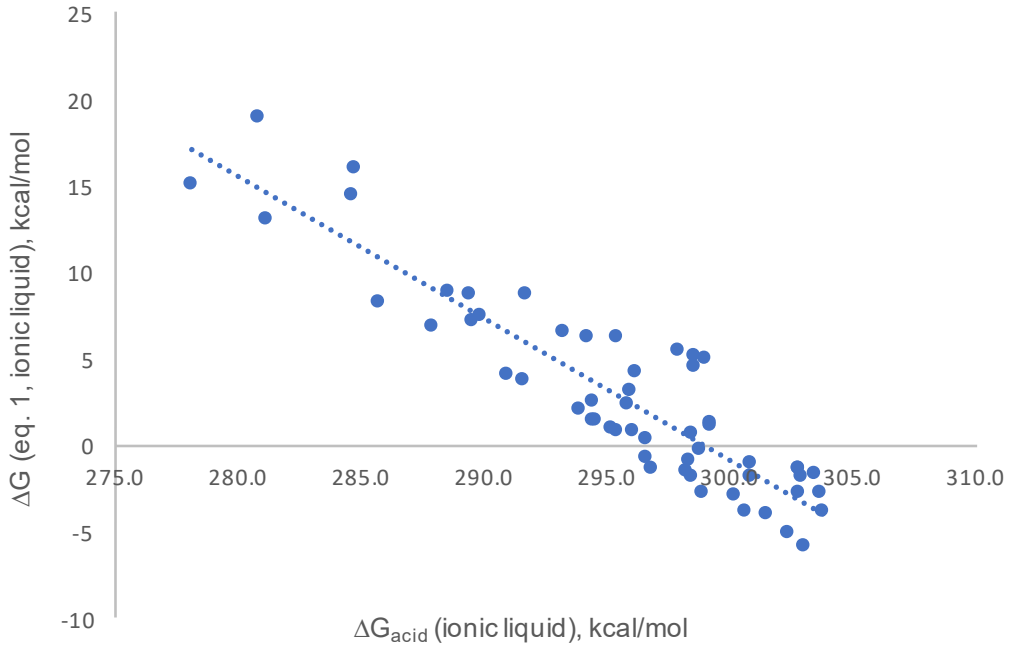

Figure 3. 6 Relationship between ΔG_{rxn} for equation 1 and $\Delta G_{acid,\ calc}$ of imidazoles in ionic liquid.

As noted earlier when we discussed imidazole acidity, the more basic imidazolates are generally substituted with more electron donating groups, such as alkyl substituents. One other observation is that substitution on the 2-position renders the addition of CO_2 less exergonic than substitution on the 4-position (CO_2 adducts shown in Figure 6). Table 3.6 lists imidazole pairs that have the same substituent, but on the 2-position versus the 4-position. The calculated ΔG_{rxn} for the addition of carbon dioxide in ionic liquid is also listed for each pair. The imidazolates that produce 4-substituted CO_2 adducts all have a more exergonic reaction than the 2-substituted analogs. This is consistent with experimental observations; 2-substituted imidazole-based ILs have generally lower CO_2 capacities than 4-substituted ILs.[31] One preliminary theory concerning this difference in reactivity was proposed by Zhu and coworkers, who noted that a substituent on the 2-position could present steric hindrance to the addition of carbon dioxide to the adjacent nitrogen anion.[31] Steric effects are typically kinetic, but our calculations indicate that there is a thermochemical preference for the formation of CO_2 adducts with the substituent at the 4-position. The issue is most probably also steric; an adduct with carbon dioxide would certainly be expected to be more sterically crowded and less stable with substitution on the 2-position versus the 4-position (Figure 3.7).

Table 3. 6 Calculated (B3LYP/6-31++G(d,p) ΔG_{rxn} for CO_2 addition for 2-substituted and 4-substituted imidazole pairs, in ionic liquid.

functional group	2-substituted structure	4-substituted structure	Is 2-substituted or 4-substituted more exergonic?

	number/ΔG for CO_2 addition, in IL	number/ΔG for CO_2 addition, in IL	
$–SO_2Cl$	**5**/+18.8 kcal/mol	**4**/+8.2 kcal/mol	4-substituted
$–NO_2$	**10**/+15.9 kcal/mol	**6**/+6.8 kcal/mol	4-substituted
–CN	**12**/+7.1 kcal/mol	**13**/+3.7 kcal/mol	4-substituted
$–CF_3$	**18**/+8.6 kcal/mol	**19**/+2.0 kcal/mol	4-substituted
$–CH_3$	**56**/–2.8 kcal/mol	**54**/–5.2 kcal/mol	4-substituted

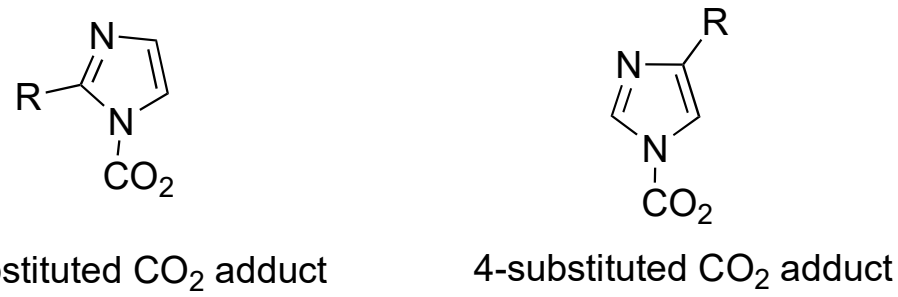

Figure 3. 7 Structures for the 2-substituted CO_2 adduct, and the 4-substituted CO_2 adduct.

Overall, our results are consistent with prior work also showing correlations between basicity of the nucleophile, and CO_2 complexation in ionic liquids.[1,13,15,16,18-30] Furthermore, Firaha, Hollóczki, and Kirchner observed that if the computed OCO angle (in a solvent dielectric of 15) is less than 140˚, then chemical absorption (nucleophilic reaction between the anion and carbon dioxide) is likely.[27] We do find that the OCO angle in ionic liquids is calculated to be less than 140˚ for all our substrates (detailed data in SI). These authors

also predict that promising anions for IL capture have calculated ΔG_{rxn} values (in a medium of dielectric 15) ranging from roughly -7 to +4 kcal/mol. As can be seen in Figure 5, should this prediction be valid, many of the imidazolates described herein are promising candidates for carbon dioxide capture.

Ultimately, our study is the first to examine a wide range of imidazolates, with experimental gas phase measurements that indicate the accuracy of the calculations. Carbon dioxide capture and storage is a matter of urgency, and our data herein will help in the understanding of the relationship between basicity of imidazolates and chemical absorption of imidazolate-containing ILs.

3.4 Conclusions

In this work, fifty-six imidazoles are examined both computationally and experimentally. These data are relevant for the improved design and tuning of anion-based ionic liquids for carbon dioxide capture. The measurements are the first for these substrates, and benchmark the calculations. A linear correlation is found between imidazole acidity and the free energy of reaction for anion-CO2 association, which is improved when an ionic liquid computational model is used. The results show the tunability of imidazolates for carbon dioxide capture.

3.5 References

(1) Cui, G.; Wang, J.; Zhang, S. Active Chemisoprtion Sites in Functionalized Ionic Liquids for Carbon Capture. *Chemical Society Reviews* **2016**, *45*, 4307-4339.

(2) Bates, E. D.; Mayton, R. D.; Ntai, I.; Davis, J. H., Jr. CO_2 Capture by a Task-Specific Ionic Liquid. *J. Am. Chem. Soc.* **2002**, *124*, 926-927.

(3) Boot-Handford, M. E.; Abanades, J. C.; Anthony, E. J.; Blunt, M. J.; Brandani, S.; Mac Dowell, N.; Fernández, J. R.; M.-C., F.; Gross, R.; Hallett, J. P.; Haszeldine, R. S.; Heptonstall, P.; Lyngfelt, A.; Makuch, Z.; Mangano, E.; Porter, R. T. J.; Pourkashaninan, M.; Rochelle, G. T.; Shah, N.; Yao, J. G.; Fennell, P. S. Carbon Capture and Storage Update. *Energy Environ. Sci.* **2014**, *7*, 130-189.

(4) MacDowell, N.; Florin, N.; Buchard, A.; Hallett, J.; Galindo, A.; Jackson, G.; Adjiman, C. S.; Williams, C. K.; Shah, N.; Fennell, P. An Overview of CO_2 Capture Technologies. *Energy Environ. Sci.* **2010**, *3*, 1645-1669.

(5) Yang, Z.-Z.; Zhao, Y.-N.; He, L.-N. CO_2 Chemistry: Task-Specific Ionic Liquids for CO_2 Capture/Activation and Subsequent Conversion. *RSC Adv.* **2011**, *1*, 545-567.

(6) Bara, J. E.; Camper, D. E.; Gin, D. L.; Noble, R. D. Room-Temperature Ionic Liquids and Composite Materials: Platform Technologies for CO_2 Capture. *Acc. Chem. Res.* **2010**, *43*, 152-159.

(7) Huang, J.; Rüther, T. Why are Ionic Liquids Attractive for CO_2 Absoprtion? An Overvew. *Aust. J. Chem.* **2009**, *62*, 298-308.

(8) Zhao, Z.; Dong, H.; Zhang, X. The Research Progress of CO_2 Capture with Ionic Liquids. *Chin. J. Chem. Eng.* **2012**, *20*, 120-129.

(9) Zhang, X.; Zhang, X.; Dong, H.; Zhao, Z.; Zhang, S.; Huang, Y. Carbon Capture with Ionic Liquids: Overview and Progress. *Eng. Environ. Sci.* **2012**, *5*, 6668-6681.

(10) Ramdin, M.; de Loos, T. W.; Vlugt, T. J. H. State-of-the-Art of CO_2 Capture with Ionic Liquids. *Ind. Eng. Chem. Res.* **2012**, *51*, 8149-8177.

(11) Zhang, J.; Zhang, S.; Dong, K.; Zhang, Y.; Shen, Y.; Lv, X. Supported Absorption of CO_2 by Tetrabutylphosphonium Amino Acid Ionic Liquids. *Chem. Eur. J.* **2006**, *12*, 4021-4026.

(12) Zhang, Y.; Zhang, S.; Lu, X.; Zhou, Q.; Fan, W.; Zhang, X. Dual Amino-Functionalised Phosphonium Ionic Liquids for CO_2 Capture. *15* **2009**, 3003-3011.

(13) Wang, C.; Luo, X.; Luo, H.; Jiang, D.-e.; Li, H.; Dai, S. Tuning the Basicity of Ionic Liquids for Equimolar CO_2 Capture. *Angew. Chem. Int. Ed.* **2011**, *50*, 4918-4922.

(14) Gutowski, K. E.; Maginn, E. J. Amine-Functionalized Task-Specific Ionic Liquids: A Mechanistic Explanation for the Dramatic Increase in Viscosity upon Complexation with CO_2 from Molecular Simulation. *J. Am. Chem. Soc.* **2008**, *130*, 14690-14704.

(15) Wang, C.; Luo, H.; Jiang, D.-e.; Li, H.; Dai, S. Carbon Dioxide Capture by Superbase-Derived Protic Ionic Liquids. *Angew. Chem. Int. Ed.* **2010**, *49*, 5978-5981.

(16) Seo, S.; Quiroz-Guzman, M.; DeSilva, M. A.; Lee, T. B.; Huang, Y.; F., G. B.; Schneider, W. F.; Brennecke, J. F. Chemically Tunable Ionic Liquids with Aprotic Heterocyclic Anion (AHA) for CO2 Capture. *J. Phys. Chem. B* **2014**, *118*, 5470-5751.

(17) Seo, S.; DeSilva, M. A.; Xia, H.; Brennecke, J. F. Effect of Cation on Physical Properties and CO_2 Solubility for Phosphonium-Based Ionic Liquids with 2-Cyanopyrrolide Anions. *J. Phys. Chem. B* **2015**, *119*, 11807-11814.

(18) Gurkan, B.; F., G. B.; Mindrup, E. M.; Ficke, L. E.; Massel, M.; Seo, S.; Senftle, T. P.; Wu, H.; Glaser, M. F.; Shah, J. K.; Maginn, E. J.; Brennecke, J. F.; Schneider, W. F. Molecular Design of High Capacity, Low Viscosity, Chemically Tunable Ionic Liquids for CO_2 Capture. *J. Phys. Chem. Lett.* **2010**, *1*, 3494-3499.
(19) Lei, X.; Xu, Y.; Zhu, L.; Wang, X. Highly Efficient and Reversible CO_2 Capture through 1,1,3,3-Tetramethylguanidinium Imidazole Ionic Liquid. *RSC Adv.* **2014**, *4*, 7052-7057.
(20) Wang, C.; Luo, X.; Zhu, X.; Cui, G.; Jiang, D.-e.; Deng, D.; Li, H.; Dai, S. The Strategies for Improving Carbon Dioxide Chemisorption by Functionalized Ionic Liquids. *RSC Adv.* **2013**, *3*, 15518-15527.
(21) Wang, Z.; Wang, F.; Xue, X.-S.; Ji, P. Acidity Scale of N-Heterocyclic Carbene Precursors: Can We Predict the Stability of NHC−CO_2 Adducts? *Org. Lett.* **2018**, *20*, 6041-6045.
(22) Gao, F.; Wang, Z.; Ji, P.; Cheng, J.-P. CO_2 Absorption by DBU-Based Protic Ionic Liquids: Basicity of Anion Dictates the Absorption Capacity and Mechanism. *Frontiers in Chemistry* **2019**, *6*, 658.
(23) Wang, C.; Luo, H.; Li, H.; Zhu, X.; Yu, B.; Dai, S. Tuning the Physicochemical Properties of Diverse Phenolic Ionic Liquids for Equimolar CO_2 Capture by the Substituent on the Anion. *Chem. Eur. J.* **2012**, *18*, 2153-2160.
(24) Venkatraman, V.; Gupta, M.; Foscato, M.; Svendsen, H. F.; Jensen, V. R.; Alsberg, B. K. Computer-aided molecular design of imidazole-based absorbents for CO_2 capture. *Int. J. Greenhouse Gas Control* **2016**, *49*, 55-63.
(25) Zhao, T.; Zhang, X.; Tu, Z.; Wu, Y.; Hu, X. Low-viscous Diamino Protic Ionic Liquids with Fluorine-Substituted Phenolic Anions for Improving CO_2 Reversible Capture. *J. Mol. Liq.* **2018**, *268*, 617-624.
(26) Vijayraghavan, R.; Pas, S. J.; Izgorodina, E. I.; MacFarlane, D. R. Diamino Protic Ionic Liquids for CO_2 Capture. *Phys. Chem. Chem. Phys.* **2013**, *15*, 19994-19999.
(27) Firaha, D. S.; Hollóczki, O.; Kirchner, B. Computer-Aided Design of Ionic Liquids as CO_2 Absorbents. *Angew. Chem. Int. Ed.* **2015**, *54*, 7805-7809.
(28) Sudha, S. Y.; Khanna, A. Evaluating the Interactions of CO_2-Ionic Liquid Systems through Molecular Modeling. *World Acad. Sci., Eng. Tech. Int. J. Chem. Molec. Eng.* **2009**, *3*, 524-527.
(29) Bhargava, B. L.; Balasubramanian, S. Insights into the Structure and Dynamics of a Room-Temperature Ionic Liquid: Ab Initio Molecular Dynamics Simulation Studies of 1-*n*-Butyl-3-methylimidazolium Hexafluorophosphate ([bmim][PF_6]) and the [bmim][PF_6]-CO_2 Mixture. *J. Phys. Chem. B* **2007**, *111*, 4477-4487.
(30) Ren, S.; Hou, Y.; Tian, S.; Chen, X.; Wu, W. What are Functional Ionic Liquids for the Absorption of Acidic Gases? *J. Phys. Chem. B* **2013**, *117*, 2482-2486.
(31) Zhu, X.; Song, M.; Xu, Y. DBU-Based Protic Ionic Liquids for CO_2 Capture. *ACS Sustainable Chem. Eng.* **2017**, *5*, 8192-8198.
(32) We note that Alsberg and coworkers (Venkatraman, V.; Gupta, M.; Foscato, M.; Svendsen, H. F.; Jensen, V. R.; Alsberg, B. K. Computer-aided Molecular Design of Imidazole-based Absorbents for CO_2 Capture. *Int. J. Greenhouse Gas Control* **2016**, *49*, 55-63) calculated and measured the pK_a in water of a series of imidazoles; while we cannot compare our values directly with theirs, since we did not calculate pK_a, we do find a clear linear relationship between his pK_a values and our ΔG_{acid} values in ionic liquid (plot in SI). .

(33) Kaljurand, I.; Koppel, I. A.; Kutt, A.; Room, E.-I.; Rodima, R.; Koppel, I.; Mishima, M.; Leito, I. *J. Phys. Chem. A* **2007**, *111*, 1245-1250.
(34) Pan, M.; Cao, N.; Lin, W.; Luo, X.; Chen, K.; Che, S.; Li, H.; Wang, C. Reversible CO_2 Capture by Conjugated Ionic Liquids through Dynamic Covalent Carbon-Oxygen Bonds. *ChemSusChem* **2016**, *9*, 2351-2357.
(35) Luo, X.; Guo, Y.; Ding, F.; Zhao, H.; Cui, G.; Li, H.; Wang, C. Significant Improvements in CO_2 Capture by Pyridine-Containing Anion-Functionalized Ionic Liquids through Multiple-Site Cooperative Interactions. *Angew. Chem. Int. Ed.* **2014**, *53*, 7053-7057.
(36) Kurinovich, M. A.; Lee, J. K. The Acidity of Uracil from the Gas Phase to Solution: The Coalescence of the N1 and N3 Sites and Implications for Biological Glycosylation. *J. Am. Chem. Soc.* **2000**, *122*, 6258-6262.
(37) Liu, M.; Xu, M.; Lee, J. K. The Acidity and Proton Affinity of the Damaged Base 1,N^6-Ethenoadenine in the Gas Phase versus in Solution: Intrinsic Reactivity and Biological Implications. *J. Org. Chem.* **2008**, *73*, 5907-5914.
(38) Sharma, S.; Lee, J. K. The Acidity of Adenine and Adenine Derivatives and Biological Implications. A Computational and Experimental Gas Phase Study. *J. Org. Chem.* **2002**, *67*, 8360-8365.
(39) Sharma, S.; Lee, J. K. Gas Phase Acidity Studies of Multiple Sites of Adenine and Adenine Derivatives. *J. Org. Chem.* **2004**, *69*, 7018-7025.
(40) Kurinovich, M. A.; Phillips, L. M.; Sharma, S.; Lee, J. K. The Gas Phase Proton Affinity of Uracil: Measuring Multiple Basic Sites and Implications for the Enzyme Mechanism of Orotidine 5'-Monophosphate Decarboxylase. *Chem. Comm.* **2002**, 2354-2355.
(41) Kurinovich, M. A.; Lee, J. K. The Acidity of Uracil and Uracil Analogs in the Gas Phase: Four Surprisingly Acidic Sites and Biological Implications. *J. Am. Soc. Mass Spectrom.* **2002**, *13*, 985-995.
(42) Liu, M.; Li, T.; Amegayibor, F. S.; Cardoso, D. S.; Fu, Y.; Lee, J. K. Gas-Phase Thermochemical Properties of Pyrimidine Nucleobases. *J. Org. Chem.* **2008**, *73*, 9283-9291.
(43) Zhachkina, A.; Liu, M.; Sun, X.; Amegayibor, F. S.; Lee, J. K. Gas Phase Thermochemical Properties of the Damaged Base O^6-Methylguanine versus Adenine and Guanine. *J. Org. Chem.* **2009**, *74*, 7429-7440.
(44) Sun, X.; Lee, J. K. The Acidity and Proton Affinity of Hypoxanthine in the Gas Phase versus in Solution: Intrinsic Reactivity and Biological Implications. *J. Org. Chem.* **2007**, *72*, 6548-6555.
(45) Chesnavich, W. J.; Su, T.; Bowers, M. T. Collisions in a Noncentral Field: A Variational and Trajectory Investigation of Ion-Dipole Capture. *J. Chem. Phys.* **1980**, *72*, 2641-2655.
(46) Su, T.; Chesnavich, W. J. Parametrization of the Ion-Polar Molecule Collision Rate Constant by Trajectory Calculations. *J. Chem. Phys.* **1982**, *76*, 5183-5185.
(47) Lee, C.; Yang, W.; Parr, R. G. Development of the Colle-Salvetti Correlation-Energy Formula into a Functional of the Electron Density. *Phys. Rev. B* **1988**, *37*, 785-789.
(48) Becke, A. D. Density-Functional Thermochemistry. III. The Role of Exact Exchange. *J. Chem. Phys.* **1993**, *98*, 5648-5652.

(49) Becke, A. D. A New Mixing of Hartree-Fock and Local Density-Functional Theories. *J. Chem. Phys.* **1993**, *98*, 1372-1377.
(50) Stephens, P. J.; Devlin, F. J.; Chabalowski, C. F.; Frisch, M. J. Ab Initio Calculation of Vibrational Absorption and Circular-Dichroism Spectra Using Density-Functional Force-Fields. *J. Phys. Chem.* **1994**, *98*, 11623-11627.
(51) Gaussian16, Rev. B.01; Frisch, M. J.; Trucks, G. W.; Schlegel, H. B.; Scuseria, G. E.; Robb, M. A.; Cheeseman, J. R.; Scalmani, G.; Barone, V.; Petersson, G. A.; Nakatsuji, H.; Li, X.; Caricato, M.; Marenich, A. V.; Bloino, J.; Janesko, B. G.; Gomperts, R.; Mennucci, B.; Hratchian, H. P.; Ortiz, J. V.; Izmaylov, A. F.; Sonnenberg, J. L.; Williams-Young, D.; Ding, F.; Lipparini, F.; Egidi, F.; Goings, J.; Peng, B.; Petrone, A.; Henderson, T.; Ranasinghe, D.; Zakrzewski, V. G.; Gao, J.; Rega, N.; Zheng, G.; Liang, W.; Hada, M.; Ehara, M.; Toyota, K.; Fukuda, R.; Hasegawa, J.; Ishida, M.; Nakajima, T.; Honda, Y.; Kitao, O.; Nakai, H.; Vreven, T.; Throssell, K.; Montgomery, J. A., Jr.; Peralta, J. E.; Ogliaro, F.; Bearpark, M. J.; Heyd, J. J.; Brothers, E. N.; Kudin, K. N.; Staroverov, V. N.; Keith, T. A.; Kobayashi, R.; Normand, J.; Raghavachari, K.; Rendell, A. P.; Burant, J. C.; Iyengar, S. S.; Tomasi, J.; Cossi, M.; Millam, J. M.; Klene, M.; Adamo, C.; Cammi, R.; Ochterski, J. W.; Martin, R. L.; Morokuma, K.; Farkas, O.; Foresman, J. B.; Fox, D. J., Gaussian, Inc., Wallingford CT, 2016.
(52) Bernales, V. S.; Marenich, A. V.; Contreras, R. H.; Cramer, C. J.; Truhlar, D. G. Quantum Mechanical Continuum Solvation Models for Ionic Liquids. *J. Phys. Chem. B* **2012**, *116*, 9122-9129.

Chapter 4 Charge-Tagged *N*-heterocyclic Carbene Catalysts

4.1 Introduction

Since the first reports of isolable, stable N-heterocyclic carbenes (NHCs) nearly three decades ago, these intriguing species have come to the forefront as important players in organic catalysis. NHCs serve as both ligands for organometallic catalysts as well as catalysts in their own right, more prominently as nucleophilic species in *Umpolung* chemistry, but also as Brønsted bases in organic transformations.

Both NHCs and tricyclohexylphosphine (PCy_3) are ligands for ruthenium catalysts used in the Grubbs olefin metathesis (Figure 4.1).[1] First generation catalysts utilized PCy_3 as ligands; second generation catalysts introduced NHC ligands that were dominated by the imidazolylidene framework. The unique features of these neutral two-electron-donors with steric demands of bulky groups, are more effective than the first generation. The increased effectiveness of the catalysts with NHC ligands might also be attributed to the higher basicity of the NHC compared to PCy_3.

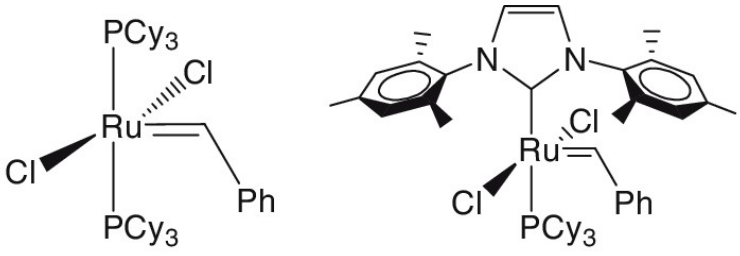

Figure 4. 1 The 1st and 2nd generations of Grubbs catalysts

Most reactions in organic synthesis can be generalized as the reaction of a nucleophile (electron donor, d) with an electrophile (electron acceptor, a). The *Umpolung* (polarity inversion) of the intrinsic reactivity of a functional group starts a new chapter in organic

synthesis. *Umpolung* is the chemical modification of a functional group with the aim of polarity reversal, which allows further reactions of this functional group that would otherwise not be available. Catalysts such as N-Heterocyclic Carbenes (NHCs) have been using to achieve *Umpolung* of electrophilic aldehydes. These aldehydes are converted to nucleophiles to react with aromatic aldehydes (benzoin condensation) or with appropriate Michael acceptors (Stetter reaction). Since Ukai and coworkers, dating back to 1943, discovered the ability of thiazolium salts to catalyze benzoin condensation (Figure 4.2), a wide variety of chiral and achiral thiazolylidene catalysts, generated in situ from thiazolium salts, have been developed to catalyze *Umpolung* reactions.[2,3]

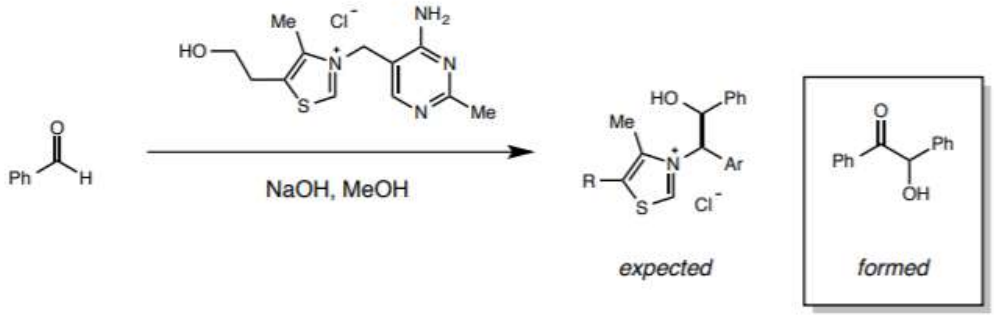

Figure 4. 2 The first benzoin condensation catalyzed by thiazolium salts instead of cyanide

In recent years, triazolylidene carbenes, instead of thiazolylidene or imidazolylidene carbenes, appeared in more and more organocatalysis-based researches. Enders and Teles first reported a triazolylidene-catalyzed asymmetric Stetter reaction in their seminal report in 1995, laying the foundation from which many more group stepped into this research field.[4-7]

Despite the importance of NHCs in catalysis, the measurement and study of NHC properties, to achieve an improved understanding of these species, as well as to increase understanding of catalytic mechanisms and to produce better catalysts, are surprisingly limited.[8] As mentioned above in **1.1.1**, Breslow and coworkers proposed a catalytic mechanism with the thiazolylidene as the catalytic species. The Breslow mechanism is commonly accepted for the benzoin condensation. Many attempts over the years to isolate the Breslow intermediate turned out to be elusive until 2012, when both a nitrogen analogue and the intermediate itself were observed and characterized spectroscopically. Lemal and Castells also proposed different mechanisms that both involved a thiazolylidene dimer, which have witnessed reported data both for and against these mechanisms.[9] On the other hand, there is even less mechanistic work existing for the Stetter reaction. The mechanism is generally assumed to be similar to that of the benzoin, as they share the same first step (NHC addition to aldehyde).

Our group has been working on elucidating mechanisms of *Umpolung* reactions using gas-phase studies with tools such as mass spectrometric measurement and quantum mechanical computation. Previous work by our group involved using two charge tagged thiazolylidene catalysts (Figure 4.3) to study *Umpolung* reaction mechanisms in the gas phase.[10,11]

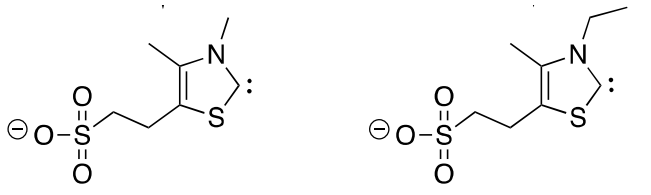

Figure 4. 3 Charge-tagged NHC catalysts designed and synthesized in our group

When we tried to use these charged thiazolylidene catalysts to "fish out" Breslow intermediate of Stetter reaction in the gas phase using mass spectrometry, however, no ion signals corresponding to the first addition product was found. We hypothesized that the formation of Breslow intermediate required an intramolecular 1,2-proton transfer, which required a too high barrier to overcome in gas-phase. In solution phase, this proton transfer can be assisted by solvent molecules. In order to test our hypothesis, we designed a sila-Breslow intermediate using an acylsilane in place of the original aldehyde to overcome the barrier of 1,2-transfer via a Brook rearrangement.[12] The peak of sila-Breslow intermediate was successfully observed which supported our hypothesis. However, the unfavorable intramolecular proton-transfer problem remains unsolved.

To further tackle this problem, two novel charge-tagged triazolylidene catalysts (**11a-anion** and **11b-anion**, as shown in Figure 4.4) designed by Dr. Tom Rovis' group attracted our attention.

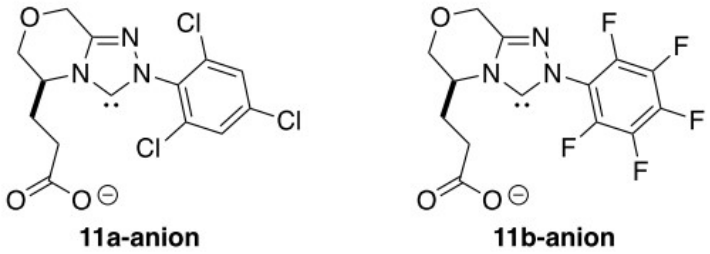

Figure 4. 4 Two novel charge-tagged triazolylidene catalysts

We are also interested in two commercially available charge-tagged NHC catalysts (imidazolylidene **6a-anion** and thiazolylidene **6b-anion**), as shown in Figure 4.5.

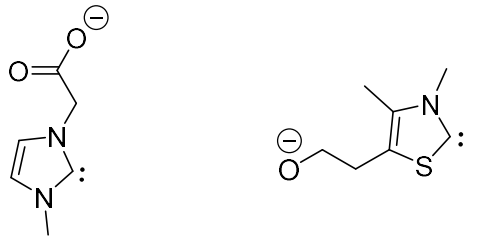

Figure 4. 5 Two commercially available charge-tagged NHC catalysts

The charge-tagged carboxylate/alkoxide groups would not only be able to make relevant species detectable via mass spectrometry, but also potentially serve as proton shuttles to effect the 1,2-proton transfer and the subsequent formation of Breslow intermediate, as shown in Figure 4.6. In addition, these new charged NHC catalysts will enable us to compare the intrinsic catalytic reactivities among triazolylidene, imidazolylidene and thiazolylidene frameworks of NHC catalysts.[13]

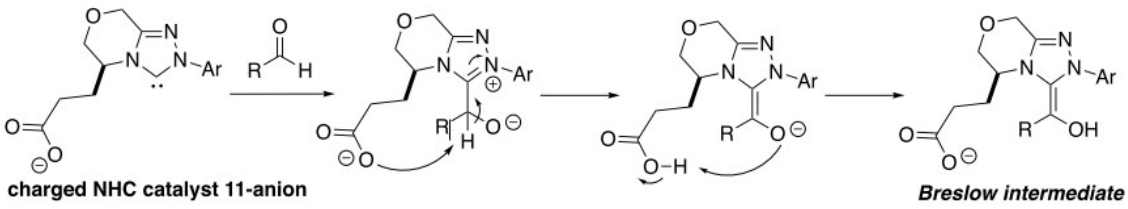

Figure 4. 6 Proposed pathway of the Breslow intermediate formation aided by charge-tagged NHC catalysts

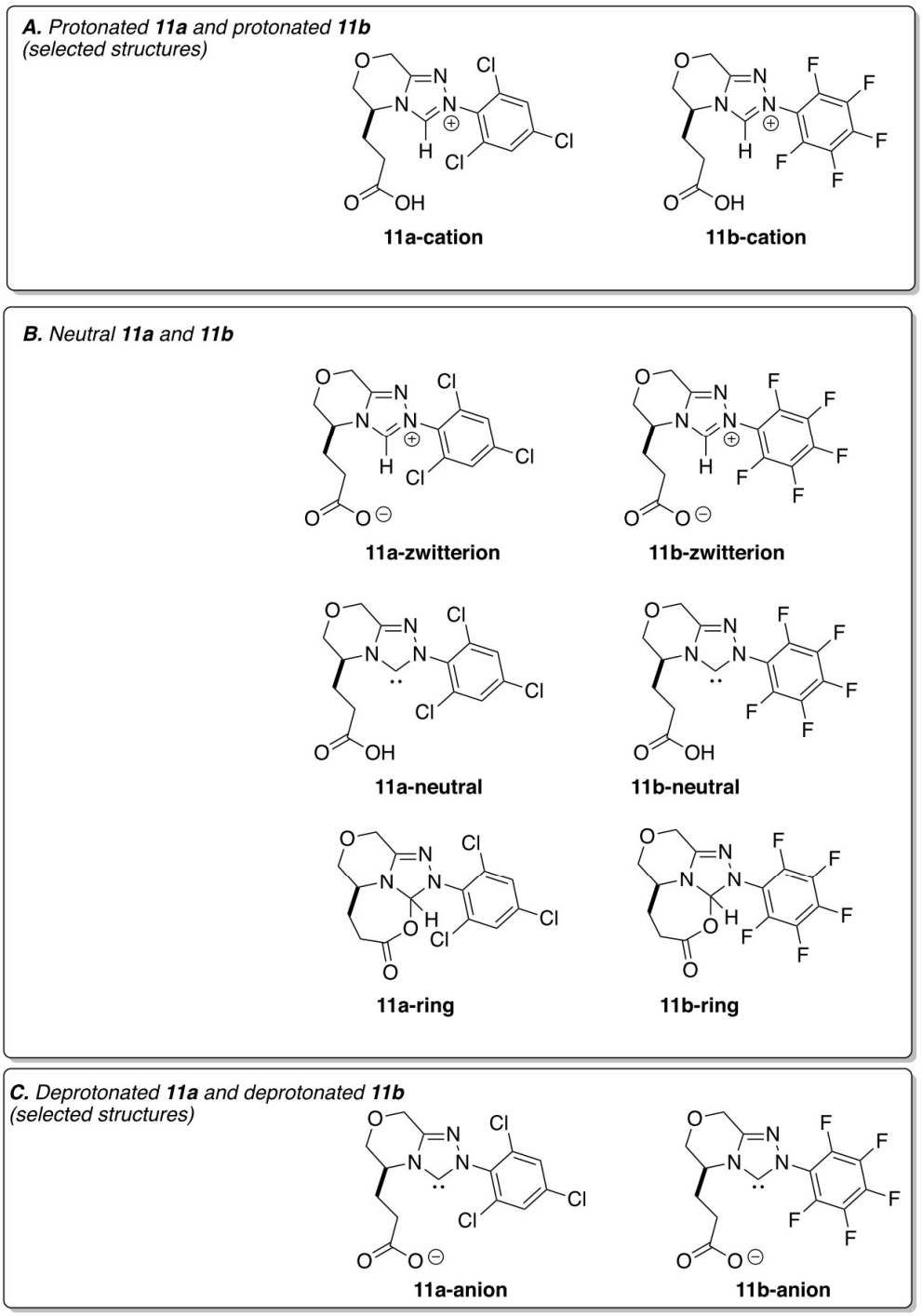

Figure 4. 7 Related species of charge-tagged triazolylidene catalysts

The relative stability in both gas phase and solution phase, as well as their fundamental thermodynamic properties such as acidity and proton affinity, of the related species of these

NHC catalysts, including their cationic, anionic and neutral configurations, are of great importance to better understanding the reaction mechanisms catalyzed by these catalysts, and to better utilizing these catalysts in various *Umpolung* reactions. Such fundamental properties for the related species of charge-tagged triazolylidene catalysts (Figure 4.7), have been previously obtained by our group.[14] In order to practically apply such NHC catalysts in the solution phase syntheses, it is important to confirm the most stably-existed structures of such charged NHCs in the solution phase. Based on our calculation results, the triazolium salt (precatalyst) goes through 1st and 2nd deprotonations by bases (e.g. KHMDS) to form the negatively-charged carbene catalyst (**11b-anion**, Figure 4.8).

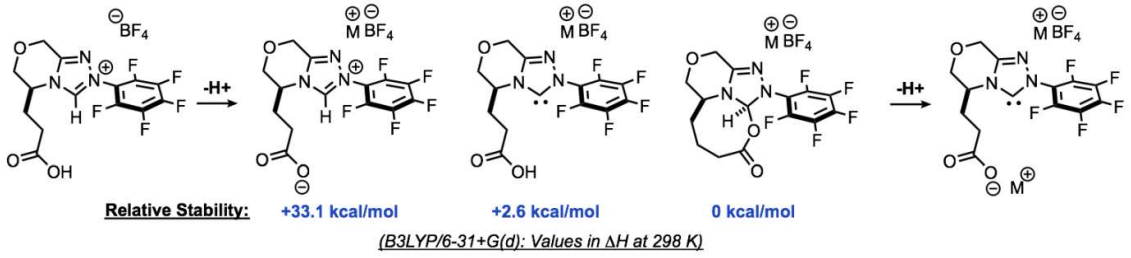

Figure 4. 8 Triazolium precatalyst goes through 1st and 2nd deprotonations by bases to form the negatively-charged carbene catalyst

While the charge-tagged triazolylidene catalysts were tested in the solution phase reactions, however, it was found that these catalysts decomposed which resulted in poor yields. In this chapter, we will report 1) theoretical calculations we used to study the possible pathways for the charge-tagged triazolylidene catalysts decomposition; and 2) computational and experimental characterizations of the fundamental properties of the two commercially available charge-tagged NHC catalysts (imidazolylidene **6a-anion** and thiazolylidene **6b-anion**).

4.2 Experimental

4.2.1 Calculation

All ground state and transition state calculations were performed using density functional theory (B3LYP/6-31+G(d)) as implemented in Gaussian 09 and Gaussian 16. All the geometries were fully optimized, and the frequencies were calculated; no scaling factor was applied. The optimized structures had no negative frequencies. The temperature for the calculations was set to be 298 K.

4.2.2 LCQ Bracketing Method

The commercially available precatalysts (5-(2-Hydroxyethyl)-3,4-dimethylthiazolium iodide and 1-carboxymethyl-3-methylimidazolium chloride) for the two charge-tagged NHC catalysts (imidazolylidene **6a-anion** and thiazolylidene **6b-anion**) were purchased and measured without further purification.

Gas-phase acidities of protonated 6a(b) were first measured by the bracketing method using a modified Finnigan LCQ ESI-3D ion trap mass spectrometer, as described in Chapter 1. We used calculational method as a guiding tool to choose a series of neutral reference bases with known proton affinities. The neutral reference bases were leaked into the ion trap with helium buffer gas flow through the house-modified cross inlet. The precatalysts of the charge-tagged NHCs were dissolved in methanol solution with a concentration of 0.1 mM, before they were injected in ESI. An ESI solution flow rate of 20 uL/min was used. The capillary temperature was 190 °C, the spray voltage was set as 4.5 kV, and the positive ion mode was used to analyze the cations. The protonated 6a(b) cation was isolated via MS/MS and was allowed to react with neutral reference bases for

time ranges of 0.03 - 10000 ms. The average spectra of up to 10 scans was collected. Reaction efficiency was used to assess the occurrence or non-occurrence of a proton transfer reaction between the analyte ions and the neutral reference bases. Reaction efficiency was defined as the ratio of the reaction rate constant and the theoretical ion-molecule collisional rate constant obtained from trajectory theory. Reactions that were less than 10% efficient were labeled "-" and reactions with efficiencies higher than 10% were labeled "+" in the bracketing table. All the reactions were performed under *pseudo* first-order conditions. In order to calculate the reaction rate constant, the pressure of the neutral bases had to be measured. We used a fast control reaction in which proton transfers from a weak base to a neutral reference base (assumed to be 100% efficient), to "back out" the reference base pressure.

4.2.3 Cooks Kinetic Method

The Cooks kinetic method was also used to study the gas-phase acidity of protonated 6a(b). A Finnigan LCQ DUO ESI-3D ion trap mass spectrometer was used to conduct Cooks kinetic experiments, as described in Chapter 1. The proton-bound dimer between an analyte and a reference base was dissociated via collision-induced dissociation (CID), and either the protonated analyte cation or the protonated reference base ion was formed (Eq. 4.1, where "A-H + " is the protonated 6a(b) cation in this case, and "B_i " stands for a series of reference bases). The ratio of these two products yielded the relative proton affinities of the two compounds.

$$AH^{\oplus} + B_i \xleftarrow{k_1} [A \cdots H^{\oplus} \cdots B_i] \xrightarrow{k_2} A + B_i H^{\oplus} \qquad \textbf{Eq. 4.1}$$

A solution was prepared by mixing the analyte and reference base in a 1:1 ratio in methanol with a concentration of 0.5 mM. The solution was then injected into the mass spectrometer with a flow rate of 20 uL/min and then ionized via ESI. The capillary temperature was set as 190 °C. The spray voltage was set to be 4.5 kV. The protonated 6a(b) cation (6a(b)-H^+), the protonated reference base, and the proton-bound dimer were detected and shown simultaneously in the full-scan mass spectrum. The proton-bound complex ion was then isolated under tandem mass spectrometry (MS/MS) and was subjected to collision-induced energy with an activation time of 30 ms. A total of 40 scans were averaged.

Data was analyzed using the Cooks "standard" and "extended" kinetic methods. Both of these methods involve acquiring ion abundance ratios at different collision energies. Different collision energies have different Teff (in Kelvin), which is the effective temperature for dissociating the proton-bound complexes. These methods allow for deconvolution of the enthalpic and entropic contributions. The analysis processes are summarized in Equations 4.2 - 4.4.

$$\ln\frac{k_1}{k_2}=\frac{[AH^{\oplus}]}{[BH^{\oplus}]} \qquad \textbf{Eq. 4.2}$$

$$\ln\frac{k_1}{k_2}=[\frac{PA(A)}{RT_{eff}}-\frac{\Delta(\Delta S)}{R}]-\frac{PA(B_i)}{RT_{eff}} \qquad \textbf{Eq.4.3}$$

$$\frac{GB^{app}(A)}{RT_{eff}}=\frac{PA(A)}{RT_{eff}}-\frac{\Delta(\Delta S)}{R} \qquad \textbf{Eq. 4.4}$$

Δ(ΔS) is the difference in the ΔS associated with the two dissociation pathways in equation 4.1. A plot of ln(k1/k2), which equals to ln([AH^+]/[BiH^+]), versus the proton affinity of a series of reference bases (PA(B_i)), yields the Teff from the slope and the GB^{app}(A) from the y-intercept (Eq. 4.3). Plotting equation 4.4 at different Teff yields the proton affinity of the unknown (PA(A)) and Δ(ΔS) for the Cooks experiments. It has been noted that the Δ(ΔS) value is related to the accuracy of the acidity measurement by the Cooks kinetic method. Ideally, the actual Δ(ΔS) value should be less than or equal to 5 kcal/mol; otherwise, the Cooks kinetic method may underestimate the measured acidity.

4.3 Results and Discussion

4.3.1 Computational Results

4.3.1.1 Reaction Energetics for the Proposed Pathways of Catalyst Decomposition

While the charge-tagged triazolylidene catalysts were tested in the solution phase Stetter reactions, it was found that 11a/b-anion might be subjected to decomposition which results in poor yields and no obvious acceleration in the reaction.[15] Two possible pathways were proposed on such decomposition (Figure 4.9).

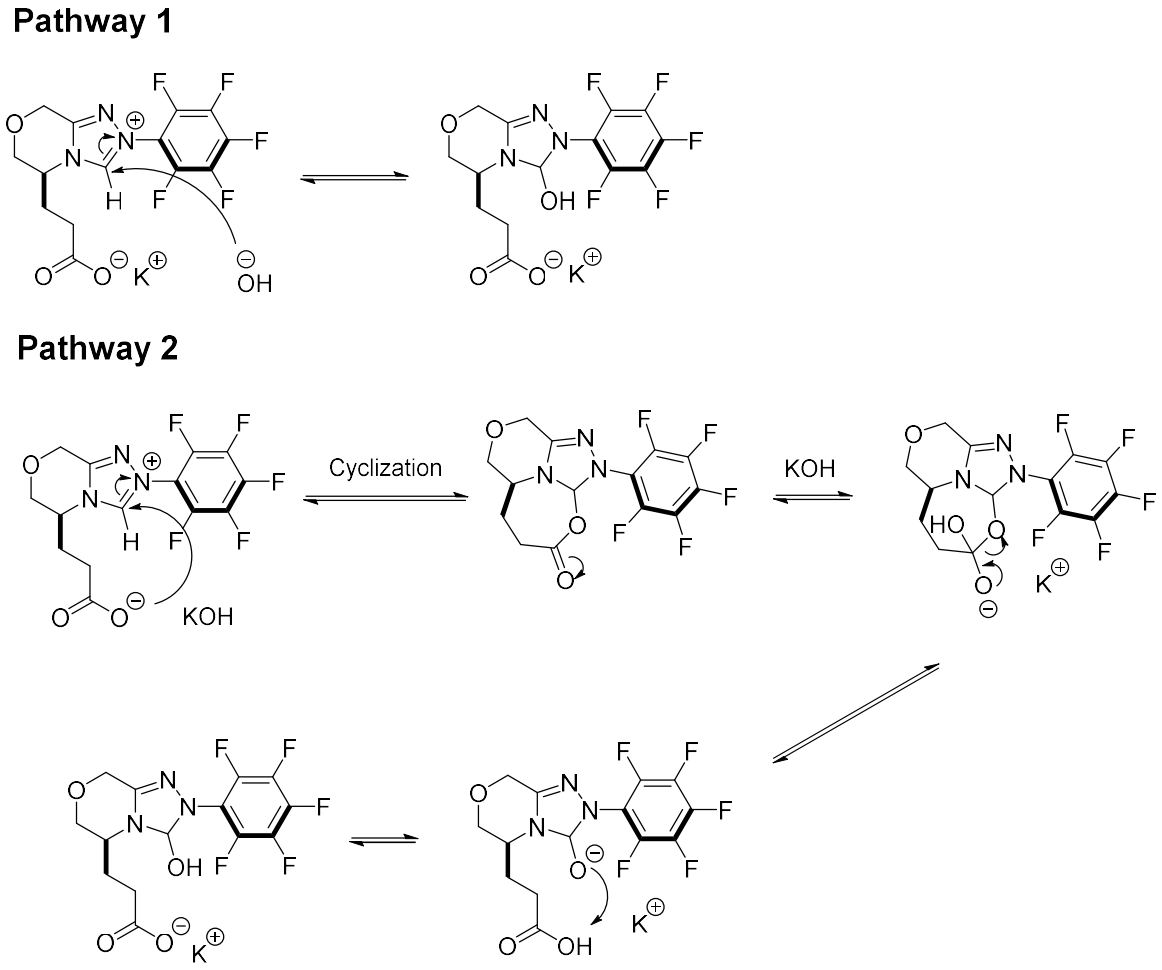

Figure 4. 9 Two proposed pathways of 11a/b decomposition

Density functional theory (DFT) calculations were employed to obtain the energetic profiles of the two proposed pathways, and the results are shown in Figure 4.10 and Figure 4.11.

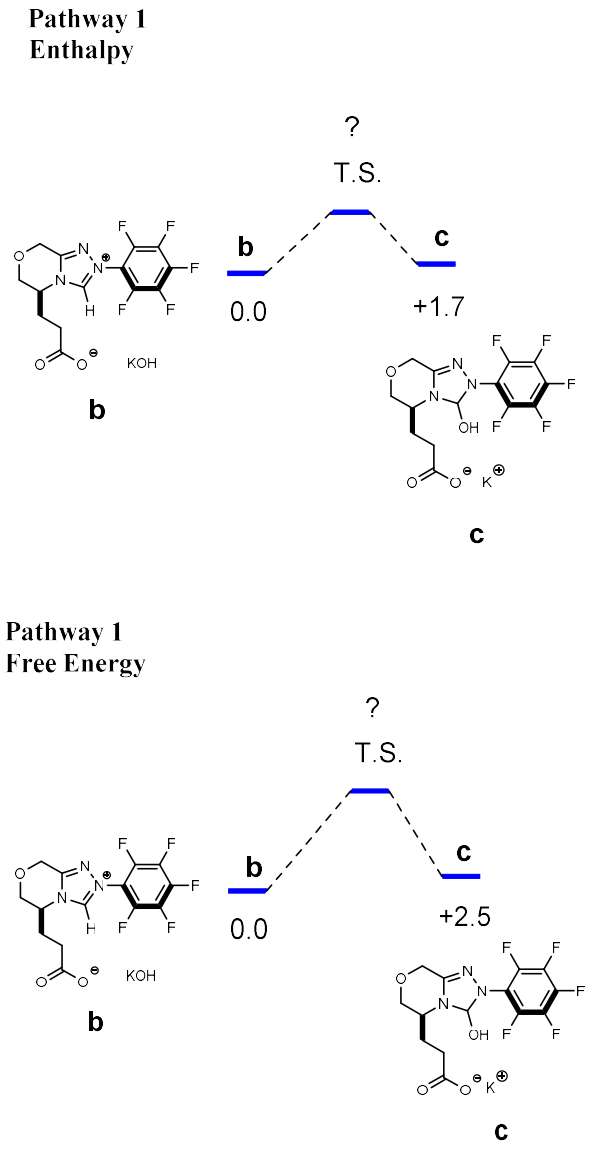

Figure 4. 10 Calculated reaction energetics for pathway 1

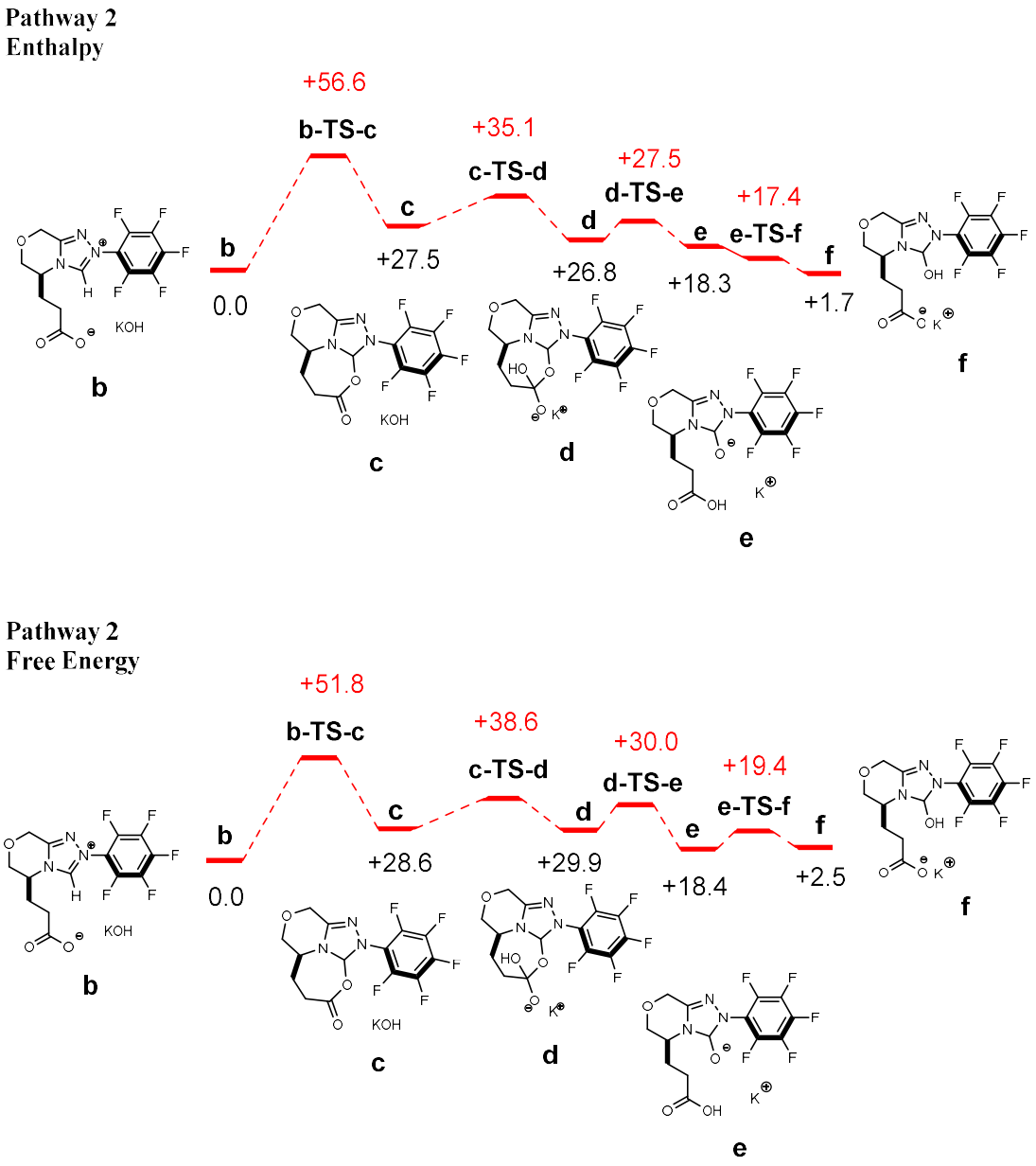

Figure 4. 11 Calculated reaction energetics for pathway 2

The energetics calculation results indicate that the 2nd decomposition pathway has pretty high energy barriers and is therefore not energetically favorable. The transition state of the 1st pathway is hard to characterize by calculations since the one-step reaction involves concerted electron transfers.

4.3.1.2 Calculations of 6a(b) and Related Species

i. Relative stability

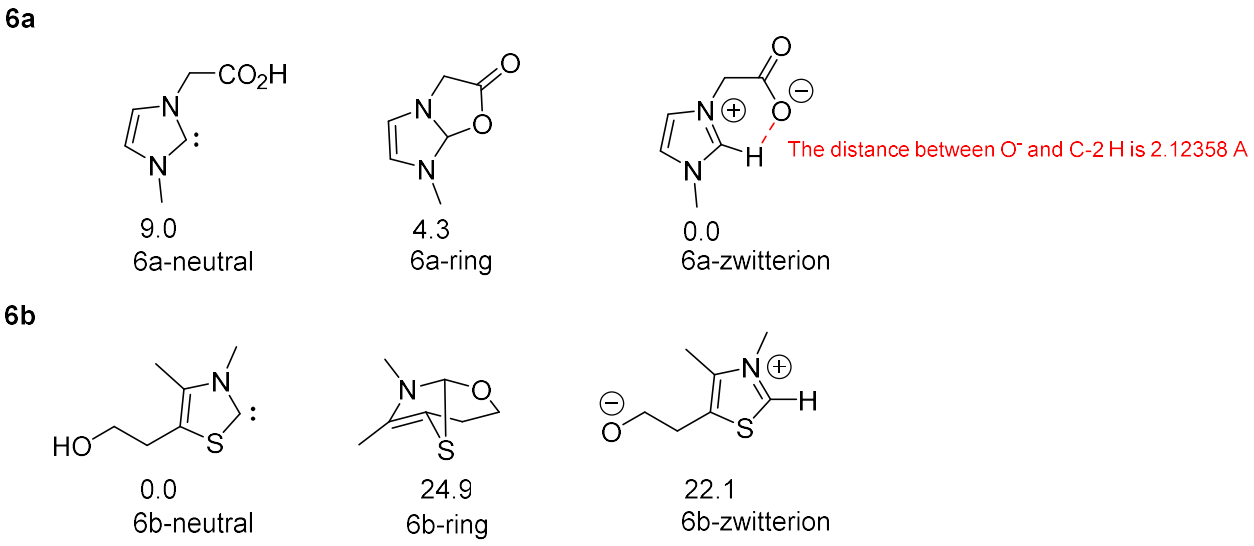

Figure 4. 12 Relative stabilities (in kcal/mol) of neutral 6a/b in the gas phase

As the neutral configuration, **6a-zwitterion** was calculated to be the most stable structure while **6b-neutral** was calculated to be the most stable among the three configurations.

It is worth noting that the distance of O^- and C-2 proton of the imidazolium ring in **6a-zwitterion** is about 2.1 Å, indicating a hydrogen bonding interaction which might stabilize this confirmation, making it the most stable among the three.

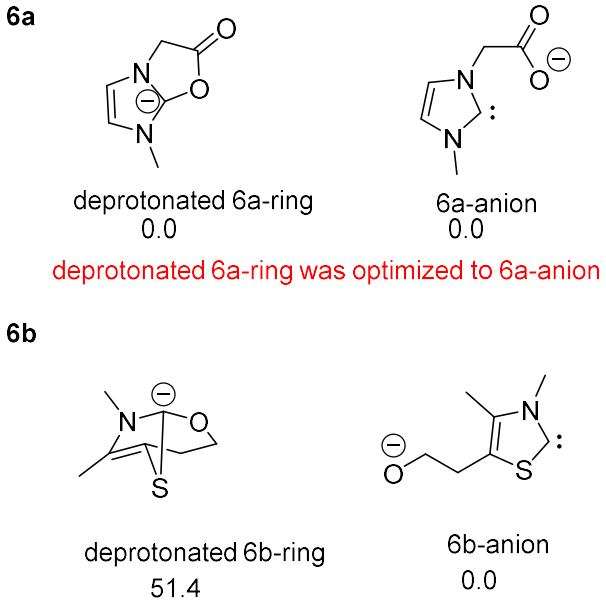

Figure 4. 13 Relative stabilities (in kcal/mol) of deprotonated 6a/b in the gas phase

The deprotonated 6a/b exist stably as negatively charged free carbene (6a/b-anion). This negatively-charged species is equipped with a reactive carbene center and a negatively charged tag, which makes it an observable NHC catalyst in mass spectrometry. The ring structures are both less stable.

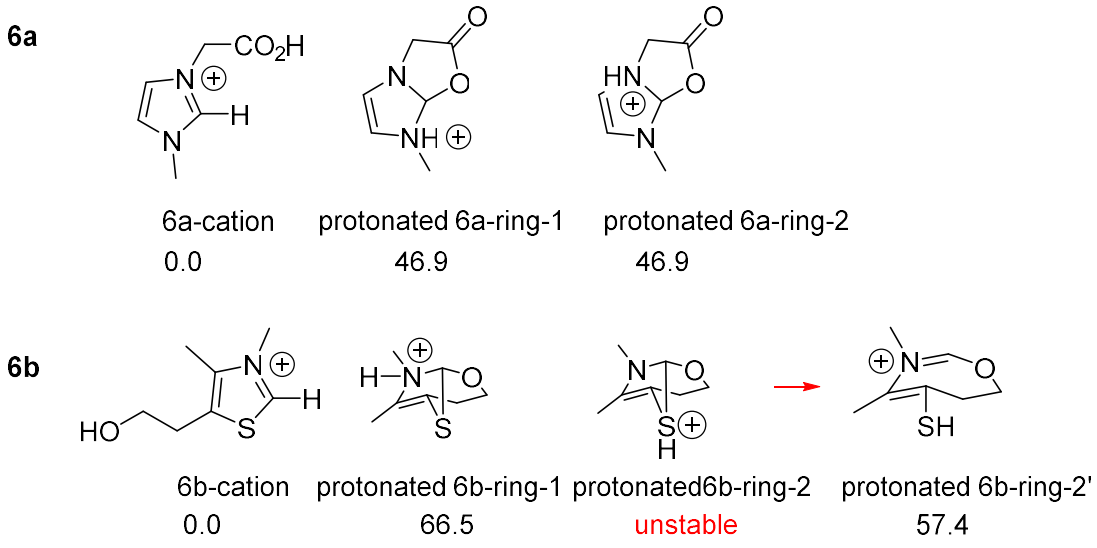

Figure 4. 14 Relative stabilities (in kcal/mol) of protonated 6a/b in the gas phase

Both protonated 6a and 6b can stably exist as azolium-based cations (6a/b-cation) in the gas phase; there might be other possible ring structures (e.g. ring-1 and ring-2), which are less stable.

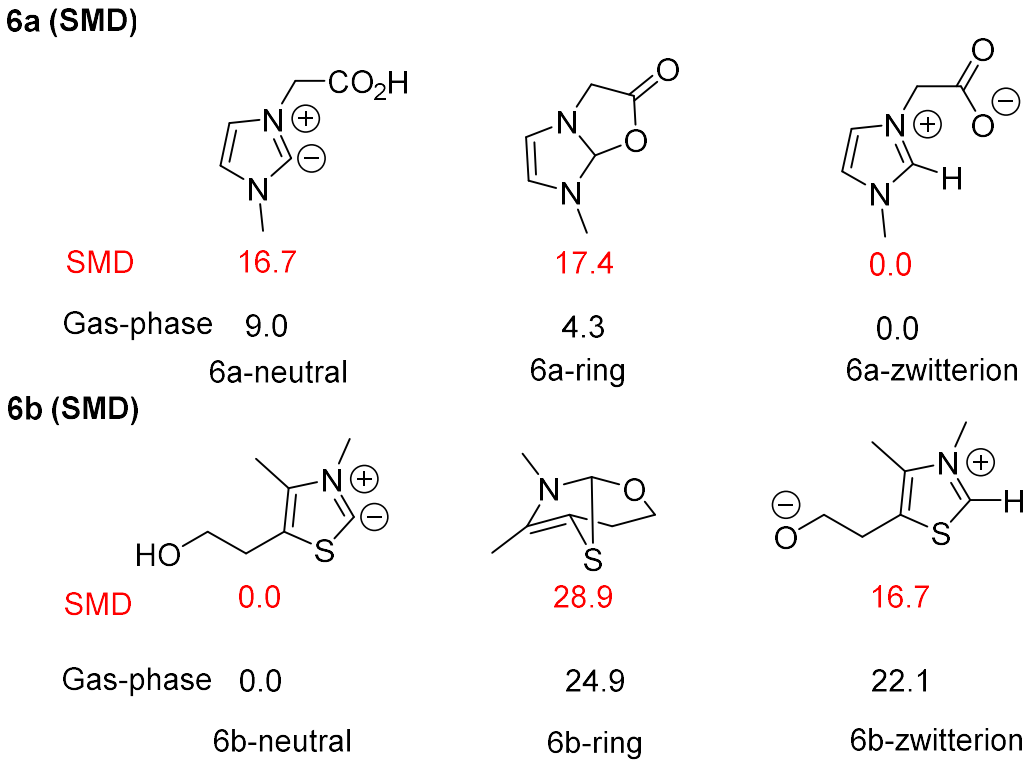

Figure 4. 15 Calculated relative stabilities (in kcal/mol) of neutral 6a/b in Solution Phase

Density functional theory (DFT) at B3LYP/6-31+G(d) was used to calculate the relative stabilities (enthalpy) of neutral 6a/b species in solution. The SCRF (Self-Consistent Reaction Field) solvation methods, SMD solvation model, was used with a dielectric constant of 20.493 for acetone to simulate a solution-phase environment. The trends for both 6a and 6b in acetone generally track with stability trends in gas-phase. One structure

stands out, though, that the free carbene structure of 6a (6a-neutral) is better stabilized in acetone than in gas phase.

ii. Acidity and Proton Affinity

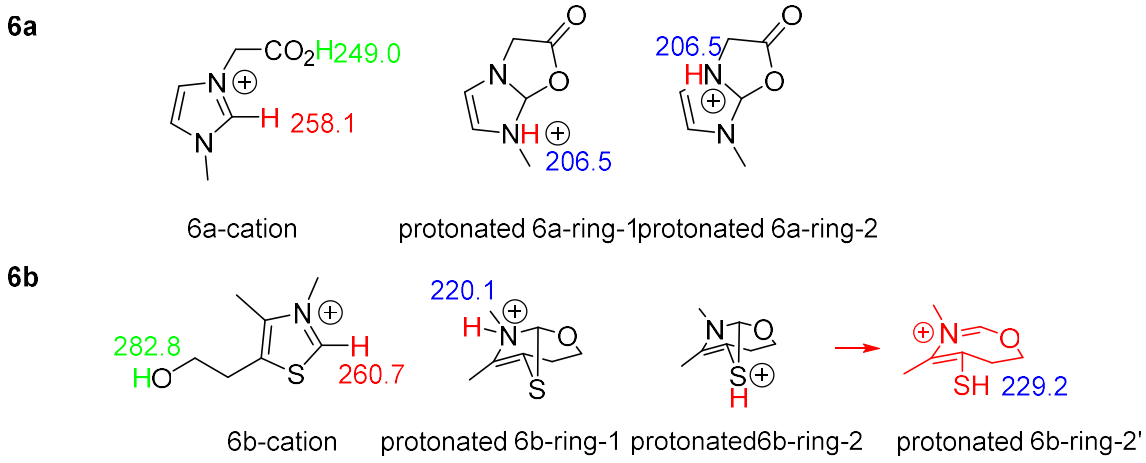

Figure 4. 16 Gas-phase acidity (kcal/mol) of Protonated 6a/b

From calculation results we can tell that the 6a C-2 site (258.1 kcal/nol) is less acidic than its carboxylic acid "handle" (249 kcal/mol). Note that both of the trends are consistent with those in aqueous solution: it is known that the triazolium salts have a pKa of 16-19 in water, and the pKa of carboxylic acid is around 5. The 6b C-2 site (260.7 kcal/mol), however, is more acidic than its alcohol "handle" (282.8 kcal/mol). The acidic sites (206-230 kcal/mol) within all other protonated ring structures are much more acidic compared with the cation structures.

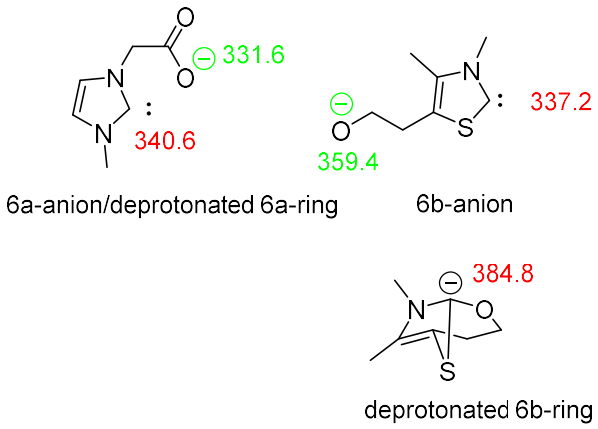

Figure 4. 17 Gas-phase Proton Affinity (PA, kcal/mol) of Deprotonated 6a/b

For the previously characterized Rovis 11a/b cations, the C-2 sites are also more acidic than its charged handles (Figure 4.18).

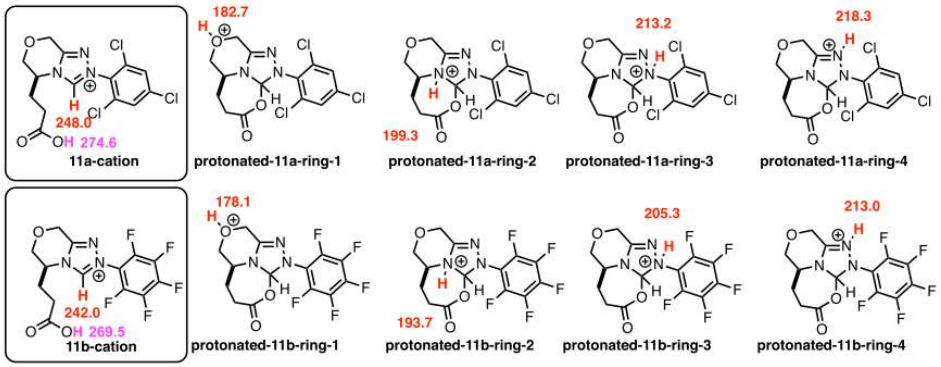

Figure 4. 18 Calculated acidities for protonated 11a(b) cations (kcal/mol)

One possible reason that accounts for this difference can be that, the negative charge on the carboxylate is better stabilized by hydrogen bonding between O- and the C-2 proton in the zwitterion structure of 6a (6a-zwitterion), compared with the zwitterion structures of 6b (6b-zwitterion) and 11a/b-zwitterion (Figure 4.19).

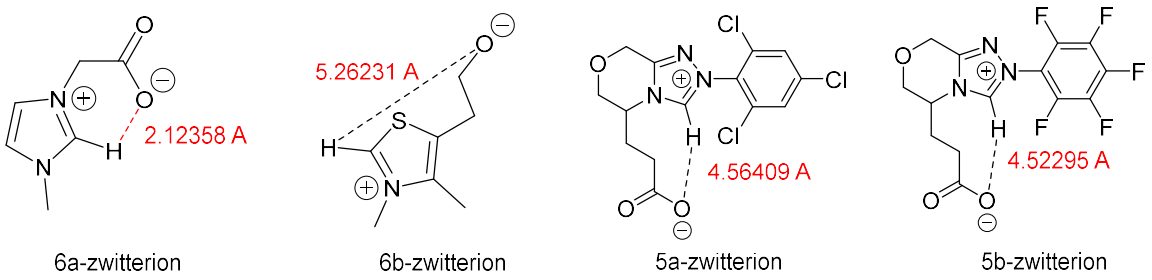

Figure 4. 19 Structures of four protonated NHC catalysts

For 6a there is only one methylene group between azolium ring and the negatively charged site, while for 6b/11a/11b there are two methylene groups. This might be one of the reasons why 6a-zwitterion has a stronger H-bonding interaction. Based on this, the relative acidities of azolium C-2 proton and –COOH/-OH can be readily tuned to be applied in catalysis.

4.3.2 Results of Bracketing Methods

The experimental bracketing results for the acidities of protonated 6a and 6b are listed in Table 4.1. The proton transfer reactions between the protonated 6a(b) and various reference bases with known proton affinities were studied in the gas phase. Electrospray ionization of the 6a(b) precatalyst successfully yielded the positively-charged protonated 6a(b) cation in the mass spectra as the major signal peak.

Eight reference bases are used. They are N,N,N',N'-tetramethylenediamine (PA = 242.1 kcal/mol), 1-(Cyclopent-1-en-1yl)pyrrolidine (PA = 243.6 kcal/mol), N,N,N',N'-tetramethyl-1,3-propanediamine (PA = 247.4 kcal/mol), MTBD (PA = 254.0 kcal/mol), HP_1(dma) (PA = 257.4 kcal/mol), $tBuP_1$(dma) (PA = 260.6 kcal/mol), $tOctP_1$(dma) (PA = 262.0 kcal/mol), and BEMP (PA = 263.8 kcal/mol). The presence of proton transfer from protonated 6a(b) to a reference base indicates that PA of the given base is higher than that of the conjugate base of protonated 6a(b) cation. In contrast, absence of proton transfer

implies a higher PA of the conjugate base of protonated 6a(b) cation than the PA of the reference base.

Table 4. 1 Summary of results for acidity bracketing of protonated 6a and 6b

Reference base[a,b]	*PA (kcal/mol)*[c]	*Proton transfer to reference base*[d]	
		6a-cation	**6b-cation**
N,N,N',N'-tetramethylethylenediamine	242.1	- (dimer)	
1-(cyclopent-1-en-1yl)pyrrolidine	243.6	- (dimer)	
N,N,N',N'-tetramethyl-1,3-propanediamine	247.4	- (dimer)	
MTBD	254.0	- (dimer)	-
HP_1(dma)	257.4	- (dimer)	-
$tBuP_1$(dma)	260.6	- (dimer)	+
$tOctP_1$(dma)	262.0	- (dimer)	+
BEMP	263.8	+ (dimer)	+

[a]Reference; [b]BEMP = 2-tert-butylimino-2-diethylamino-1,3-dimethylperhydro-1,3,2-diazaphosphorine; tOctP 1 (dma) = tert-octylimino-tris(dimethylamino)phosphorane; tBuP 1 (dma) = tert-butylimino-tris(dimethylamino)phosphorane; HP1(dma) = imino-tris(dimethylamino) phosphorane; MTBD = 7-Methyl-1,5,7-triazabicyclo[4.4.0]dec-5-ene. [c]Reference base PAs typically have an error of ±2 kcal/mol. [d]The "+" symbol indicates the occurrence and the "–" symbol indicates the absence of proton transfer.

HP_1(dma) (PA = 257.4 kcal/mol) cannot deprotonate **6b-cation**, but $tbuP_1$(dma) (PA = 260.6 kcal/mol) can, bracketing the acidity of **6b-cation** to 259 ± 4 kcal/mol; $tOctP_1$(dma) (PA = 262.0 kcal/mol) cannot deprotonate **6a-cation**, but BEMP (PA = 263.8 kcal/mol) can, bracketing the acidity of **6a-cation** to 263 ± 3 kcal/mol.

6a-cation formed hydrogen-bonded dimers (noted as "dimer" in Table 4.1) with all eight reference bases, which made it difficult to find specific cut-off points and draw a solid conclusion about the gas-phase acidity of protonated 6a. The "-/+" symbols of 6a-cation in

Table 4.1 were based on the data processing where the dimer peaks were considered as reactant (protonated 6a) peaks.

Cooks kinetic method was further used to measure the acidity of protonated 6a(b) cations (section **4.3.3**).

4.3.3 Results of Cook Kinetic Methods

For our acidity studies of protonated 6a(b) using Cooks kinetic experiments, we utilized eight reference bases and measured the product ion distributions three separate times to ensure reproducibility. The reference bases were *N,N,N′,N′*-tetramethyl-1,3-propanediamine (PA = 247.4 kcal/mol), DBN (PA = 248.2 kcal/mol), DBU (PA = 250.5 kcal/mol), MTBD (PA = 254.0 kcal/mol), HP_1(dma) (PA = 257.4 kcal/mol), $tBuP_1$(dma) (PA = 260.6 kcal/mol), $tOctP_1$(dma) (PA = 262.0 kcal/mol), and BEMP (PA = 263.8 kcal/mol).

Based on data analysis using Cooks "extended" kinetic method, the acidities of protonated 6a and 6b were determined as 251 ± 3 kcal/mol, and 258 ± 3 kcal/mol, respectively.

4.4 Discussion

The experimental and calculational results of protonated 6a/b are summarized in Table 4.2. For 6b cation structure (6b-cation) the bracketed acidity (259.0 ± 4 kcal/mol) benchmarked its calculated acidity of 260.7 kcal/mol on the C-2 site, so it's highly probable that 6b cation exist in gas phase as the 6b-cation structure. For 6a, the acidity was measured by Cooks method to be 251 ± 3 kcal/mol which is consistent with the calculated acidity (249 kcal/mol)

of the charged handle site (-COOH), and it's likely that 6a cation exist in the gas phase as the 6a-cation structure. Another optimized 6a-zwitterion structure where there is no hydrogen bonding existing (where the distance of COO- to C2-H is 4.34817 Å, compared to 2.12358 Å where there is H-bonding, see Figure 4.19) was also calculated, and the acidity of the charged handle site was calculated to be 252.6 kcal/mol which is more closely consistent with the Cooks method results.

Calculation

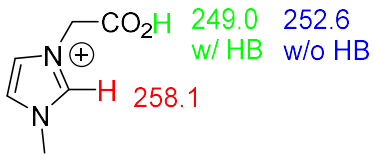

6a-cation

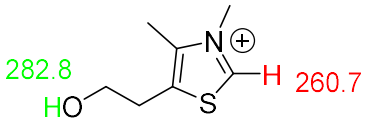

6b-cation

LCQ Bracketing

262.9 ± 3	259.0 ± 4

Cooks Method

251.3 ± 3	257.6 ± 3

Figure 4. 20 Comparison of experimental and calculational data of 6a/b cations

It is worth noting that the LCQ bracketing results of 6a (263 ± 3 kcal/mol) is quite different from its calculation results. It might be that when the reference bases with PAs below ~260 kcal/mol were used, they only deprotonated the –COOH site which is more likely to stay as a proton bound dimer; while reference bases with PAs above ~260 kcal/mol deprotonated the C2-H site, and a carbene formed so that we could observe the proton transfer.

Table 4. 2 Calculated (B3LYP/6-31+G(d); 298K) and experimental acidities for protonated 6a and protonated 6b

6a/b cation	Calc acidity	Experimental acidity
6a-Cation-C2	258.1	
6a-Cation-COOH	249.0	251.3 ± 3 (Cooks)
6a-ring1	206.5	262.9 ± 3 (Bracketing)
6a-ring2	206.5	
6b-Cation-C2	260.7	
6b-Cation-OH	282.8	257.6 ± 3 (Cooks)
6b-ring1	220.1	259.0 ± 4 (Bracketing)
6b-ring2	229.2	

4.5 Conclusions

In order to employ the charge handled NHC catalysts to organocatalysis where they could serve as proton shuttles to accelerate reaction, and also make relevant species detectable in mass spectrometer, it is very important to ascertain the fundamental properties, e.g. the most stable structures, of the charged-handle NHCs (both in gas phase and in solution phase), and their relative acidity/PA between their carbene (C-2) sites and charged handle sites.

4.6 Reference

(1) Samojłowicz, C.; Bieniek, M.; Grela, K., *Chem. Rev*. **2009**, *109*, 3708.
(2) Ukai, T.; Tanaka, R.; Dokawa, T., *J. Pharm. Soc. Jpn.* **1943**, *63*, 296.
(3) Sheehan, J. C.; Hunneman, D. H*., J. Am. Chem. Soc.* **1966**, *88*, 3666.
(4) Enders, D.; Breuer, K.; Raabe, G.; Runsink, J.; Teles, J. H.; Melder, J.-P.; Ebel, K.; Brode, S., *Angew. Chem., Int. Ed. Engl.* **1995**, *34*, 1021.
(5) Enders, D.; Breuer, K.; Runsink, J.; Teles, J. H., *Helvetica Chimica Acta*, **1996**, *79*, 1899.
(6) Knight, R. L.; Leeper, F. J., *J. Chem. Soc. Perkin Trans.* **1998**, *1*, 1891.
(7) Flanigan, D. M.; Romanov-Michailidis, F.; White, N. A.; Rovis, T., *Chem. Rev.* **2015**, 115, 9307.
(8) Stetter, H.; Schreckenberg, M., *Angew. Chem. Int. Ed*. **1973**, *12*, 81.
(9) Lemal, D. M.; Lovald, R. A.; Kawano, K. I. *J. Am. Chem. Soc.* **1964**, *86*, 2518.
(10) Tian, Y.; Lee, J. K. *J. Org. Chem.* **2015** , *80*, 6831.
(11) Zeng, H.; Wang, K.; Tian, Y.; Niu, Y.; Greene, L.; Hu, Z.; Lee, J. K. *Int. J. Mass Spectrom.* **2014**, *369*, 92.
(12) Brook, A. G. *Acc. Chem. Res.* **1974**, *7*, 77.
(13) Lalli, P.; Rodrigues, T. S.; Arouca, A. M.; Eberlin, M. N.; Neto, B. A. D., *RSC Adv*. **2012**, *2*, 3201.
(14) Yijie, N. Gas Phase Kinetic and Thermodynamic Studies of Organic Species Using Mass Spectrometry. Ph.D. Dissertation, Rutgers, the State University of New Jersey, 2017.
(15) Alberto M.; Tomislav R. Unpublished work.

Chapter 5 Heterocycle-based Ionic Liquids (ILs) Applied as Electrolytes in Anhydrous Fuel Cells

5.1 Introduction

Room temperature ionic liquids (RTILs) are liquids at ambient or even far below ambient temperature. These are comprised entirely of ions and are gathering more and more interest in multidisciplinary areas for their unique physicochemical properties such as high thermal stability, negligible vapor pressure, relatively high ionic conductivity, good tunability, and excellent electrochemical stability. After the discovery of air- and water-stable RTILs by Cooper and Sullivan and Wilkes et al.,[1] many RTILs have been extensively explored, and their remarkable utility in diverse fields has been discovered. From the viewpoint of electrochemistry, RTILs themselves are ionic conductors and in many aspects excel typical ionic conductors for which the use of a solvent is a prerequisite to reveal ionic conductivity in electrochemical devices. Carlin et. al. , back in 1994, constructed dual intercalating molten electrolyte batteries, wherein they used RTILs as an electrolyte.[2] RTILs have come to the forefront as effective electrolytes since then, either independently or as incorporated into polymer matrix or membrane. Protic ionic liquids have a long history since the first discovery of a protic ionic liquid, EtH_3NNO_3, and the use of an amine base-protonic acid system as a proton conductor in nonaqueous states was first reported by Takahashi et al. in 1976.[3] The recent research hotspot, high temperature polymer electrolyte fuel cells (PEFCs), possess advantages over conventional PEFCs which exhibit poor proton conductivity above 100°C due to their temperature and humidity dependence.[4] Therefore, ionic conducting membranes based on low-volatility solvents, i.e., heterocycle-based polymer or ILs-based polymer, have been widely studied. Heterocycles such as imidazole,

pyrazole, triazole, and benzimidazole have been considered as proton solvents to replace water, so that high temperature polymer electrolyte fuel cells would be possible.

Despite the widespread applications of protic ionic liquids, reports focusing on their intrinsic properties are relatively rare. Our gas-phase study is conducted in anhydrous conditions where the properties of the heterocycle-based electrolytes could be characterized *in vacuo*. By establishing the relationship between heterocycle properties and proton conductivity in fuel cells we could provide guidance for rational electrolytes design for novel anhydrous high temperature fuel cells.

5.2 Experimental

5.2.1 Calculation

All the calculations were performed using density functional theory (B3LYP/6-31+G(d)) as implemented in Gaussian 09 and Gaussian 16. All the geometries were fully optimized, and the frequencies were calculated; no scaling factor was applied. The optimized structures had no negative frequencies. The temperature for the calculations was set to be 298 K.

5.3 Results and Discussion

5.3.1 Computational Results

i. Gas-phase acidity vs. Ionic Conductivity

First we calculated the gas phase acidity of a series of amines. The results are shown in Table 5.1. Taking trifluoromethanesulfonimide (HTFSI) as the pre-anion (Brønsted acid) and different amines as pre-cations (Brønsted bases), the calculated gas phase acidities are plotted against the ionic conductivity data reported previously in the literatures (Figure 5.1).[5]

Table 5. 1 Calculated gas phase acidities of a series of amines

Pre-anion	Pre-cation	Calculated acidity (kcal/mol)	[a]Ionic Conductivity (10^{-2} S*cm^{-1})
trifluoromethanesulfonimide	Pyrazine	209.6	3.38
	Pyrazole	213.7	2.65
	Quinoxaline	216.0	1.65
	Butylamine	220.2	1.04
	Morpholine	220.9	1.08
	Pyridine	222.3	3.04
	Imidazole	225.3	2.71
	Pyrrolidine	226.6	3.96
	Benzimidazole	228.0	1.31
	Piperidine	228.0	2.35
	Dimethylethylamine	229.5	4.60
	Dibutylamine	231.5	1.26
	Diethylmethylamine	232.1	4.10
	triethylamine	234.7	3.23
	Diphenylamine	214.9	0.85
	4,4'-Trimethylenedipyridine	224.9	1.05

[a]All the Ionic conductivity data were measured at 120°C, except for Dimethylethylamine and Diethylmethylamine which were measured at 130°C.[5]

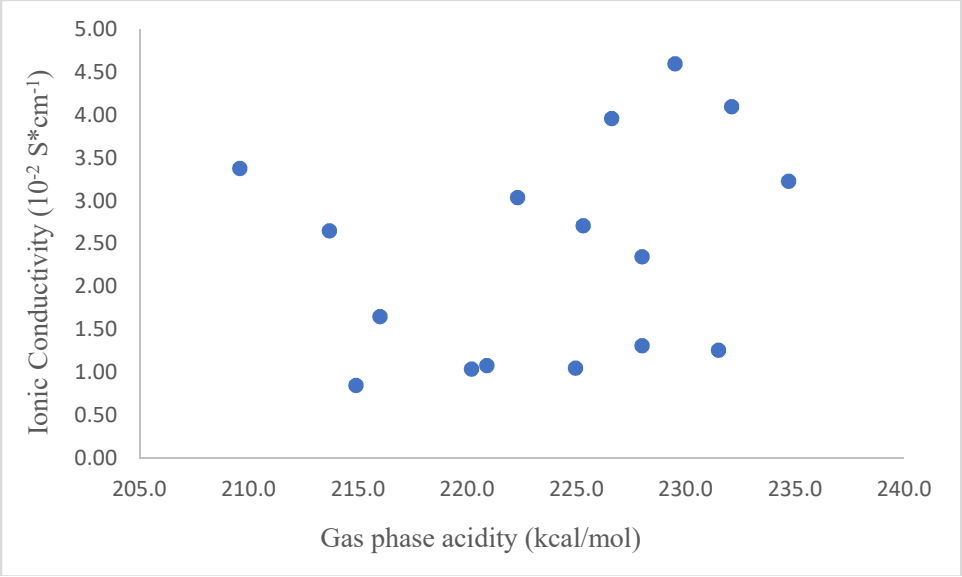

Figure 5. 1 Calculated gas phase acidities of pre-cations vs. ionic conductivity.[5]

The correlation between the calculated gas phase acidities and the ionic conductivity is not clear in Figure 5.1. Regarding the structural variations among the pre-cations studied, we categorized these pre-cations into different groups, and the subsequent plot is shown in Figure 5.2. The categorized structures were highlighted in colors while the un-highlighted structures were in black. The correlations between the calculated gas phase acidities and the ionic conductivity are relatively clearer after the categorization, yet more pre-cation/anions would need to be measured before any conclusions are made.

Table 5. 2 Calculated gas phase acidities of a series of amines (categorized)

Pre-anion	**pre-cation**	**Calculated acidity (kcal/mol)**	**Ionic conductivity (10^{-2} S*cm^{-1})**
trifluoromethanesulfonimide	dimethylethylamine	229.5	4.60
	diethylmethylamine	232.1	4.10
	triethylamine	234.7	3.23
	Pyrazine	209.6	3.38
	Pyrazole	213.7	2.65
	Quinoxaline	216.0	1.65
	Morpholine	220.9	1.08
	Imidazole	225.3	2.71
	Benzimidazole	228.0	1.31
	Pyrrolidine	226.6	3.96
	Piperidine	228.0	2.35
	Diphenylamine	214.9	0.85
	Butylamine	220.2	1.04
	Dibutylamine	231.5	1.26
	Pyridine	222.3	3.04
	4,4'-Trimethylenedipyridine	224.9	1.05

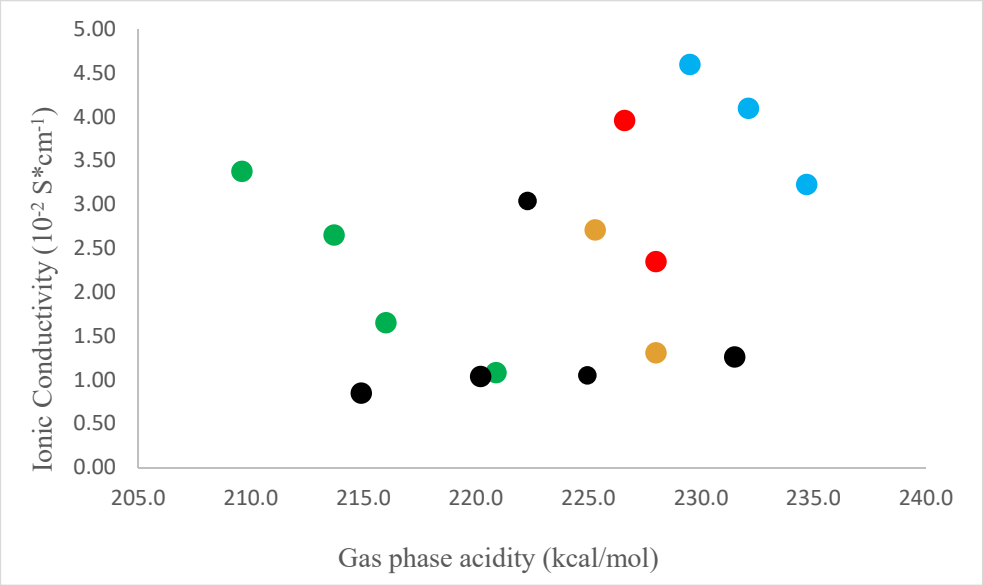

Figure 5. 2 Calculated gas phase acidities of pre-cations vs. ionic conductivity (categorized)

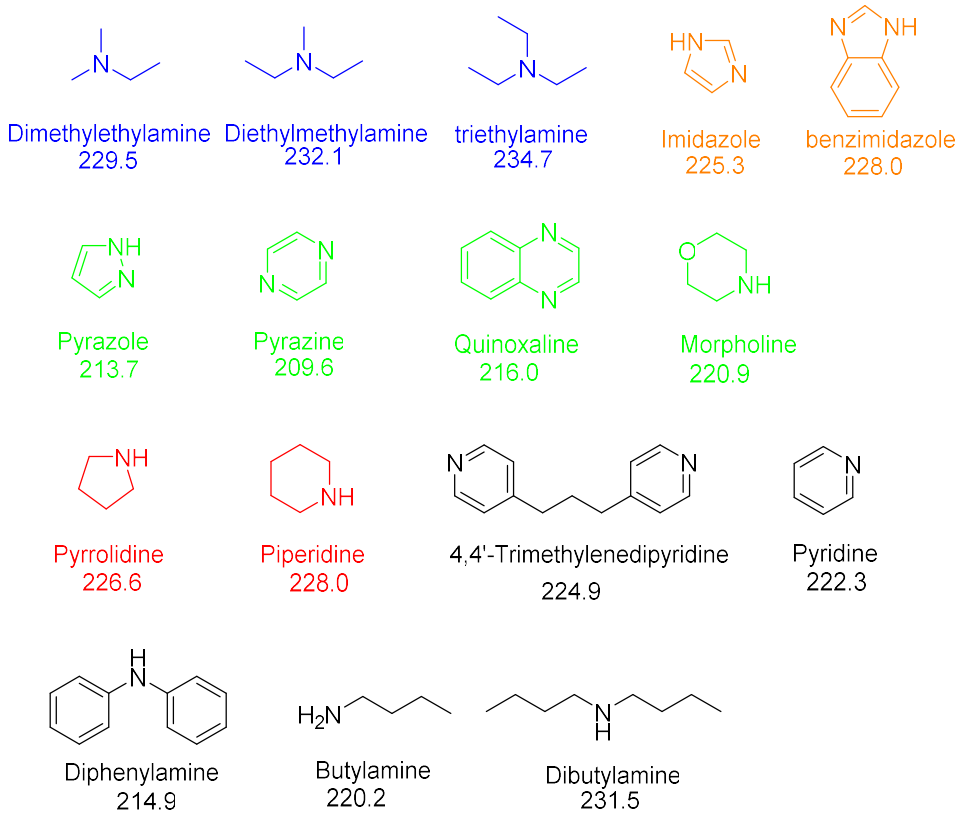

Figure 5. 3 Structures of pre-cations (categorized)

ii. Gas-phase acidity/proton affinity vs. Open-Circuit Potential (OCP)

Open-Circuit Potential (OCP) is the difference of electrical potential between two terminals of a device (solar cell, fuel cell, etc.) when disconnected from any circuit. Alternatively, the open-circuit potential may be thought of as the voltage that must be applied to a fuel cell or a battery to stop the current. OCP, besides ionic conductivity, is another indicator of how well the electrolytes would facilitate proton transport in fuel cell. Inspired by Watanabe's report in 2013 (Figure 5.4 redrawn from reference),[6] we also plotted the difference of calculated anion PA and cation acidity, against the fuel cell OCP values (Figure 5.5). The results indicate that the gas phase thermodynamic properties such as acidity and proton affinity could also correlate with OCP and provide information on how efficient an ionic liquid is as electrolyte for fuel cells.

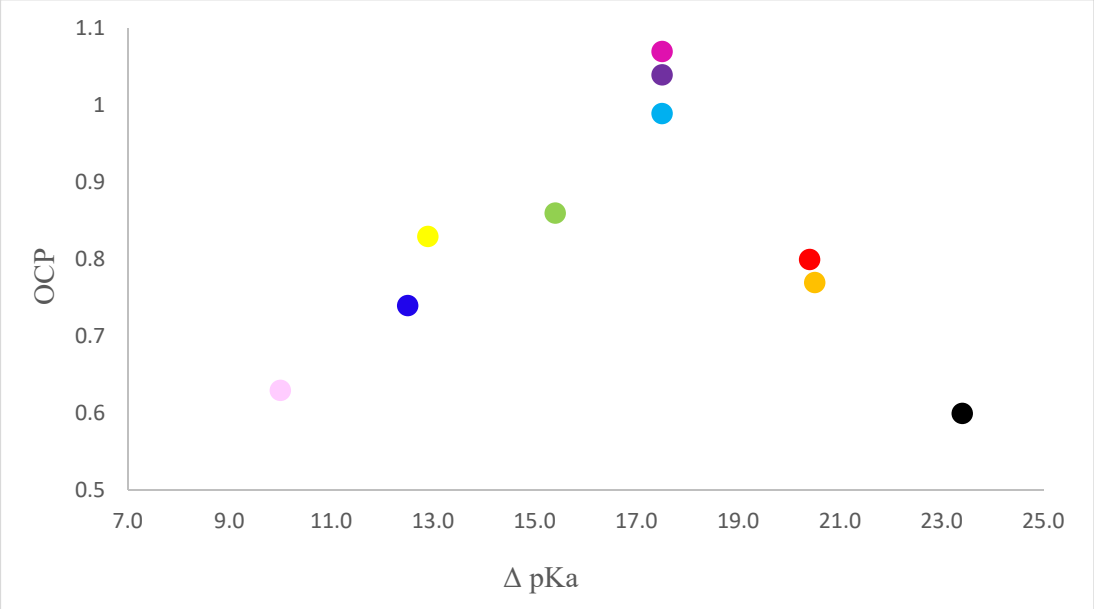

Figure 5. 4 ΔpKa of the IL cation/anion vs. the fuel cell OCP.[6]

Table 5. 3 Calculated gas phase acidities and PAs (kcal/mol) of a series of cations and anions

anion	A. anion proton affinity	cation	B. cation acidity	Δ (A-B)	OCP
$CF_3CO_2^-$	313.4	dema-H^+	230.3	83.1	0.63
	313.4	DBU-H^+	250.7	62.8	0.83
$CH_3SO_3^-$	315.5	dema-H^+	230.3	85.2	0.74
	315.5	DBU-H^+	250.7	64.9	0.86
$CF_3SO_3^-$	295.7	dema-H^+	230.3	65.4	1.04
	295.7	DBU-H^+	250.7	45.1	0.8
	295.7	empa-H^+	231.1	64.6	0.99
$C_4F_9SO_3^-$	292.6	empa-H^+	231.1	61.5	1.07
$(CF_3SO_2)_2N^-$	291.3	dema-H^+	230.3	61.0	0.77
	291.3	DBU-H^+	250.7	40.7	0.6

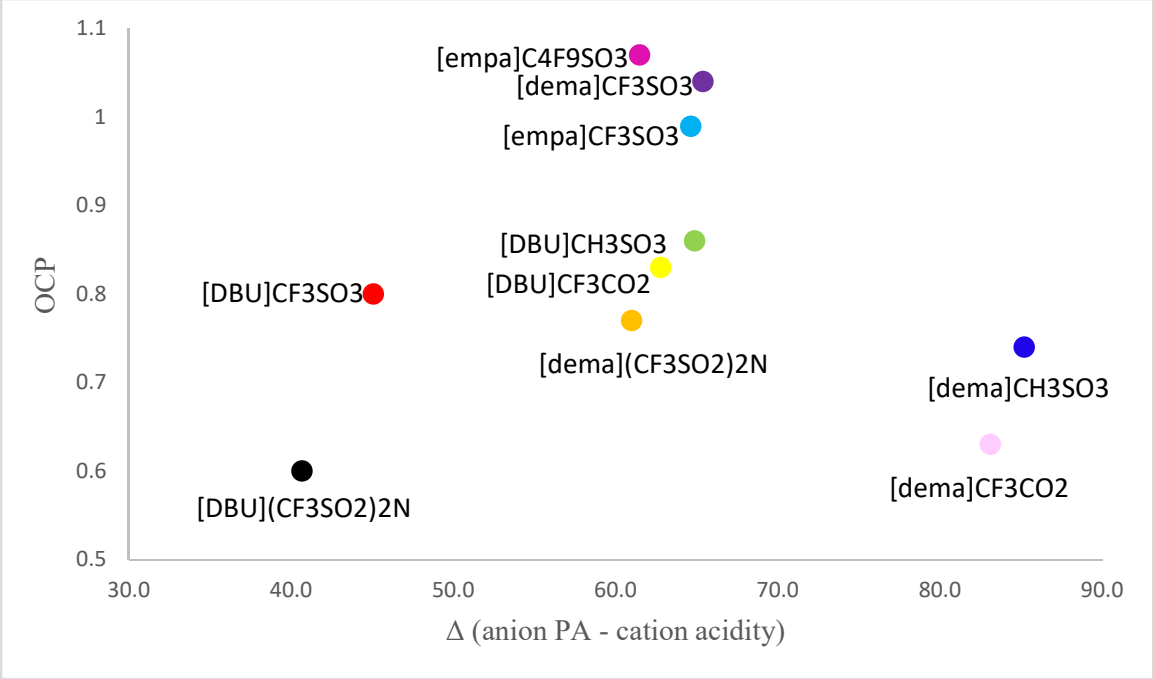

Figure 5. 5 Δ (anion PA - cation acidity) of the IL cation/anion vs. the fuel cell OCP

5.4 Conclusion

We calculated the gas phase acidities and proton affinities for a series of acids and bases that could be used to make protic ionic liquids applied as anhydrous fuel cell electrolytes. From these preliminary results we could tell that the gas phase thermodynamic properties have the potential to be considered as useful tools for rational anhydrous electrolyte design. Further calculational and experimental data on a broader range of cation/anion candidates need to be collected for a deeper understanding.

5.5 References

(1) Cooper, E. I.; Sullivan, E. J. M. In Molten salts VIII; Gale, R.J., Blomgren, G., Kojima, H., Eds.; *The Electrochemical Society Proceedings Series*; Electrochemical Society: Pennington, NJ, 1992; Vol. 92-16, p 386.
(2) Wilkes, J. S.; Zaworotko, M. J. J. J. o. t. C. S., *Chemical Communications.* **1992**, 965.
(3) Takahashi, T.; Tanase, S.; Yamamoto, O.; Yamauchi, S. J. *J. Solid State Chem.* **1976**, *17*, 353.
(4) Cho, E.; Park, J.-S.; Sekhon, S.; Park, G.-G.; Yang, T.-H.; Lee, W.-Y.; Kim, C.-S.; Park, S.-B. J. *J. Electrochem. Soc.* **2009**, *156*, B197.
(5) Noda, A.; Susan, M. A. B. H.; Kudo, K.; Mitsushima, S.; Hayamizu, K.; Watanabe, M. J. T. *J. Phys. Chem. B.* **2003**, *107*, 4024.
(6) Miran, M. S.; Yasuda, T.; Susan, M. A. B. H.; Dokko, K.; Watanabe, M. J. *RSC Advances,* **2013**, *3*, 4141.